Development of a miniature novel biopsy instrument for ductoscopy

by

K.A. Snaar

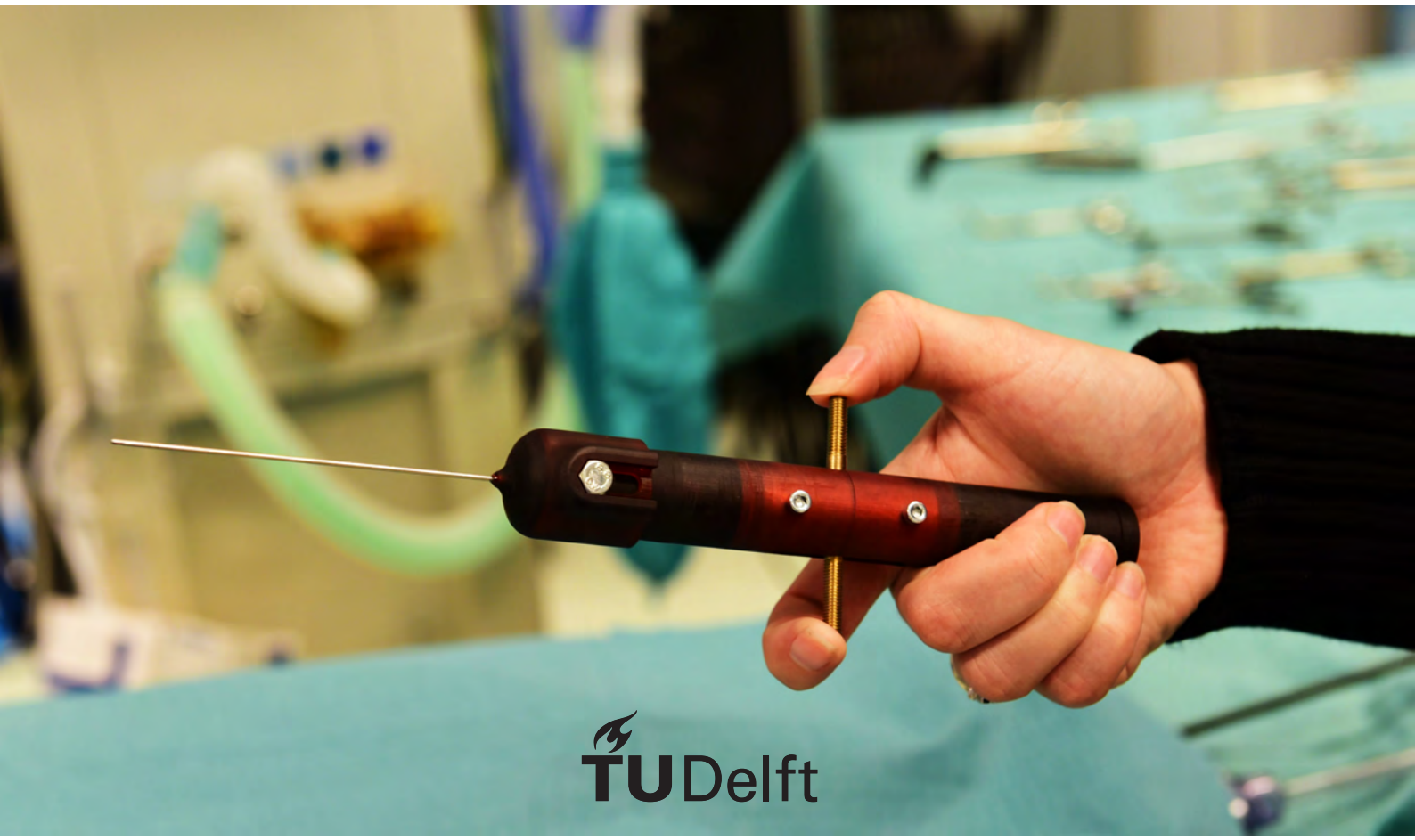

Development of a miniature novel biopsy instrument for ductoscopy

by

K.A. Snaar

To obtain the degree of Master of Science
at the Delft University of Technology,
to be defended publicly on Wednesday March 12, 2017 at 10:00 AM.

Student number:	4010434	
Project duration:	September 1, 2017 - March 12, 2017	
Thesis committee:	Prof. dr. ir. P. Breedveld,	TU Delft,
	Ir. A. Sakes,	TU Delft
	Ir. J. W. Spronck,	TU Delft
	Dr .ir. G. Smit,	TU Delft

TU Delft

Abstract

Background: Ductoscopy is a minimally invasive procedure, using a sub millimeter fiber optical camera, to explore the mammary ductal epithelium for Pathological Nipple Discharge (serous fluid discharged from the milk duct) and breast cancer, detecting lesions up to eight years before other modalities. Although ductoscopy can revolutionize breast disease screening, an improved method to take a biopsy during the procedure is needed. The goal of this study was, therefore, to develop a new biopsy method for the removal of a small tissue sample during ductoscopy for the pathological examination and a definite diagnosis.

Method: In order to develop the novel biopsy instrument the clinical situation and cutting forces were analyzed. The novel biopsy instrument, contains $\varnothing 1.0x0.1$ *mm* and $\varnothing 1.2x0.1$ *mm* needles including a knife design at the tip. The needles are actuated by the handle design, able to create a single- and a counter rotating motion. Subsequently the fully functioning prototype has been evaluated on its mechanical functionality and biopsy capabilities. In these experiments three different tip geometries: The Straight-, Beveled- and Reverse beveled-knife, were evaluated based on the resection time, displacement, operation force Biopsy points and sample volume. To mimic the ductal wall and tumorous tissue, gelatin with a Young's modulus of $150kPa$ was used.

Results: Comparison of the two rotational configurations demonstrated a decrease in all tested variables (resection time, displacement and tissue cut angle), using the counter rotation configurations. The Beveled tip designs showed an inability to debulk the lesion, however the other two geometries, the Straight and Reversed beveled tip proved to be able to debulk the breast mimicking phantom. The resected volume was 1.0 mm^3 sufficient for future pathological examination.

Conclusion: The experiment has revealed the potential clinical application of the instrument to debulk lesions found in the mammary ductal epithelium. Even so, more knowledge on the biomechanical properties of the lesions and an in-vivo experiment is needed, to find an optimal knife design for the different clinical situations. In future the novel instrument could be combined with a ductoscope, improving the diagnosis of breast cancer patients in an early stage of the disease.

Contents

1 Introduction

1.1 Ductoscopy

A minimally invasive surgery called "ductoscopy", "mammary ductoscopy" or "breast endoscopy" uses a submillimetre fiberoptic micro-endoscope, which is inserted into the breast milk ducts via the nipple surface, to facilitate the inspection of the mammary ductal epithelium for breast diseases [1]. It is suspected that the majority of benign and malignant lesions of the breast arise from the ductal epithelium and the terminal duct-lobular unit (TDLU), [2–4], see Appendix A.1. Ductoscopy could revolutionise breast disease screening, induced by the increased ability to visualize these lesions compared to modern mammography, ultrasound, and MRI (Appendix A.2).

Current breast cancer diagnosis modalities play a vital role in primary screening, diagnosing and characterizing of lesions, treatment selection, progression monitoring and in determining cancer recurrence. However, by the time a lesion is found by the patient or with the preferred population based method, namely mammography, the lesion is been growing for approximately 8 years. The cancerous breast tissue is usually about 10 *mm* at the time it is palpable, and 5-10 *mm* when detected by mammography [5, 6]. Hence, No single modality currently exists, better able to diagnose breast cancer in its early stages. However research is still conducted trying to improve the differentiation from normal and benign tissues, based on the physical, chemical, and biological properties of cancerous breast tissue. Ductoscopy is currently the best screening modality. Cancer is a disease without a specific cure, therefore early detection of breast cancer plays a vital role in the survival rate of women [7]. Therefore Ductoscopy could be the future of both Pathological Nipple Discharge (PND) and breast cancer diagnosis. Ductal Carcinoma In Situ (DCIS) and Lobular Carcinoma In Situ (LCIS) are non-invasive or pre-invasive breast cancer types. Invasive forms are Invasive Ductal Carcinoma (IDC) and Invasive Lobular Carcinoma (LIC). Of all breast cancers DCIS is the most common and best treatable.

In 1988 ductoscopy was first introduced by Teboul, for evaluating patients with spontaneous bloody nipple discharge. The ductal cavity was first observed using a rigid endoscope with an outer diameter of 1.7 *mm*, under the guidance of ultrasound. The early ductoscopic attempts were not very successful because of the large size of the endoscopes, lack of good resolution, small size images, and lack of a biopsy capability [6, 8].

Later Okazaki and Fujikura Co., developed smaller fiber-optic ductoscopy device with a 0.8 *mm* outer diameter, and an even later version had a 0.45 *mm* outer diameter [6]. This small diameter made it possible to observe the ductal appearance and measure the distance from the ductal orifice to the lesion, to determine the involved risk.

Presently, ductoscopy is performed in three different fields: as a screening tool for women with PND, during breast conserving surgery for cancer, and in screening procedures of high risk women [3, 9–11]. To implement ductoscopy as the cancer screening modality some aspects need to be improved. Although current ductoscopic instruments have excellent scopes, instruments containing better optics, smaller diameters, increased ability to negotiate tight turns and allow for the obtainment of biopsies during the procedure, are needed.

Furthermore, a downside of ductoscopy is the occasional lack of findings caused by luminal occlusion from scarring and sclerosis and the limited accessibility to the peripheral lesions created by the scope length (60-100 *mm*) [12].

1.2 Goal of the study

The functionality of the ductoscope could be increased when a biopsy tool is implemented in the instrument. Therefore recent research is conducted to combine the ductoscope with a biopsy instrument (Appendix A.3), to create a screening device which can directly take a sample of the abnormality. However current biopsy tools are not suited for the implementation of a ductoscope. Therefore the desire for an innovative ductoscopic instrument, which is able to perform the diagnosis of both PND and breast cancer, with integrated biopsy functionality, has emerged into a global description of the study objective:

"Develop a new biopsy method to take a tissue sample during ductoscopy"

1.3 State of the art

1.3.1 Current ductoscope

The ductoscope used in the University medical centre of Utrecht (UMCU) contains a cannula (stainless steel- or polyethylene tube (Polyshaft) (Fig.1 ①) and a ductoscope or a small fiber optical camera (Fig.1 ⑦). During the first surgical step, the nipple duct is enlarged using the lumen expander (Fig.1 ⑭), followed by the insertion of the Polyshaft/cannula containing the ductoscope. The images are obtained by, an auto fluorescence (AF) ductoscope coupled, via a custom-made eyepiece (Fig.1 ②), to an AF endoscopic imaging system (Fig.1 ④, ⑤ and ⑦) (OncoLIFE, Xillix Technologies Corporation, British Columbia, Canada, now Pinpoint, NOvadaq Technologies Corporation, Ontario Canada). When the milk duct is entered a salt solution is used to enlarge the milk ducts diameter (Fig.1 ⑥). After the entire breast is examined the instrument is extracted, finishing the procedure.

Endoscopic auto fluorescence imaging (AFI) uses the natural emission of tissue fluoresences of collagen, nicotinamide, adenine dinucleotide, flavin and porphyrins, induced by excitation light to create real-time pseudocolor images. AFI is able to visualize lesions undetectable by conventional white light endoscopy (WLE) [13–15].

1.3.2 Biopsy instruments

Performing a biopsy can be performed by guiding some sort of instrument through the scope 2. Examples are retrieval baskets, brushes, forceps, scissors, and magnetic extraction devices. Another method is image guided biopsy, including

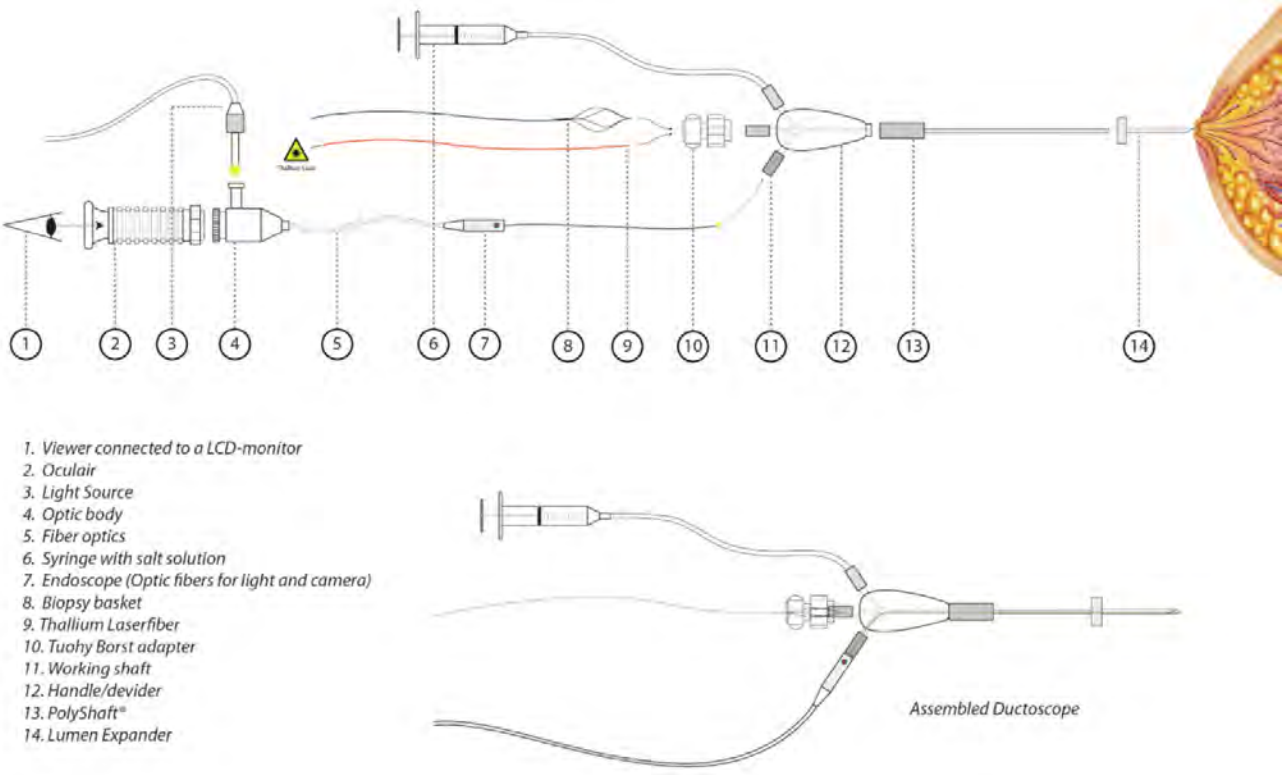

Figure 1: Ductoscopic overview.

Figure 2: Biopsy modalities inserted via a scope, from left to right: Snare, forceps, stone retrieval basket and cytology brush [16].

biopsy needles and guide wire devices. Although all of these modalities work for specific procedures most of them are not suited in combination with ductoscopy. For example, the biopsy brushes can only be used during procedures containing fluids or fluid like tissue such as saliva [17].

Other modalities are unable to take tissue samples from the ductal epithelial tract, due to the small diameter of the ducts. Only a limited amount of biopsy instruments could be found, which are usable [18]. The retrieval baskets used during some of the ductoscopic procedures were initially designed to remove stones [19], and are unable to cut the tissue from the ductal wall. Due to the fact that most of the devices have no hollow center, they can't be used while the ductoscope is inside the duct, enabling the user to visualise what is happening. The only biopsy modality available that is using a hollow center is the biopsy needle.

Biopsy needle types

For percutaneous breast biopsy different needle types are available. The simplest form is fine needle aspiration using a bevel shape needle attached to a syringe to collect a sample of cells or fluid from the lump, providing the material for cytological analysis. Core needle biopsy, on the other hand makes use of a hollow needle to remove tissue samples from the breast mass, preserving the obtained tissue architecture, enabling histological analysis, thereby being the preferred method (see Appendix A.3).

There are two types of core needle biopsy instruments used on the market. Core needles that can be advanced manually or semi-automatic, most often spring driven. Automatic spring driven needles provide more tissue than manually advanced needles of the same type, usually with little or no compressed tissue at the edges of the specimen, due to the high velocity cut. [20, 21]. However the surgeon is unable to determine the debulking velocity.

Biopsy needle tip designs

Biopsy needles take a tissue sample using a side cut or an end cut tip design, as will be explained next.

Side cut

Side cut biopsy needles consist of an inner stylet with a side notch and an outer cutting needle. The side-notch needle type is also called “Tru-cut" after the first commercial model, introduced by Allegiance [22]. These type of needles are introduced with the stylet slightly in front of the cutting needle. Subsequently, the needle tip is advanced into the lesion, by advancing the cutting needle over the stylet, resulting in the containment of the tissue inside the side notch. (Fig. 3).

During cryobiopsy a solid needle is placed in the targeted tissue. The tip-temperature is then lowered to approximately -10°C, this temperature freezes the tissue onto the needle, however there is no tissue necrosis. A slightly bigger outer rotating cutting cannula is then advanced over the inner needle. Thereby finishing the biopsy procedure, where after the device containing a single sample is removed from the breast (Fig 5). The advantages of this method are; the local anaesthetic effect created during the cooling process, the ability of the device to spear and stabilize a lesion, and the absence of a trigger mechanism. These advantages have the largest effect when a mobile lesion close to the skin or chest wall is fount [23].

End cut

The BioPince (Argon medical devices, Plano, Texas) end cut design is based on three separate parts: a sharp inner stylet, an inner coring cannula and an outer cannula with a pincer. During a biopsy the needle is advanced with the stylet slightly protruding from both cannulas. Near the lesion the inner coring cannula is advanced over the stylet, cutting the tissue, where after the outer cannula, and the pincer, slide over the inner coring cannula to cut off the tissue core. The pincer is positioned against the inner coring cannula, sealing of the cutting tube and holding the tissue in its place (Fig. 4).

Vacuum Assisted Biopsy (VAB)

Vacuum assisted biopsy devices most often exist of a sharp inner stylet and an outer cutting needle. The handling of a VAB is comparable to the side cutting needles except for the removal of the tissue sample, this is done by rotating the needle to take a sample (Fig 5). At the margin of the lesion the stylet is removed, followed by an applied vacuum during the advancement of the cutting needle. Hence, a core sample is cut from the target tissue using the entire length of the cutting needle. This needle type is most often advanced manually. The drawback of VAB is the inferior results compared to those of a semi-automatic tru-cut needle [24]. However the probe can be rotated up to 360° to retrieve multiple samples via a single insertion in the skin. These larger tissue volumes reduce the incidence of the spreading of breast diseases, such as atypical ductal hyperplasia (ADH) or DCIS, on consecutive biopsies [25].

1.4 Design direction

Despite the large amount of biopsy needles, there is no biopsy instrument in existence capable to combine biopsy abilities with a ductoscopic instrument. When looked upon the fine needle aspiration biopsy needles the downside is the inability to perform additional studies. Therefore only core needles and VAB will be considered. When the actuation of the instrument is considered for this particular application, the manual instruments have an advantage because the surgeon can control the velocity of the debulking process, which is important to precisely cut the lesion along the ductal wall, as the margin of error is very slim. However the actuation of the biopsy tip and the design of the biopsy tip itself will be addressed in later chapters.

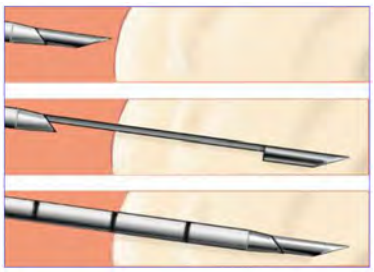

Figure 3: Side cut Biopsy needle (Tru-Cut, Allegiance, USA) [26].

Figure 4: End cut Biopsy needle (BioPince, Argon medical devices, Plano, Texas). Colour references: Grey: Outer cannula with Pincer, Purple: Inner couring cannula, Green: Stylet and Red: Tissue [22].

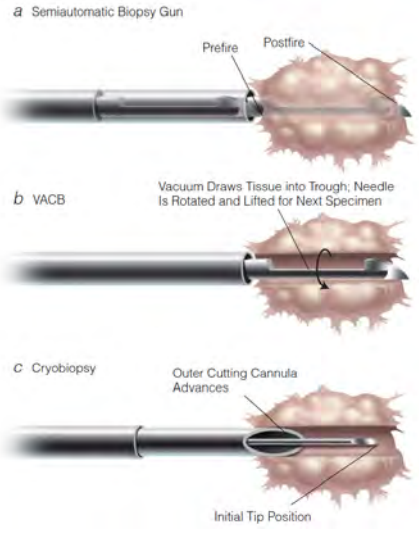

Figure 5: Different Biopsy needle types: A) Semiautomatic biopsy gun, uses a side cut biopsy needle to withdraw the sample. B) Vacuum assisted core biopsy (VACB), a vacuum is applied to remove the sample. C) Cryobiopsy, takes a tissue sample using cold temperatures. Colour references: Brown: Tissue and Grey: the instrument [23].

Although the Tru-Cut and BioPince are excellent in taking a sample from a densely packed tissue, they have some drawbacks. The Tru-cut is only able to work in areas where the tissue density is very high. This dens tissue pushes itself into the compartment where after the tissue is debulked. Without the pressure of the surrounding tissue, the compartment will stay empty, as will be the case when using the Tru-cut in the ductal tract, then the stylet will only push the lesion further into the duct.

When the BioPince is considered the drawback is the automated actuation, this reduces the ability of the surgeon to control the debulking velocity, increasing the risk for complications. Together with the large axial force pushing the lesion further into the duct.

Concluding, a novel biopsy instrument is needed, able to cope with the screening ability of the ductoscope.

1.5 Layout of the report

This study covers the theoretical derivation of promising biopsy methods, resulting in a final design of the biopsy tip. Subsequently, an actuation mechanism able to cope with the biopsy tips is designed. Followed by a translation of the two designs into one functional prototype. Where after a proof of principle experiment is performed by validating the ability of the instrument through experimentation.

2 Tip design

2.1 Requirements

The corporation with the UMCU included specialist consult on the current ductoscope. The questionnaire (Appendix A.4) gave a better understanding on the desires for the novel biopsy instrument and resulted in the requirements for the ductoscopic biopsy instrument, which are described as:

- The existing cannula dimensions are desired for easy integration. Hence, the cannula has a length of 100 *mm* and an inner and outer diameter of 1.15 *mm* and 1 *mm*, respectively.
- The optical fiber should fit inside the biopsy instrument: The optical fiber is 0.55 *mm* in diameter (LaDuScope T-flex, Polydiagnost), with a working length of 100 *mm* and a 0° angle direct view, otherwise explained as a field of view of 180° degrees.
- Irrigation of a duct enlargement fluid should be possible. During ductoscopy an enlargement fluid is used to expand the duct, enabling the surgeon to fit the instrument.
- The cutting structure of the instrument should contain an end-cut or a side cut mechanism, with a slide preference towards the end-cut mechanism.
- The biopsy method allows to cut all breast cancer types and Papilloma.
- To obtain a sample usable in pathology, the sample cells need to be intact, therefore the instrument should perform a cut, without destroying the obtained sample.
- During the removal of the instrument the tissue should be confined inside the cannula or grasped by i.e a vacuum, to reduce the risks of cancerous tissue spread.
- To create a clear vision on the milk duct, the ductoscope should be positioned close to the operation site, at the distal end of the cannula, when an end-cut is used. In the case of a side cut, the camera is positioned at the proximal end of the cutting window.

One of the requirements state that the biopsy instruments should be able to debulk all different possible tissues found during ductoscopy. The found cancerous tissues consist of LCIS DCIS and IDC. Harmless Papilloma are found during PND screening. In literature the elasticity stiffness values are reported to be between 36.5-83.3 *kPa* for LCIS, 69.6-97.4 *kPa* for DCIS and 144.5-149.7 *kPa* for IDC. Where Papilloma have an even lower stiffness value. [27–30] Hence, the biopsy instrument should be able to exert a pressure of at least 150 *kPa*.

2.2 Categorization

2.2.1 Clinical situation

For the design of a novel biopsy instrument all possible debulking methods need to be considered, therefore the clinical situation of the ductal lesion, the involved debulking forces and the force directions are evaluated.

The clinical situation found in the ductal tract is divided in three configurations. The first situation describes lesions found inside the ductal wall, while the second category contains lesions partially filling the duct, the final category portrays lesions filling the entire duct (see Fig. 6).

When the clinical situations are observed from a mechanical point of view, a better understanding of the needs for a biopsy tool, inside the ductal tract, are presented. To allow the instrument to contain lesions as described in the first category, the biopsy tool should be able to cut with a diameter larger than the ductal diameter, mechanically explained as the expansion of the instruments diameter at the location of the lesion, an example of such an instrument are tweezers. Instruments used in the second and third situation are permitted to stay inside the duct, thereby keeping a constant outer radius, which in these small diameter instruments is the preferred option.

The largest difference between the partially filled, (situation 2) and completely filled duct (situation 3) is the instruments position during the biopsy process. If the lesion covers the entire duct the instrument should be able to take an end cut. When a partially filled duct is found the instrument is allowed to cut from the side as well, in the case that the cannula is small enough to be manoeuvred round the lesion.

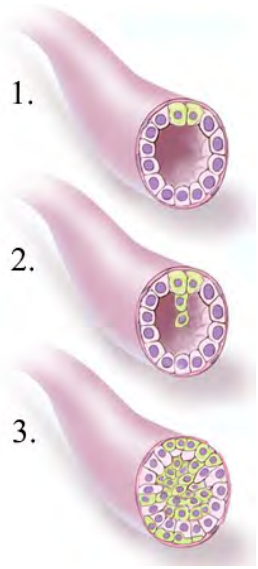

Figure 6: Situation 1: Lesion found inside the ductal wall, Situation 2: Partially filled duct, Situation 3: Completely filled duct. Green: Cells representing harmful lesions.

2.2.2 Debulking forces

For a fundamental analysis, the different debulking forces are categorised. To create a better understanding of the different designs possibilities.

Action force direction

When the biopsy process is observed on a fundamental level, the force delivered by the biopsy tip plays an important role in the ability to perform a cut. This force will be referred to as the action force. To categorise the different action forces a division is made based on the actional debulking force direction. Three force directions are identified: axial, radial, and tangential. In the axial category, an action force in the direction of the longitudinal axis of the instrument, is exerted on the tissue. In the radial category, an action force; along the radial axis (lateral axis), is exerted on the tissue. In the tangential category, a tangential force that follows the tangent of the instruments shaft, is exerted on the tissue. Schematic drawings of the action force directions can are found in Tables 1 and 2.

Reaction force delivery

After dividing the action forces in categories. The next logical step was to search for categories classifying the reaction forces. During the debulking of tissues two fundamental methods can be observed, instruments that only generate an action force, referred to as single-sided debulking and a second method, in which both the action and reaction force are generated by the instrument to cut, called double-sided debulking (see Fig.7). In single-sided debulking only one instrumental action force is used, to debulk the tissue; creating a large force loop, due to the force distribution. The reaction force is delivered by the environment, in the case of slow knife movement caused by the large force loop, or it is delivered by the tissue, in the case of fast knife creating enough inertia to keep the force loop small. An example of a single-sided debulking instrument is a knife. Double-sided debulking, on the other hand, exerts both the action and reaction force during the debulking process, causing a predetermined well-positioned, small force loop.

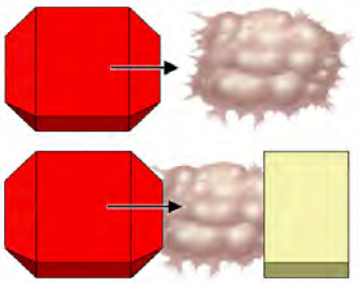

Figure 7: Top: Single-sided debulking. Bottom: Double-sided debulking. Red: Action force. Yellow: Reaction force.

In the remainder of this article single-sided debulking using slow knife movement will be referred to as "Environmental" while fast knife movement will be called "Tissue", the reaction force obtained during double-sided debulking on the other hand will be called "Device". An example of a biopsy instrument, which uses a single-sided axial debulking is Fine needle aspiration biopsy (FNAB), during this type of procedures a hollow needle is forced into the tissue, where after a syringe is used to pull the tissue through the needle, due to the slow pull movement, caused by the vacuum in the syringe, this method is referred to as an "Environmental" reaction force. The reactional forces are portrayed on the left axis of Table 1.

2.3 Concept selection

2.3.1 Overview

Considering the lesions clinical situation, the reaction forces and the action force directions results in the solutions found in Tables 1 and 2. Where Table 1 only uses basic ideas to show the different possibilities, Table 2 uses designs combining the action force directions, to find more intricate designs. After introducing basic biopsy tip designs, a design selection needed to be made. To complete this task selection criteria were created, as will be described in the next section.

2.3.2 Criteria

The damage caused to the ductal wall was examined and ought to be minimized. To reduce the damage to the surrounding environment, biopsy tips generating a small force loop are preferred. Structures creating a small force loop either use a reaction force supplied by the device, or a biopsy tip containing a quick moving knife.

The millimeter scale dimensions of the instrument, present a reduced feasibility to integrate a hinge in the instrument. Due to the extreme small size of these hinges, they can causes weakness and unreliability in the instrument. When hinges are used the forces acting on these small hinges should be extremely small, otherwise the hinges could fail. Minimizing the forces acting on a hinge is fairly hard, although there are instruments using a hinge, such as the BioPince, developing such an instrument is more time

Table 1: An overview of possible debulking structures, positioned in the different categories.

Table 2: Debulking structures combining two action forces, during the debulking process. i.e. a diagonal cut made using both the axial and a radial force.

consuming and precise knowledge on the dynamical effects and material properties is needed. Therefore instruments using a hinge are secondary to instruments without a hinge.

Another requirement was caused by the very limited design space, which meant that the manufacturability difficulty would increase exponentially, therefore concepts using fairly basic ideas had a preference over more intricate designs. Basic ideas use the already existing tube shape, were more advanced ideas add structures to the cutting tube.

2.3.3 Most promising concepts

After the incorporation of the new selection criteria three concepts were chosen as the most promising solution. The first biopsy tip concept uses a cone shape to make a diagonal cut, as can be seen in Figure 8. The second concept uses a sharpened tube, which is advanced rapidly along the ductal wall to debulk the lesion, (Fig. 9). The third concept uses two tubes containing a cut out, allowing the instrument to debulk the tissue when one or both knifes are rotated, (Fig. 10).

Finding the best solution out of these three concepts entailed a selection procedure, evolving the consideration of the biopsy tips downsides, together with some other important design factors.

The different clinical situations are an important factor in choosing the design for the biopsy tool, because the lesions, in situation 2 and 3, are connected to the ductal wall, the biopsy tip should be able to cut directly along the ductal wall. This eliminates designs that use a radial force to take the biopsy. The elimination of the radial action force combined with the rejection of hing designs created very limited design space, for solutions closing of the end of the tube. Although the cone concept is perfectly able to take a biopsy in situation 3, it is unable to cut along the ductal wall resulting in the rejection of the cone concept.

During the procedure controlling the tissue is an important factor. Tissue control is defined as the surgeons ability to slowly and precisely debulk the desired tissue area. However, the downside of the sharpened tube concept is the inability to debulk the tissue in a controlled manner. Due to the rapid movement of the sharpened cutting tube (Fig. 9). Another result of the rapid moving knife is the propulsion of the debulked tissue further into the milk duct, increasing the risk of harmful tissue spread. The protruding movement also results in a decreased ability to capture the debulked tissue.

Concluding, a biopsy tip, allowing the surgeon to position the knifes slowly and precisely, creating a controlled cut, while the debulked tissue should stay as close to the end of the biopsy tip as possible, is desired. The biopsy tip should also be able to penetrate tissue using the frontal surface, in the case of an entirely filled duct, and when the lesion is expanding over a distance longer than the cut outs length. The Cut out concept fits perfectly to this necessities. It uses two counter rotating knifes to debulk the tissue, slowly yet precisely, and because of the tangential motion the debulked tissue remains near the debulking tip. While the simple design of the knifes is easy to fabricate. The concept can be explained as an instrument containing two rotatable shafts with a cut out at the end of the shaft. The tangential motion ensures debulking along the ductal wall, while allowing the surgeon to control the knife movement. Possible biopsy tips are illustrated in Figure 11. The cut out concept will be further elaborated in the next section.

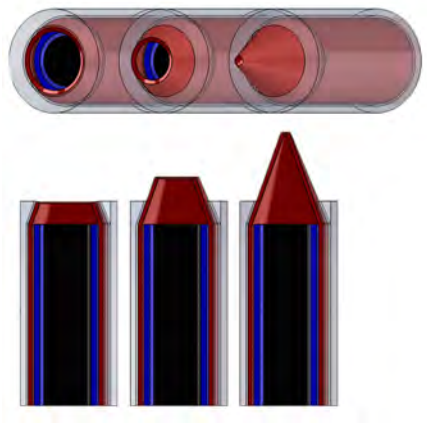

Figure 8: Cone concept: The flexible cutting tube (Red) is pushed against the outer tube (Grey) to change the cutting direction which allows the cutting tube to debulk the tissue.

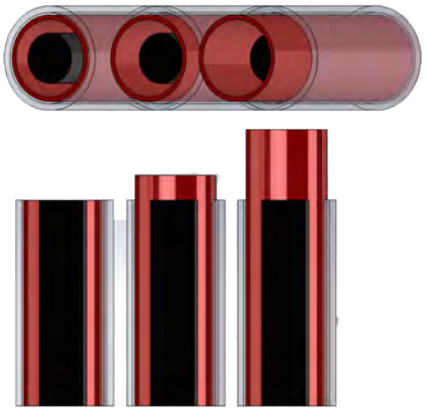

Figure 9: Push concept: The instrument containing a outer tube (Grey), which protects the ductal wall from the sharp cutting tube (Red). The cutting tube is advanced rapidly when a lesion is detected.

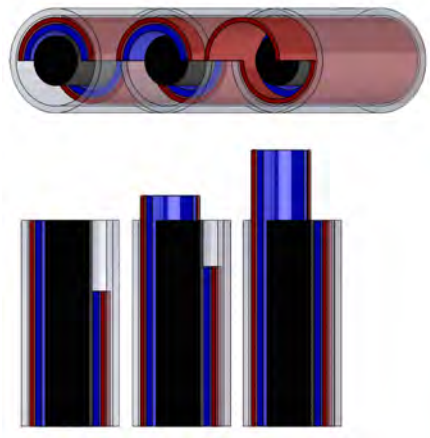

Figure 10: Cut out concept: The two cutting tubes (Red and Blue) are advanced out of the protection tube (Grey), where after the cutting tubes are counter rotated to cut the lesion.

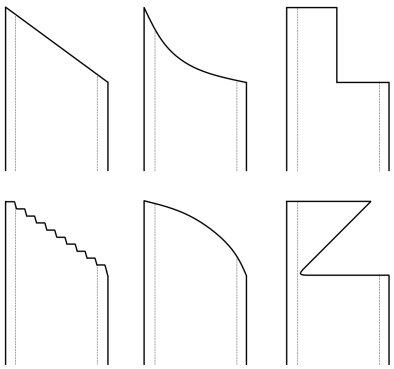

Figure 11: Examples of different Cut-Out profiles. Fairly basic ideas are portrayed due to manufacturability reasons.

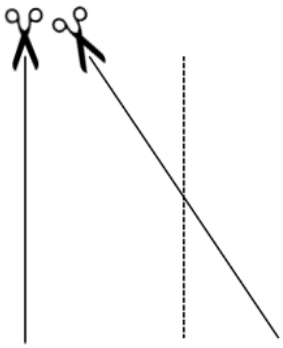

Figure 12: Difference between a symmetrical cut and an asymmetrical cut, on the left the result of a cut performed by counter rotating knifes. The right side shows the outcome of a single rotating and a fixated knife.

2.4 Final concept

2.4.1 Counter- vs. single-rotation

The biopsy tip design chosen in the previous section will be developed into a structure that is able to be constructed. The entire concept consists of an outer sleeve, protecting the ductal wall from the two cutting tubes. The cutting tubes contain a biopsy tip at the end, the design of this structure, also referred to as the knife design, will be further elaborated in the upcoming sections.

This paragraph will further address the debulking process and the reason to use two rotating knifes. The difference between a single rotating knife and counter rotating knifes is the ability to perform a double sided cut, resulting in a smaller force loop, reducing the possibility of harming surrounding tissue. If the counter rotating knife is compared to a configuration using one beveled rotating knife and a fixated beveled knife. The counter rotating knife will create a symmetrical cut while the single rotating knife will result in an asymmetrical cut. The asymmetrical cut will not follow the axial axis, but a diagonal line describing the knifes shape. This diagonal cut is longer compared to the symmetrical, straight cut created when using two counter rotating knifes. (Fig. 12).

Due to the longer length of the asymmetrical cutting line, more damage is done to the surroundings and therefore it could be considered as the lesser of the two. However, the involved force directions are of greater importance, when a symmetrical cut is preformed the forces are orthogonal to the axial axis, exactly the desired direction to shear off the tissue. When an asymmetrical cut is considered the force directions are orthogonal to the shape of the cut out, which could lead to an undesired shearing movement. Due to the small sizes involved the differences between the two could be minimal and therefor experiments are needed to determine if this is the case.

2.4.2 Knife design

For the development of the biopsy tip the knife design is of great importance. The shafts cutting tips should minimize the tissue deformation and the force needed to debulk the tissue, to protect the surrounding tissue.

Due to the small size in combination with the debulking of soft tissue, and the shearing movement of the knifes, available knife design information was fairly limited. Therefore multiple knife designs will be created. Where after the different knife geometries will be manufactured to test which design is best suited to debulk the tissue.

However in advance of the experiment several criteria are developed to compare the different knife designs. When tissue is debulked, in theory the contact area needs to be as small as possible to cut. Therefore the first criteria concerns the area which is used to debulk the tissue, referred to as the debulking surface.

The second criteria is based on the debulking force direction. An important factor in the ability to cut the tissue, when the direction is directed into the instruments shaft the tissue will be pushed in. Consequently if the debulking force is directed outwards it will push the tissue out of the cutting tube, resulting in a reduced ability to debulk the tissue. However knife designs exerting an outwards push have an advantage when looked upon the frontal surface and should therefore be tested.

Structures integrity is another factor taken into account when choosing a knife designs. Some of the potential knifes reduce the structures ability to withstand load, while others keep the structures integrity intact.

Due to the small tube diameter, the cut out area is fairly small. Therefore the ability to fabricate the different knifes is of importance in choosing a design. Therefore the last criteria is based on the knife's manufacturability.

After creating the criteria, designing the knifes could start. Comparing the different knife geometries, is the aim of this study. To improve the ability to test these geometries, the knife designs were separated in different categories to to determine the pro's and con's of each design. The most basic category describes a knife design, which exists of a 90 degree angle, further referred to as the Straight knife (red). The next category describes a beveled knife (blue), the Reversed beveled knife is the third category shown in green, in Figure 13.

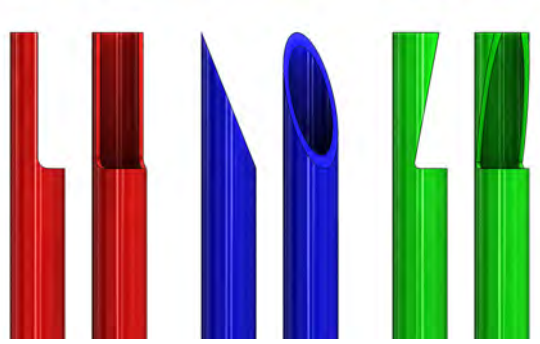

Figure 13: The different knife design categories; Red: Straight knife, Blue: Beveled knife, Green: Reverse beveled knife.

All of these categories have a downside as well as an upside therefore it is hard to determine in advance, which shape is preferred. To determine the exact differences between the shapes an experiment is needed. However the pro's and con's will be examined in advance. The drawback of using a Straight knife is the large surface area debulking the tissue, which in theory will be infinitely longer than a cut out under an angle. However the manufacturability to create a Straight knife is high and the debulking force direction is favorable over the bevelled angle category.

The debulking force direction of the Beveled knife is pointing away from the cutting tube thereby pushing the tissue, in an undesired direction, away from the instruments shaft. The advantage on the other hand is the frontal surface area, which is much smaller resulted in a lower penetration force when a completely filled duct is found.

The disadvantage of the Reversed beveled knife is the increased insertion surface, due to the larger frontal area. This design also reduces the structural integrity, caused by the sharp angle between the shafts center and the debulking line. The advantage of using this type of knife is the direction of the debulking force, which is pointed down, causing the tissue to be forced into the instruments shaft.

Although in theory these designs could all be made the structures integrity would suffer, with in the worst case scenario a structural failure as a result. Failures at a stress point does often occur when a squared corner or a bolt hole is placed too close to the material's edge, causing slowly forming cracks to form, which progress through cyclic loading. Failure generally occurs when the cracks reach a critical length, causing breakage to happen suddenly under normal loading conditions [31]. Hence, in the theoretical knife categories squared or sudden corners should be reduced to a minimum by using a radius instead of a corner. The designs shown in Figure 13 take this factor in consideration.

3 Handle design

3.1 Requirements

The actuation mechanism should allow the user to take the biopsy with the biopsy tip. Both of these structures needed to take the fiber optical camera into consideration and therefore should contain a hollow space in the center.

After deciding to experiment on the knife designs shown in Figure 13. The process of taking a biopsy needed to be determined. To allow the surgeon to take a sample of the suspected lesion the two knives and the sleeve needed to be moved in a specified order. To determine the best suited sequence, operating the biopsy tip, all possibilities need to be considered, described by:

1. The sleeve is moved down where after the outer knife starts to rotate, the inner knife is fixated.
2. The sleeve is moved down followed by the rotation of the inner knife, the outer knife is fixated.
3. The sleeve is moved down where after the outer knife starts to rotate clockwise and the inner knife is rotated counterclockwise.
4. The sleeve is fixated, both the knifes are moved up followed by the rotation of the outer knife, the inner knife doesn't rotate.
5. The sleeve is fixated, both the knifes are moved up followed by the rotation of the inner knife, the outer knife doesn't rotate.
6. The sleeve is fixated, both the knifes are moved up followed by the counter rotation of the knifes.

Applications using a fixed sleeve and two axially movable knifes were excluded due to the much harder application (4,5 and 6). Because no articles were found on debulking tissue using a tangential movement on this scale, it was decided to experiment on the remaining configurations and to create an actuation method, allowing the user to test the different possibilities.

Therefore the actuation mechanism should be adaptable, to create the counter rotating knifes as well as a single rotating knife. The instrument should be able to rotate the knifes in a counter clockwise direction, while they are rotating with the same velocity. The identical velocity ensures for comparable results during the experiments. To obtain even better experimental results the user should be able to exert the exact same rotating velocity, of which the magnitude could be varied during the tests to compare the tissue deformations.

The mechanisms should also be able to fix one of the knifes, while the the other is rotated, to see whether the tissue is debulked differently when a single rotating knife configuration is used. However the outer sleeve should also be able to move over the axial axis to protect the knifes, allowing the user to move the sleeve in the desired position.

Further requirements are caused by the usability of the actuation mechanism. The mechanism should allow the user to position the knifes into any desired position using one hand. The mechanism should also allow the user the incorporate the ductoscope.

3.2 Concept selection

Allowing the user to counter rotate the two cutting tubes with the same velocity was the most difficult part in developing the actuation mechanism, therefor this was the main

focus during the concept phase. In order to create solutions the task was described in a fundamental fashion by: two axially and radially fixated disks, which are tangentially movable and are able to counter rotate, with the same velocity, when actuated.

Gearwheel concept

An existing solution is a gear wheel solution. The drawback of this concept is the ability to fit the gears inside the instrument, while being small enough to be used by one hand. While taking the adaptation of the ductoscope in consideration. The dimensions of the gear wheels will be small, resulting in a weak instrument, in which alignment problems are unavoidable. Using a gear wheel construction will also create problems in switching from a counter rotating movement to one rotating cutting tube.

Disk concept

Another concept uses two discs that are hold by a construction as is shown in Figure 14. This concept enables the user to turn the disks by hand. The disadvantages of this concept are the alignment, due to the small sizes of the tubes, and the inability to perform an exact counter rotating movement.

Intricate gearwheel concept

Intricate gearwheels such as found in Figure 15 form another possibility. However, the manufacturability of these intricate gear wheels is a large hurdle, because they should be fabricated using a 5-axis CNC-machine, using a geometrically advanced operating program. Transforming the counter rotating movement of the described solution to a rotating cutting tube will be a difficult adaptation as well.

Camera lens concept

Camera lens designs were also considered, although they combine an axial and tangential movement, the working principle of the helix pattern could be used in the actuation mechanism. Camera lenses are designed to have little friction and allow the user to precisely maneuver the lens in position.

Helix concept

Because the camera lens/helix pattern only needed a little adjustment, were all other concepts had an obvious drawback, implementation possibilities of the camera lens/helix design will be considered.

To use the helix pattern in the biopsy tool some changes needed to be made. The first thing to adjust was the ability to rotate only one object. The biopsy instrument should be able to counter rotate two objects, therefore a second helix path was needed. To create the counter rotating movement the helix paths rotate in opposite direction.

Another adjustment needed to be made was found in the direction of movement. In a camera the disks translate as well as rotate over the axial axis, while the housing is fixated. For the biopsy instrument to work, the disks can only rotate over the axial axis, while the outer body is only allowed to move over the axial axis.

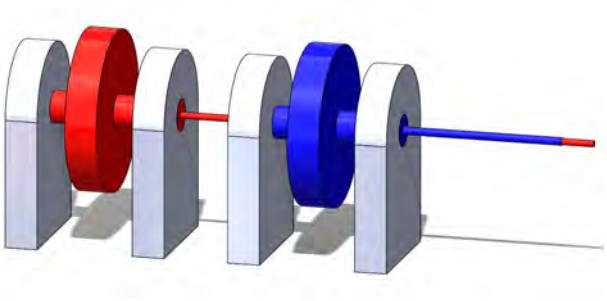

Figure 14: Disc concept: Two disks are used to rotate the Outer knife (Blue) and the Inner knife (Red).

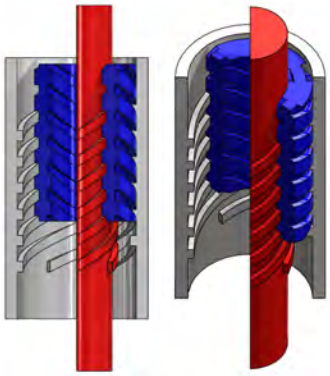

Figure 15: Cut through of an intricate gear wheel, the Outer knife (Blue) and the Inner knife (Red). Adapted from [32].

3.3 Final concept optimization

3.3.1 Design possibilities

Implementing the said adjustments into a working actuation mechanisms could be done in several ways. Therefore multiple concepts were created, two of these concepts will be explained.

Helix number 1

The concept shown in Figure 16, uses two tubes (*B* and *D*) that contain a helix pattern. The inner tube (*B*) fits inside the outer tube (*D*) and both of the tubes have the disk mounted at the top. The helix tubes (*B* and *D*) are axially fixated by the outer sleeve (*A*), while able to rotate about the axial axis. A push mechanism (*D*), existing of 4 bars and two rings is used to rotate the helix tubes (*B* and *D*). The two rings are positioned between the three tubes (*A*, *B* and *D*), where the four bars are fitted in both helix slots. The push mechanism (*D*) is allowed to translate over the axial axis thereby rotating both helix tubes (*B* and *D*).

Helix number 2

The second concept, shown in Figure 17, combines the two helix tubes, used in the previous concept, into one helix tube (*C*). This tube contains two helix patterns, one helix rotates counter clockwise and the other clockwise, allowing for the desired counter rotating movement of the rotating mechanisms (*B* and *D*). The helix tube (*C*), is hold in its place by the positioning slots (*A*), creating the ability to only translate over the axial axis. The rotation mechanisms (*B* and *D*) can only rotate over the axial axis, caused by the positioning

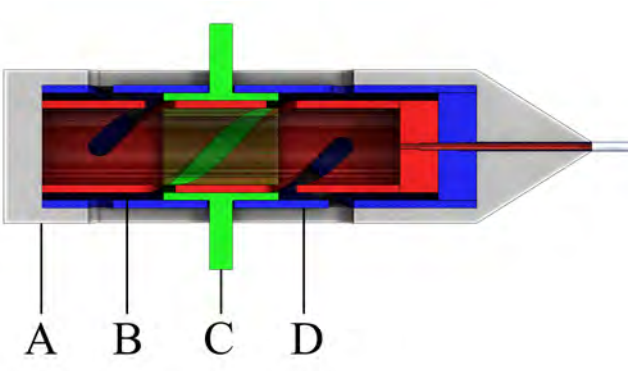

Figure 16: Cut through of Helix concept 1. A: The Outer sleeve, B: Helix tube inner knife, C: Push mechanism and D: Helix tube outer knife.

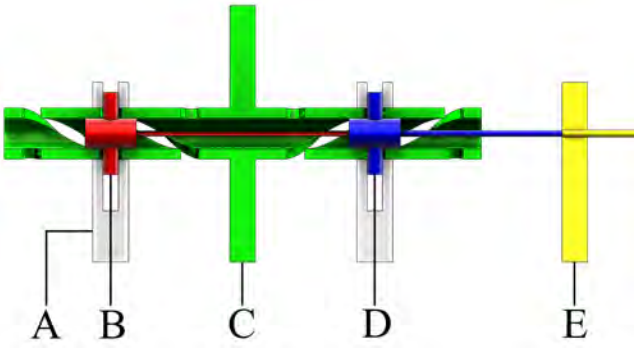

Figure 17: Cut through of Helix concept 2. A: The positioning slots, B: Rotation mechanism inner knife, C: Helix tube D: Rotation mechanism outer knife E: Outer sleeve and holder.

slots (A) and the helix patterns. The outer sleeve (E) is used to position the sleeve over the inner and outer cutting tube for protection and exact positioning.

3.3.2 Comparison

When the previously explained actuation concepts, pro's and con's are examined, the most important factors to consider are the friction forces and the manufacturability. When the friction forces in concept one (see Fig.16) are considered the tubes diameter and thickness are most important. Because the moment arm effects friction, the smaller the diameter the less the friction will influence the forces. However, there are limitations to the diameter of the tubes, caused by the cutting tubes as well as the limited abilities to fabricate the helix tubes in small dimensions.

The largest impact of the friction forces found in concept two (see Fig.17), will be at the point where the rotation mechanisms are axially fixated, however this can be done in various ways, giving the ability to choose the best possibility.

The use of bearings is important when the manufacturability is considered, were the first concept needs several bearings, the second concept doesn't need any, if designed correctly. The advantages of concept two over concept one are clear, therefore the second concept is developed further. During the design process friction and manufacturability will be kept in mind.

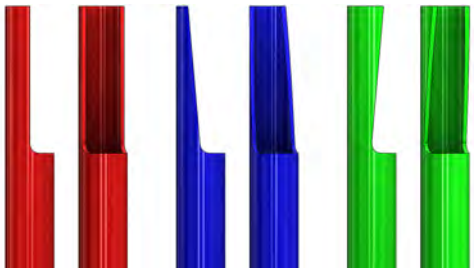

Figure 18: The final tips. Red: The Straight knife. Blue: The Beveled knife. Green: The Reversed beveled knife.

4 Prototype

4.1 Combining both designs

4.1.1 Tip

The objective for developing a functional prototype was to examine the functionality of the instruments design, rephrased as the ability to take a biopsy using the tip design actuated by the handle design.

The knife designs described in section 2.4.2, were improved before an actual prototype could be manufactured. Figure 18 shows the tip designs, made out of capillary stainless steel tubes $\varnothing 1.2x0.1$ *mm* in the case of the outer tube and $\varnothing 1.0x0.1$ *mm* for the inner tube. Using a 0.2 *mm* radius in all the angles, and a cut out length of 3 *mm* reduces the possibility of deformation during the debulking process. Comparing the knife designs was important, therefore the angle of the Beveled knife and the Reverse beveled knife was set to 5° in both cases.

Now the cut out dimensions are known the penetration forces can be determined using the tissues Young's modulus. In section 2.1, IDC is described as the strongest tissue with a Young's modulus of almost 150 *kPa*. The surface area of the Straight beveled knife is $3 \cdot 0.1 = 0.3\,mm^2$. When these two values are used, a rough estimation of the penetration forces ($F_{penetration}$) is found using:

$$\begin{aligned} F_{penetration} &= E \cdot A \\ &= 4.5 \cdot 10^{-2}\ [N] \end{aligned}$$

This force is an estimation, which doesn't include the nonlinear effects of gelatin, the sharpened edges and the different cut out designs. However, when these characteristics are accounted for the force will be in the same range.

To determine if the $1.2x0.1$ *mm* tube, containing a Straight knife design with a cut out length of 3 *mm*, is strong enough to withstand the penetration forces, a rough estimation of the maximal stress (σ_{max}) exerted on the tube is made using the following formula:

$$\begin{aligned} \mathrm{I} &= (D^4 - d^4)/145.7 - D^2 \cdot d^2 (D-d)/(56.5(D+d)) \\ &= 1.40 \cdot 10^{-14}\ [m^4] \end{aligned}$$

$$\begin{aligned} \sigma_{max} &= M \cdot y/\mathrm{I} \\ &= 2.89 \cdot 10^{6}\ [Pa] \end{aligned}$$

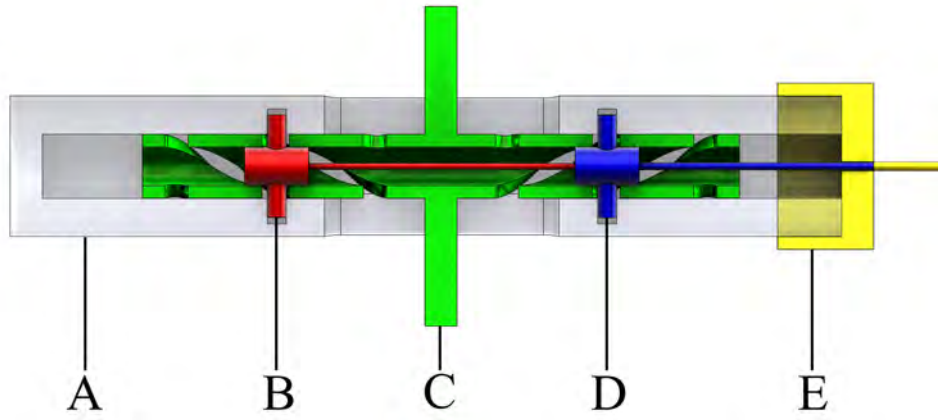

Figure 19: Cut through of the final conceptual design. A: The outer shell, B: Rotation mechanism inner knife, C: Helix tube D: Rotation mechanism outer knife E: Outer sleeve.

Where I is the moment inertia of half a circle [33], with $D = 1.2\ mm$ the tubes diameter and $d = 0.1\ mm$ the tubes thickness. The length orthogonal to the force exertion point is $y = D/2 = 0.6\ mm$, and $M = F_{penetration} * r = 4.5 \cdot 10^{-2} * 1.5 \cdot 10^{-3} = 6.75 \cdot 10^{-5}\ Nm$ the moment obtained by the force needed to cut the tissue, were r is half the cut out length, due to the assumed constant force distribution.

The capillary tubes made out of stainless steel (AISI 304) have a minimal compressive strength of 205 MPa [34]. Comparing this value to the maximal stress on the cut out (2.89 MPa), exerted to cut the tissue gives a large difference, therefore it can be concluded that the cut out is strong enough.

4.1.2 Handle

After developing the biopsy tip and the actuation mechanism, the two needed to be combined into one working instrument. The instrument could be described with five main parts, as is illustrated in Figure 19: (A) The outer shell, (B) Rotation mechanism in, (C) The helix tube (D) Rotation mechanism out and (E) The outer sleeve.

The function of the outer shell (A) is to precisely position the helix tube (C) and the rotating mechanisms (B and D), thereby allowing only rotation over the axial axis for the rotation mechanisms (B and D), and locking the helix tube (C) in its position. Another function of the outer shell (A) is created by the slot, this slot allows the helix tube (C) to be translated a precise distance over the axial axis. The function of the helix tube (C) is to counter rotate the inner rotating mechanism (B) and the outer rotating mechanism (D), when translated. Both rotation mechanisms (B and D) keep the helix tube (C) concentric in the outer shell (A) and allow cutting tubes to rotate. The outer sleeve (E) is connected to the outer shell (A), while the outer sleeve (E) is still able to axially translate a short distance. Its function is the protection of both cutting tubes during insertion, where after the outer sleeve (E) is withdrawn to allow the cutting tubes to debulk the lesion.

The actuation mechanism movement is shown in Figure 22, the biopsy tip is operated by the movement of the

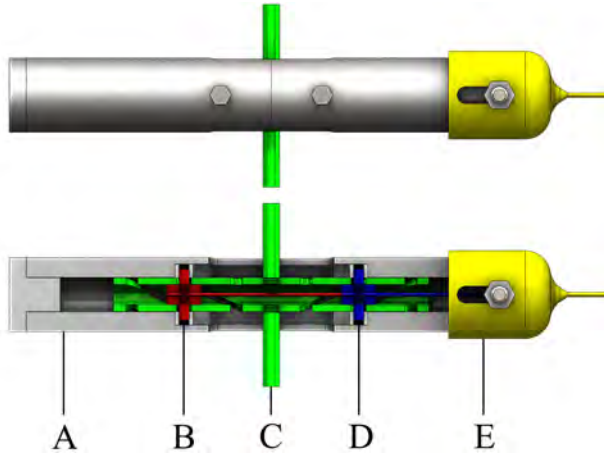

Figure 20: Prototype, top figure shows the intact instrument. the lower figure shows a cut through, with: A: Outer shell B: Rotation mechanism inner knife, C: Helix tube, D: Rotation mechanism outer knife, E: Outer sleeve.

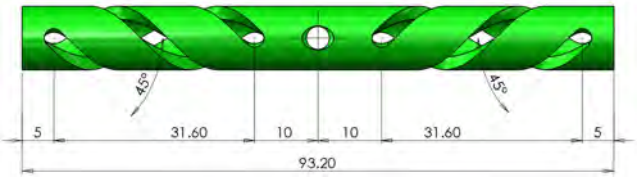

Figure 21: Helix tube dimensions.

helix tube, the 45° steps show the exact working of the handle in combination with the biopsy tip as was described in section 4.1.1.

The process from the conceptual design to a prototype mainly consisted of the dimensioning of the parts. Furthermore, a method to assemble the instrument needed to be developed. All parts have been designed using Solidworks 2015 (SolidWorks Corp.,Dassault Systemes, France). The resulting prototype is shown in Figure 20, an exploded view of the finalized prototype design is presented in Figure 23

The final design exists of the Helix tube (C_1) constructed out of a $10.0x2.0\ mm$ tube, with a length of $93.2\ mm$ containing two helix slots rotating in opposite direction (see Fig. 21). The critical factors for the helix dimensions are

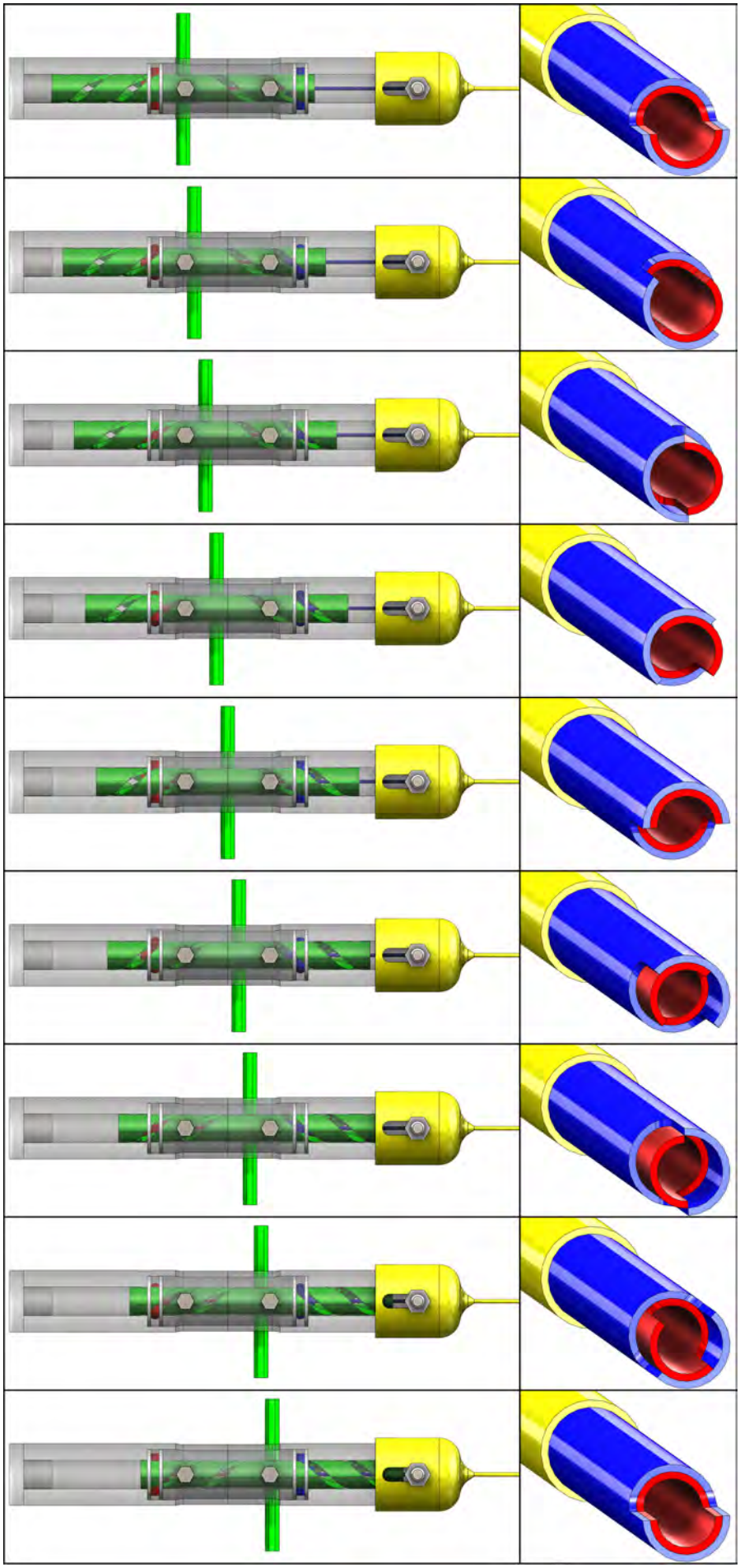

Figure 22: Prototypes working principle. The left figure shows the handle movement from 0° till 360° with 45° steps. The right figures show the according biopsy tip movement.

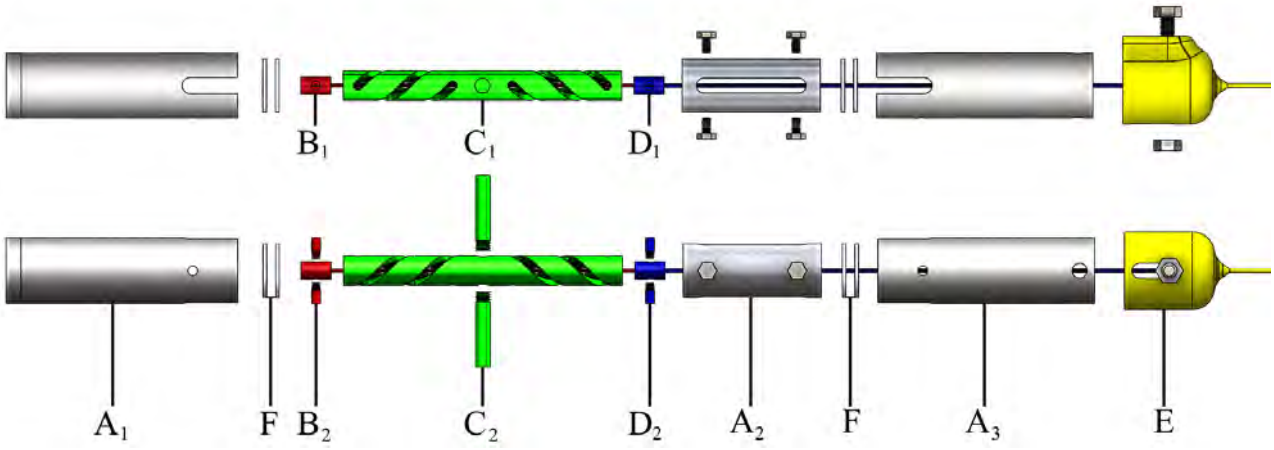

Figure 23: Exploded view of the prototype: A_1: Outer shell bottom, A_2: Outer shell middle, A_3: Outer shell top, B_1: Inner bearing, B_2: Inner Bearing rotating pins, C_1: Helix tube, C_2: Helix locating bars, D_1: Outer bearing, D_2: Outer bearing rotating pins, E: Outer sleeve and F: Rings.

the helix slot's angle and slot thickness. The 45.0° slot angle allows the user to translate the helix in both directions without creating a larger friction force in one of the directions.

The slot thickness was mostly influenced by the manufacturability of the Helix tube. A 3.0 *mm* slot was considered the best choice. The outer diameter of 10.0 *mm*, created a ridged tube, able to withstand the forces.

To allow the user to maneuver the helix, two ∅5.0 *mm* "Helix locating bars" where positioned in the middle of the tube, 10.0 *mm* from the center of both helix slot ends. The center of the slots starting points are positioned 5.0 *mm* from the outer edges.

The ∅3.0 *mm* helix slots have a length of $10.0 * \pi = 31.42$ *mm*, and are positioned 5.0 *mm* from the outer edges. The Helix tube (C_1) also contains two M5 screw holes, placed in the center of the Helix tube (C_1) opposite of each other. These two holes allow for the insertion of two Helix locating bars (C_2) with a length of 20.0 *mm*, M5 thread is placed at the end of both bars to allow fixation inside the Helix tube (C_1).

The Outer shell (A) needed to be constructed out of three peaces to assemble the instrument, it consists of: A Bottom tube (A_1), Middle tube (A_2) and Top tube (A_3). The Helix tube (C_1) is positioned inside the Middle tube (A_2), consisting of a ∅18.0*x*4.0 *mm* tube with a length of 46.2 *mm*, containing two ∅5.0 *mm* straight slots placed opposite of each other, only allowing the Helix tube (C_1) and the Helix locating bars (C_2) to translate about the axial axis, without rotation.

To connect the Middle tube (A_2) to the Bottom- and Top tube (A_1 and A_3), four M3 bolts are used. Two of the bolts are placed near the top and two near the bottom of the instrument. Both the Bottom- and Top tube (A_1 and A_3) are made of a 22.0*x*5.9 *mm* tube with a length of 72.4 *mm*. The tubes (A_1 and A_3) contain a 28.5 *mm* long, 2.7 *mm* indent, giving it the same outer diameter as the Middle tube (A_2) to ensure concentricity, and a slightly larger diameter than the Helix tube (C_1), allowing free movement of the Helix tube (C_1). The 28.5 *mm* indent length is chosen to fit the Middle tube (A_2), the Bearings (B_1 and D_1) and the Rings (F) perfectly.

Inside the Helix tube(C_1) the Inner- and Outer-bearings (B_1 and D_1) are positioned, which are ∅6.0 *mm* bars with a length of 10.0 *mm*. These two bearings (B_1 and D_1) act as plain bearings, allowing free translation of the Helix tube (C_1) along the axial axis, while being mounted exactly concentric to the Middle tube (A_2). The Inner bearing (B_1) contains a ∅1.0 *mm* hole to fit the Inner cutting tube, while the Outer bearing (D_1) contains a ∅1.2 *mm* hole fitting the Outer cutting tube. The Inner cutting tube ∅1.0*x*0.1 *mm* with a length of 228.2 *mm*, has been manufactured multiple times to implement the different tip designs. The same goes for the ∅1.2*x*0.1 *mm* Outer cannula with a length of 176.6 *mm*.

Bearing rotating pins (B_2 and D_2) are ∅3.0 *mm* bars used to connect the two bearings (B_1 and D_1) to the cutting tubes, using screw thread. While on the other end the Bearing rotating pins (B_2 and D_2) fit exactly, through the helix slot, between the Rings (F). The Rings (F) are fitted between the Middle tube (A_2) and both the Bottom- and Top tube (A_1 and A_3), thereby fixating the Inner- and Outer bearing (B_1 and D_1) as well as the cutting tubes and Bearing rotating pins (B_2 and D_2) axially, while allowing for the desired rotation.

The Outer sleeve (E), which acts as a protection for the cutting tubes tips, is attached to the top. The top can be moved to a desired position were a M5 bolt and Nut are used to lock it in position.

The used nut and bolts are of the shelf, the other prototype parts have been manufactured in various ways. Parts (A_1), (A_3), (C_1) and (E) have been manufactured at DEMO, TUDelft, while the rest of the parts are made using a turning- and a milling-machine. The Helix tube (C_1) is constructed by means of computer numerical control (CNC) milling and turning, parts (A_1), (A_3) and (E) have been 3D-printed.

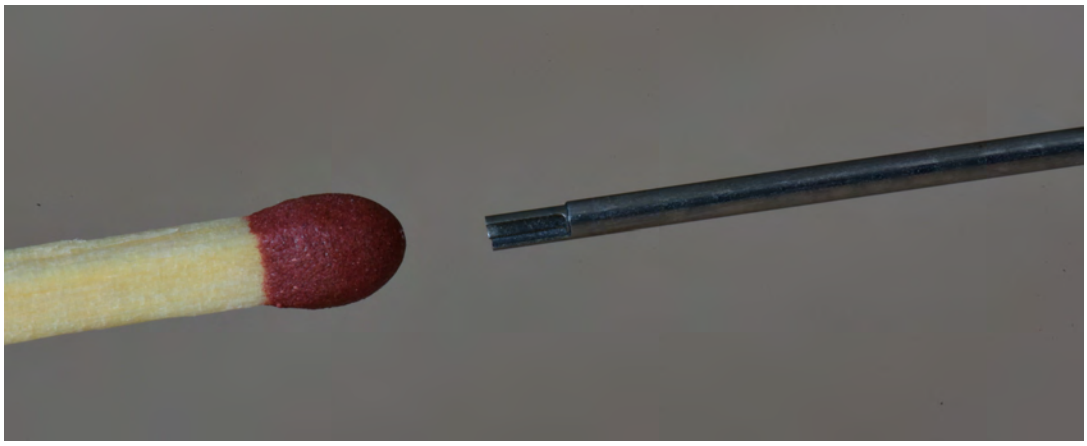

Figure 24: The Straight knifes compared to a Lucifer to create a perspective of the tip size.

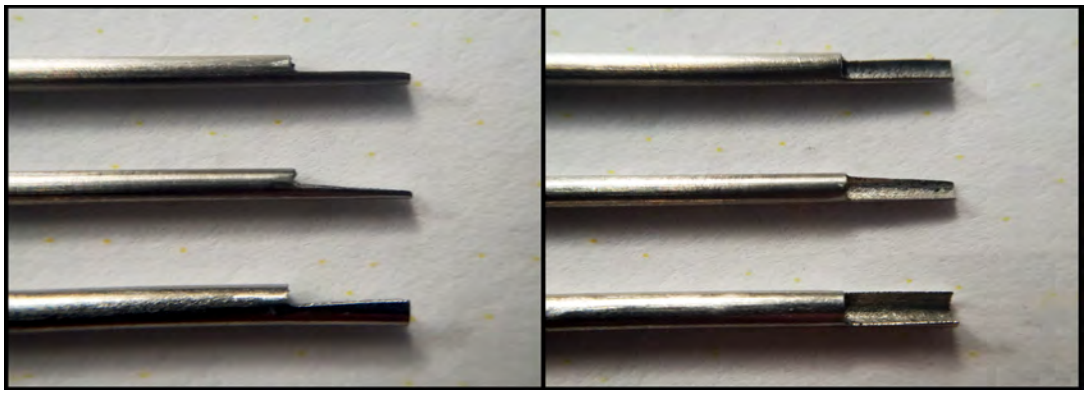

Figure 25: The finished Straight- Beveled- and Reversed beveled-knife. A side view and an isometric view.

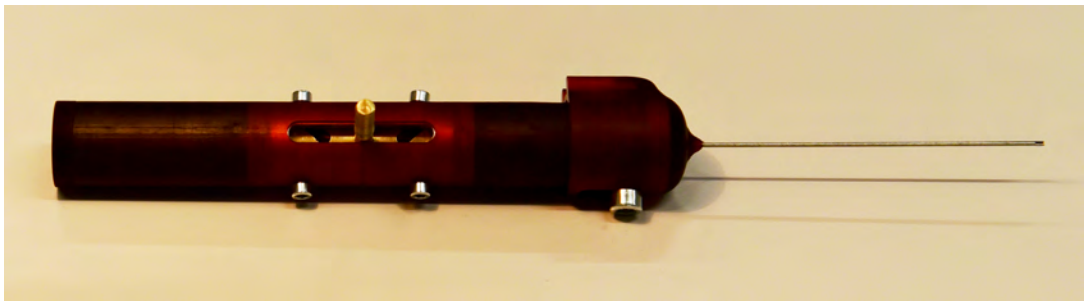

Figure 26: The finished prototype.

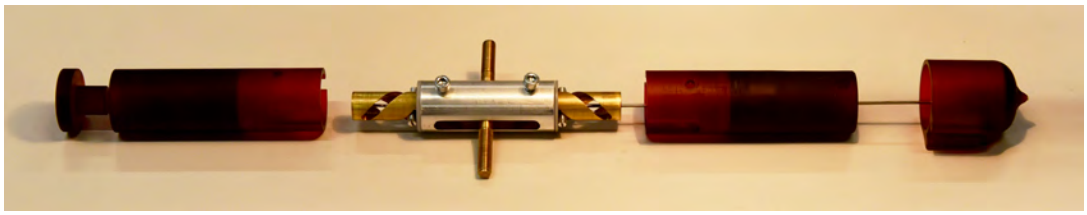

Figure 27: The finished prototype, after removing the 3D-printed parts, exposing the helix assembly.

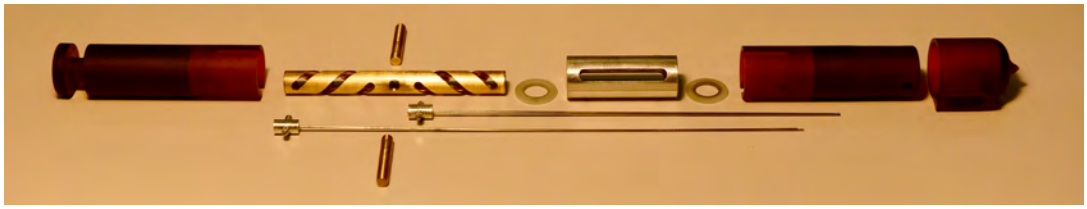

Figure 28: The finished prototype, showing all parts.

4.2 Material selection

Because of the translation and rotation of the components, friction can cause failure and increases the chances that the surgeon needs to exert a higher force to operate the instrument. To reduce the friction to a minimum, the material selection was based on friction properties of these materials. Some of the parts needed to be machined by hand, therefore aluminum was chosen as the material for component (A_2), (B_1), (B_2), (D_1), (D_2), (G) and (H), due to aluminum's workability.

Plane bearings

The surfaces of the sliding bearings, if properly lubricated, do not touch the adjacent surface. Then almost any material that meets the other constraints of the design will do. The key material properties are strength (to carry the bearing loads), lack of corrosion and resistance [35].

Materials

The selection of brass, for part (C_1) and (C_2), was made to allow easy sliding, caused by the low dynamic friction factor in combination with aluminum. Brass, allows for a low friction factor when oiled and is easy to machine. The rings (F) are in contact with both the aluminium and the brass, therefore a different material was chosen, which had a low friction in both cases, after conducting some research Nylon was the best choice, having a low friction coefficient in combination with aluminum as well as brass.

4.3 Images and assembly

The prototype is described following the 3D-drawings, however this section will show the actual prototype and how to assemble the instrument.

The finished manufactured prototype is shown in Figure 26. When the 3D-printed Outer shell parts (A_1, A_3 and E) are removed, the Middle outer shell (A_2) and the helix assembly are exposed (Fig. 27). After removing all the elements from the helix tube (C_1) all parts are exposed, see Figure 28. Some detailed pictures of the biopsy tips are shown in Figure 25, the pictures show the different knife designs.

To assemble the instrument a specific order needs to be followed. The first step is to position the Inner and Outer cutting shaft correctly, in other words the cutting edges of the shafts are positioned right next to each other, under the same angle. The second step is to place both the bearings (B_1 and D_1) over the shafts, where after the Helix tube (C_1), Middle outer shell (A_2) and two nylon rings (F) are positioned to fit the bearing ends, allowing for the desired rotational motion of the cutting shafts. Then the other two Nylon rings (F) are positioned together with the helix locating bars (C_2). The next step is to put the Bottom- (A_1) and Top-outer shell (A_3), and the Outer sleeve (E) in place.

5 Experiment design

5.1 Research questions

Several theoretical models describing the needle-tissue interaction, in terms of displacements and forces, are developed [36–39] These models have been validated with experimental data, contributing to the implementation in medical applications.

A great number of variables, influencing the mechanical needle-tissue interaction in biological tissue were unidentified, such as needle characteristics, tissue characteristics and insertion methods all influence the interaction.

However, if these relations hold, for the novel biopsy instrument is uncertain. Hence, one of the targets of this study is to collect experimental data that shows whether the tangential force has a similar influence on the tissue. Resulting in the ability to use needle insertion models.

The experiment focuses on the puncture of the breast mimicking phantom, which will be explained in section 5.3.4. The puncture process is performed using different needle tip designs, under predetermined conditions. A camera is used to observe the different biopsy process phases described in section 5.2.3.

The primary research question entails if the biopsy instrument works, when this is the case the research determines if the force and displacement metrics relate to the different needle tip geometries and configurations, under the set conditions.

The secondary question correlates to the controllability of the knifes, relating the influence of the knife velocity to the ability to perform a cut, using the preferred knife geometry, found after examining the first research question.

5.2 Variables

5.2.1 Independent variables

Determining the capability of the novel biopsy instrument is done by changing several independent variables: the biopsy tip velocity, knife design and knife rotation configurations, to proof if the needle-tissue interaction models hold for the novel biopsy instrument. While the independent variables influence the dependent variables the tissue stiffness is kept constant. The dependent variables are: resection time, displacement, tissue cut angle, operation force, biopsy process phases and sample volume.

The independent variables, otherwise referred to as design variables, influence the outcome of the experiment. To check whether these variables can be found, a pilot test will be performed to determine, if all independent variables can be changed and whether the dependent variables can be measured. The results of the pilot experiment are described in Appendix A.5.

Biopsy tip velocity

An important factor in using the biopsy instrument is found in the controllability of the cut. As was explained before the controllability is the ability to precisely position the

knifes where after the surgeon is able to cut at any desired velocity. Changing the knife rotation velocity enables the surgeon to minimize the damage to the surrounding tissue for the found clinical situation. Reducing tissue damage is done by determining the ideal knife velocity, by varying it, where after the data is analyzed. The chosen knife velocities are 15.76 *RPM*, 31.51 *RPM*, 55.15 *RPM* and 94.54 *RPM*. These velocities were based on the possible velocity variations of the linear stage, determined during the pilot experiment (Appendix A.5).

Knife design

The tip design is thought to influence the debulking forces and the ability to exert as little damage to the surrounding as possible. To determine which of the designs is best suited the three tip designs, addressed in section 4.1.1, will be tested. The three tip designs have a variation of 5° in the debulking angle.

Knife rotation configurations

Comparing the biopsy tips is not only done by changing the knife designs. Another variable examined is the difference between an instrument using the counter rotating knife configuration and an instrument operating one rotating knife. Changing the knife rotation configuration is done to examine the difference between the symmetrical and a-symmetrical cut, as was explained in section 2.2.2.

5.2.2 Constant variables

Tissue stiffness

After determining the influence of the debulking velocity, the knife design and the knife rotation configurations, the influence of another variable needs to be considered namely the stiffness of the tissue. Because the pilot experiment, see Appendix A.5.4, showed an inability to use low stiffness gelatin sheets, of 0.5 ± 0.1 *mm*, it was determined to use a 150 *kPa* gelatin, mimicking the stiffest and most common invasive breast cancer, IDC. More information on the tissue mimicking phantom is given in section 5.3.4.

5.2.3 Dependent variables

The dependent variables are the variables, influenced by the independent variables. Hence, these variables could not be changed without changing any of the independent variables.

Resection time

The resection time, defined as, the time needed for the biopsy tip to completely debulk the tissue, is measured during all tests. The resection time can also be explained as the time it takes from the moment of initial contact ($t = 0.00\ s$) until the moment the tissue is completely resected. Determining this time for all tests gives the opportunity to compare the different configurations.

Displacement

To evaluate the difference in knife design and knife rotation configuration, the displacement will be measured. The knife displacement is defined as the distance the inner and outer knife overlap, at the moment the tissue is completely debulked. This value can show a debulking advantage of one of the configurations.

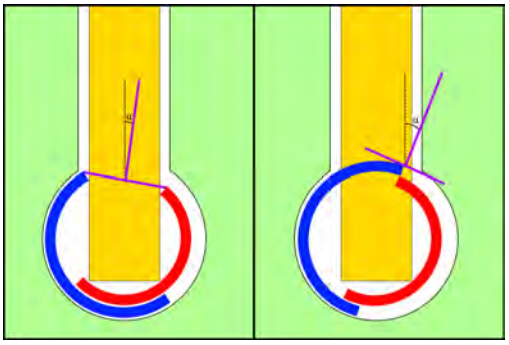

Figure 29: Tissue cut angle. Left: Initial angle at moment of contact (8°). Right: Angle at moment of tissue debulking (22°). Resulting in a Tissue cut angle of 14°.

Tissue cut angle

Another configuration comparison method is the tissue cut angle. The angle of the cut describes how the forces are acting on the gelatin and condition under which the lesion/gelatin is sheared of the ductal wall. The tissue angle is determined by placing a line between the top of the inner- and outer-knife at the moment of contact ($t = 0.00\ s$), where after a perpendicular line is drawn, the angle of this line is then measured. Followed by determining the angle at the moment the tissue is debulked, this angle is measured by placing a line at the intersection points of both knifes, followed by a line orthogonal to the intersection line (Fig. 29).

Where after both angles are subtracted to determine the tissue cut angle. The subtraction is needed to compare the different configurations, were in an ideal situation the angle between the knifes at the moment of contact would be zero, in reality this is most probably not the case.

Operation force

The operation force is measured during all tests to determine if there is a difference in the exerted force during the counter rotating knife movement and the single rotating knife movement. The operation force also shows if the user is able to actuate the handle by hand.

Needle-tissue interaction phases

The biopsy process is fairly similar to that of a needle, which is inserted into soft-tissue, described in [39]. The relative motion of the needle to the surrounding tissue is considered, rather than the absolute motion of the needle. When the position of the needle or the biopsy instruments knife relative to the tissue boundary is considered, three basic phases of interaction could be described (Fig. 30). Repetition of these phases may occur when the biopsy instrument encounters internal structures or variations in tissue properties.

The purpose of determining these phases is to find if the ideal velocity, knife design and tissue stiffness influence these moments in time, thereby being able to find results without the unusable force measurements, see Appendix A.5.3.

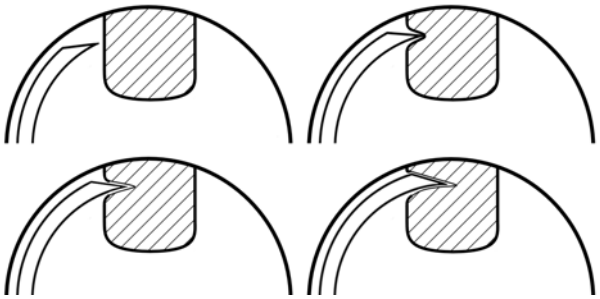

Figure 30: Needle-tissue interaction phases. Phase 0: No interaction. Phase 1: Boundary displacement. Phase 2: Knife insertion. Phase 3: Shaft insertion.

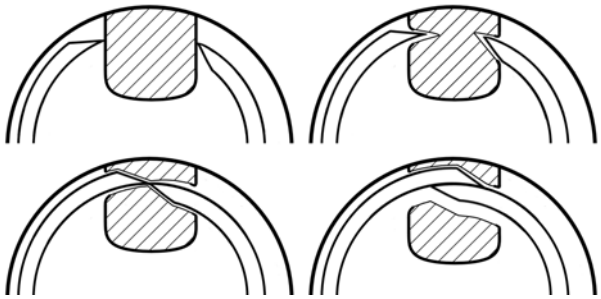

Figure 31: The Biopsy process points. Point 1: Initial contact. Point 2: Outer knife penetration. Point 3: knife intersection. Point 4: Complete debulking.

Phase 0: No Interaction

This phase describes the period before the needle or biopsy instrument interacts with the tissue boundary, until the tip touches the tissue. During this phase the boundary is not influenced by the instruments movement.

Phase 1: Boundary displacement

The first phase (Fig.30b) is initiated when the tip comes into contact with the tissue boundary, and ends at the moment the tissue boundary is breached. The boundary breach is also referred to as the puncture event.

During the boundary displacement phase, the load applied by the tip causes the tissue boundary to deflect, however the tip doesn't penetrate the tissue. The movement of the tip results in the displacement of the tissue boundary, the load at the tips edge will increase, as well as the stresses occurring in the tissue surrounding the contact area. When these stresses exceed a critical value, a crack will be initiated in the tissue and the needle tip or biopsy knife will start to penetrate the tissue [40].

Phase 2: Tip insertion

The second phase (Fig.30c) describes the period from the moment the tissue boundary is breached, by the knifes edge, until the tissue-boundary expands over the entire knifes edge and reaches the knifes shaft. During this phase, the knifes edge is advanced into the tissue, causing the crack in the tissue-boundary to expand.

The crack can grow either gradual, stable crack growth, called cutting, or sudden, unstable crack growth referred to as rupture, depending on the local properties of the tissue

Phase 3: Tip and shaft insertion

The third phase (Fig.30d) occurs after the transition from the edge to shaft. It ends when the knife is stopped or when a new (internal) tissue boundary is encountered.

During phase 3, the contact area between knife and tissue as well as the size of the hole in the tissue boundary remain more or less constant. Only the contact area between shaft and tissue increases as the knife is advanced further into the tissue. During this phase the needle is subject to cutting (or rupture) forces at the tip, and to a varying fluid friction force that is due to the increasing contact area between shaft and tissue.

Biopsy process points

During the biopsy process, changes in the phantom deformation rate (phantom velocity), are assumed to portray similar to the needle-tissue interaction phases. These events are thought to be interesting because they can show when the tissue has failed and when the biopsy is finished. For example when the rate of phantom deformation starts to differ from the tip rotation (constant velocity), tip insertion must have occurred and the phantom has failed. When the biopsy process phases can be determined the different tip configurations can be compared.

However, one of the needle-interaction phases is not applicable in this experiment, due to the small size of the tip. The sharpened edge of the knife, has an edge of no more than 0.05 *mm*. Therefore phase 2, the tip insertion phase will be impossible to detect, resulting in the combination of phase 2 and 3 into one phase.

During the pilot experiment (Appendix A.5) the remaining needle-tissue interaction phases are occurring, as will be seen in Figure 41 and 42, made during the actual tests. Despite this, additional phases should be added. A new phase occurs at the moment the knifes intersect, referred to as the intersection point. While the phase ends when the tissue is completely debulked. Combining both moments in time results in the actual debulking process referred to as the debulking phase. These two moments give an understanding of the penetration depth and the involved forces.

Although the knife insertion phase gives information about the sharpness of the knife, on which side the initial penetration occurs depends on the positioning of the gelatin inside the perspex duct. Exactly positioning the tissue phantom for every test will be very difficult and could result in a difficult comparison between the tests, and although the initial penetration phase is important the actual debulking phase is more interesting and easily visible.

During the pilot experiment (Appendix A.5) determining the phases was harder than expected, due to the magnification factor of the camera. This created an inability to determine the exact location of the gelatin boundary. Therefore instead of using the phases initially explained, moments in time will be described as the points of reference to analyse the biopsy process.

Figure 31 shows a schematic drawing of the biopsy process, the images show the decisive moments during this process. The points chosen are: The moment of initial contact

Figure 32: Positioning box (G), consisting of two T-profiles (G_1) and two blocks (G_2).

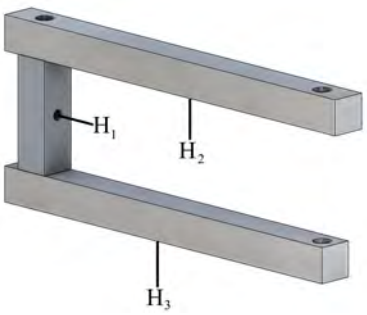

Figure 33: U-profile (H), Middle bar (H_1), Top bar (H_2) and Bottom bar (H_3).

of both knifes ($t = 0.00\,s$), the moment the outer knife is inserted, the point both knifes intersect and the moment of the complete debulking. All of these points in time can be estimated using the video images and enable the user to compare the biopsy tips.

Sample volume

When the instrument works, the main objective of the experiment is to determine if the biopsy needle is able to debulk a tissue sample usable in pathological examination. To establish if this is the case the volume of the taken tissue samples is measured.

5.3 Measurement facility

5.3.1 Exact Instrument positioning

After building the biopsy instruments prototype an experimental setup was designed. Its main purpose is to obtain repeatable results, caused by the fixation of the instrument and by a rigid U-profile triggering the instrument.

The fixation of the instrument is done using a positioning box (G), see Fig.32, consisting of two T-profiles (G_1) and two blocks (G_2). The T-profiles ((G_1) are $56x56\ mm$ with a length of 80 mm) contain four ($\varnothing 5.5\ $)$mm$ holes (positioned 7 and 46 mm from the top and 4 mm from the side of the T-profile), allowing four M4 bolts to connect the two T-profiles to the two metal blocks (G_2). The metal blocks (G_2) (are $56x56\ mm$ with a thickness of 8 mm), contain four M4 holes, (positioned 7 and 46 mm from the top at the center of the two sides). Both metal blocks contain a $\varnothing 22\ mm$ hole, located at the center of the block, (18 mm form the top). The block distal from the needle ($G_{2-distal}$) also contains a ($\varnothing 15\ mm$) hole, located at the center of the block, (34 mm form the top) to fit the U-Profile (H), see Fig. 33. This profile is made of ($10x10\ mm$) bars, where the Middle bar (with a length of 32 mm) contains a M3 hole in the middle of the bar, while on both ends a M5 hole is made in the center, to lock both the Top- and the Bottom bar (G_2 and G_3). (The Top bar has a length of 125 mm and has two $\varnothing 5\ mm$ holes in it, 10 mm from the ends. The Bottom bar is 120 mm long and contains two $\varnothing 5\ mm$ holes, one of which is located 5 mm and the other 10 mm from the end.)

Assembly

After assembling the instrument, it needs to be fitted inside the experimental setup, or Positioning box (G) as will be explained in the next chapter. To place the instrument it is fitted inside the holes of the positioning box (G), where after the Bottom- (A_1) and Top-outer shell (A_3) are bolted down onto the Middle outer shell (A_2) with four M3 bolts. Then the two fasteners are screwed down to stop any movement of the instrument. Then the U-profile is positioned where after the Helix locating bars (C_2) are connected to the profile using M5 nuts.

5.3.2 Instrumentation and measurement apparatus

The instrumentation and measurement apparatus are depicted in Figure 38. For the movement of the helix tube (Fig.22), a horizontally positioned linear motion stage is used. The linear motion stage is an Almotion LT50-TR-G8 with 200 mm travel (Almotion, Elst, The netherlands) driven by an integrated step-servo motor the SSM 24Q-3AG (Moons Industries, Shanghai, China). The step-servo motor is powered by a Delta Elektronica ES 030-5 power supply (Delta Elektronica,Zierikzee The Netherlands).

A load cell, Futek LSB200, 2 lb (Thomas, Irvine, USA), is mounted to the motion stage using an aluminium base. To keep the output of the load cell constant a CPJ Rail strain gage conditioner is used made by Scaime (Scaime, Juvigny, France). The load cell is subsequently connected to the helix tube using the U-profile (H).

For exact positioning of the helix tube movement a Feteris OptoNCDT, ILD 1300-50(00) Laser displacement sensor with a range of 50mm is used (Micro Epsilon, Birkenhead CH41, UK). The displacement sensor is also powered by the Elektronica power supply.

To initialize the step-servo motor, the load cell and the distance sensor, a Multifunction Data Acquisition system the NI USB-6008 is used (National Instruments, Austin, Texas, United States)

The high speed camera and long distance microscope are positioned 120 mm from the needle tip. The high-speed camera is a Fastcam APX RS capable of 3000 fps with a $1024x1024$-pixels resolution and a pixel size of 17 μm (Photron, San Diego, California, USA), which is connected to a long distance lens, the Questar QM1 with a magnification factor of 11/2 (Company seven, Montpelier, Maryland, USA).

The used frame rate of the camera, needed to be determined using the following formula:

$$\text{Frame rate} = \frac{\text{Velocity} \cdot \text{Magnification factor}}{\text{Pixel size}}$$

Data acquisition and position control of the linear stage are achieved using a dedicated Laptop (Intel(R) Core(TM) i7-4700MQ, 8GB RAM, MS Windows 10 Home) equipped with Labview to initialize the data acquisition (National instruments, Austin, Texas, United States), Q-programmer feeding the step-servo motor (Moons Industries, Shanghai, China), and Photron Fastcam Viewer to record the camera feed (Photron, San Diego, California, USA), Appendix D.

The camera images are analyzed using Photron Fastcam Analysis (Photron, San Diego, California, USA). Where after Data analysis is performed using Matlab R2014a software (The Mathworks Inc., Natick, USA).

5.3.3 Phantom puncture

During the biopsy process a tissue sample is taken, in Ductoscopy the desired tissue is growing on the ductal wall, therefore the instrument should be able to puncture this tissue, further referred to as the phantom. The process called "Phantom puncture" is defined as:

The process starting at initial contact between the knife's edge and the phantom, lasting until the point the phantom is fully penetrated and the knife is moved completely through the phantom.

The physical properties of phantom puncture need to be found to contemplate the tissue damage, patients discomfort, knife accuracy, knife geometry etc. To find these properties the tangential forces arising from the axial movement of the helix (Fig. 22), need to be determined, however these values are subjected to friction forces and when perfectly isolated only provide a limited amount of information. In addition to the force measurement a video feed is used allowing a clear vision on the tissue penetration process. This section will elaborate further on how the phantom penetration is measured.

In the case of the novel biopsy instrument, the phantom penetration is facilitated by the rotation of both, or one of the biopsy tips. Therefore it is assumed that tip geometry must play an important role in the penetration process. The difference in tip geometry could be measured using the tangential forces created by these tips, during tissue penetration. Although, due to internal friction forces inside the instrument the ability to measure these tangential forces is not certain. When the involved forces can be determined, the influence of the tip geometry, should show in the relation between the force and the tissue deformation depth.

5.3.4 Breast mimicking phantom

The stiffness of the breast ranges from 911-928 kg/m^3 and 1041-1060 kg/m^3 respectively for breast fat and the breast gland's. The Young's modules has been reported to range from 12-26 kPa for breast fat and from 22-76 kPa for glandular breast tissue.

Figure 35: Biopsy needle inside the perspex duct.

Figure 36: Mimicking the ductal lesion, using a perspex block with a key hole, to fit the gelatin sheet and to mimic the ductal tract.

Although these values are important, the most important factor is the elasticity stiffness value, or Young's modules, of the suspected lesions. The highest Young's modules is found for IDC with values ranging between 144.5 and 149.7 kPa, as was mentioned in Section 2.1. Hence, the phantom should allow the user to mimic a Young's modulus of 150 kPa.

The most widely used phantom material is gelatin, because it is safe to use, inexpensive easy to manufacture, behaves the same under impulse as natural tissue and a lot of research has been performed on, mixtures with comparable mechanical properties to breast tissue.

Ballistics gel, a testing medium comparable to human muscle, has been assessed as having an elastic modulus of 100-150 kPa when made from a 20 $wt\%$, 250 Bloom type A gelatin [41–43]. The gelatin bloom value is defined by the Gelatin Manufacturers Institute of America by measuring the weight, needed for a displacement of 4 mm using a 0.5 in diameter piston, into solid gelatin.

Creating a 100 $gram$ breast tissue mimicking phantom involves: Mixing 20 $gram$ of gelatin powder with 80 mL of water in a sanitized saucepan, able of holding all the phantom's volume. Where after the mixture solves for 10 minutes. Than it is heated while thoroughly stirred until all the gelatin is fully dissolved, resembling a uniform liquid. This mixture is allowed to cool to $40°C$ before pouring it into the final phantom mold.

Ductal lesion mimicking

The purpose of the experiment is to simulate conditions comparable to the real conditions. In this case a simulation was needed of the ductal tract, containing a lesion. The ductal tract was simulated using a perspex block, containing a $\varnothing 1.2$ mm hole. The lesions were mimicked using 0.5 mm thick sheets, placed inside a 0.7 mm wide groove in the perspex. The gelatin sheets are ± 2.9 mm wide to allow the 3.0 mm long cut outs to debulk along the entire gelatin sheet width. The groove thickness was deliberately

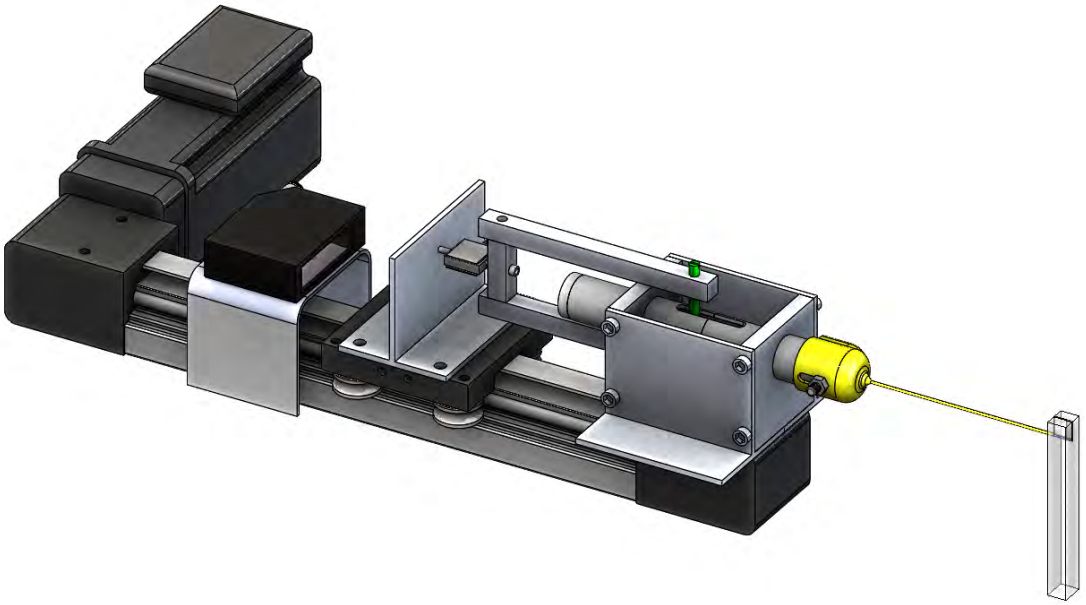

Figure 34: Experimental setup created in Solidworks.

chosen 0.2 *mm* wider, than the 0.5 ± 0.1 *mm* thick gelatin sheet. Allowing the gelatin to move inside the groove mimicking the real conditions. Instead of a fixated gelatin sheet which could only be found under ideal conditions.

5.4 Measurement protocol

Before the actual experiment, a pilot test was conducted, see section A.5. This test determined if all variables, described in section 5.2, could be analysed. The pilot test also determined the best suited knife velocity for the comparison of knife designs, as well as the knife velocity used during the experiment comparing the counter rotating knifes and single rotating knifes.

During the actual experiment the goal is to answer the primary research questions. To accomplish this goal a total of 18 penetration tests were performed on the breast mimicking phantom, described in section 5.2.3, to compare the knife designs and knife rotation configurations. Three experiments were conducted for each of the biopsy tip configurations.

After testing the needle tip geometries, the best suited knife geometry is chosen to be tested. Followed by a total of 12 experiments, three for each velocity, to determine the variation in debulking behavior using different knife velocities. Varying the knife velocity between 15.76 *RPM*, 31.51 *RPM*, 55.15 *RPM* and 94.54 *RPM*.

Biopsy tip comparison

The difference in knife design was tested using three different designs as explained in section 2.4.2. The five degrees variation in the cutting angle was the main difference between these designs. At first the three knife designs were tested three times, while both knifes were rotated in opposite direction.

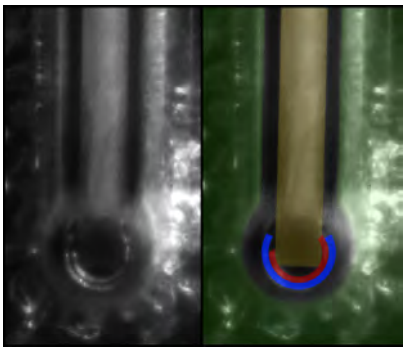

Figure 37: A video capture of the instrument in the perspect ductal tract containing the gelatin. Left: the actual image, Right: an enhanced version, Blue: the outer knife, Red: The inner knife, Yellow: The gelatin and Green: The perspex duct.

Where after the inner knife was fixated while the outer knife was still able to rotate. When the single rotating knife configurations were tested, the fixated knife was positioned as close to the gelatin as possible creating the ability to compare the counter rotating knifes and the single rotating knife.

During these tests a fixed velocity of 15.76 *RPM* was used to penetrate the phantoms, with a constant stiffness of 150 *kPa*. The next chapter will elaborate more on the fixed velocity of 15.76 *RPM* and the constant gelatin stiffness. After each test the phantom was replaced by a new one. The process was repeated three times for each configuration. Where after the configuration was changed repeatedly until all configurations were tested.

The adapted biopsy process phases as are explained in section 5.2.3 will be observed with the help of a high speed camera, boundary displacement, the outer knife tip insertion and the complete debulking phase, were estimated using the video footage. The biopsy phases were identified and evaluated.

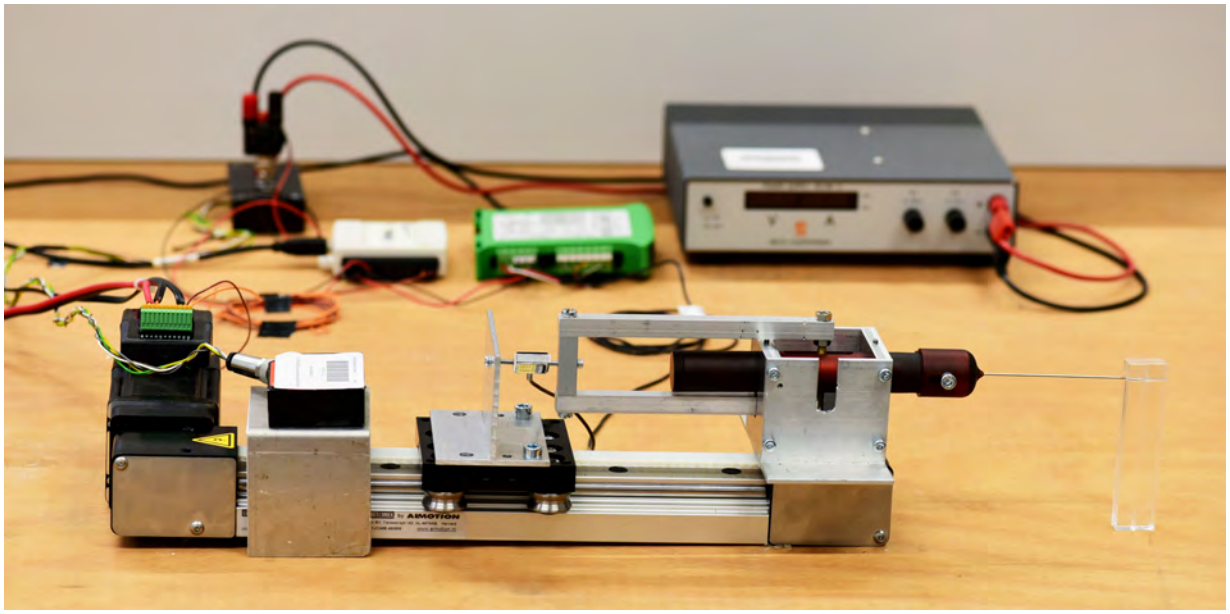

Figure 38: Experimental setup, containing the prototype and the ductal mimicking setup.

5.5 Data analysis

The experimental measurement facility, shown in Figure 38, yields time-series of the absolute axial force and position of the Helix tube (C) (Fig. 20). With the helix position, the tip position and rotational velocity can be determined, the axial forces, on the helix, allow the user to determine the operational force of the instrument. These parameters are then coupled to the corresponding high speed video recordings, showing the tissue deformation.

The video feed produced by the Fastcam APX RS is analysed to compare the different biopsy tip configurations. To analyse the video footage Photron Fastcam Analysis (Photron, San Diego, California, USA) is used. Where after Data analysis is performed using Matlab R2014a software (The Mathworks Inc., Natick, USA).The video footage is used to determine the displacement, tissue cut angle and resection time, to compare the biopsy tips and configurations, since the tangential force measurements were unable to provide sufficient data.

The maximal operation force, or the maximum force exerted onto the helix during operation, is measured, with the Futek load cell. The operation forces are determined for the counter rotating knifes, single rotating knifes and one rotating knife. The configuration using one rotating knife is used to determine the friction effects inside the instrument. This data combined with the helix position, the tip position and rotational velocity data is analysed using Matlab R2014a software (The Mathworks Inc., Natick, USA).

In the knife design comparison the linear motion stage, moving the helix, thereby inducing the rotational movement of the knifes, is moving at a velocity of 15.76 RPM. The used frame rate is 100 Hz. During the variation of the knife velocity the frame rate is adjusted accordingly, to a maximum of 500 Hz for the run with a rotational velocity of 94.54 RPM.

The initial camera feed shown in Figure 37, contains an image after focusing the camera on the tip of the instrument and positioning the perspex duct, containing the gelatin, mimicking the circumstances found during ductoscopy. In the figure the left image shows the obtained camera view, the right figure shows an enhancement of the initial image, performed by hand, improving the analysing quality. The shown enhancement will be used during all further video analysis.

In all videos the point of contact is chosen as the starting point, being a noticeable point to start the comparison of the video images.

6 Results

6.1 Operation force

After conducting the previously described experiment, this chapter will present the retrieved results. Followed by a discussion of the results in the next chapter.

The average maximal operation force during counter rotation configuration runs was 3.75 N with a minimum and maximum value of 3.37 N and 4.41 N respectively, the highest value found was 4.41 N. Experiments including a single rotating knife combined with a fixed knife gave an average maximum force of 1.76 N (1.56-1.95 N), the maximal exerted force was 1.95 N (see Fig. 39). Throughout the entire study the values are indicated as Mean (Min value - Max value), when the three tests are compared, in the case of a single value the measurement tolerance is often indicated (Value $\pm$ Measurement tolerance).

6.2 Knife design comparison

Examples of video images for the Straight knife, the Reverse beveled knife and the Beveled knife are shown in Figures 41 to 43 respectively.

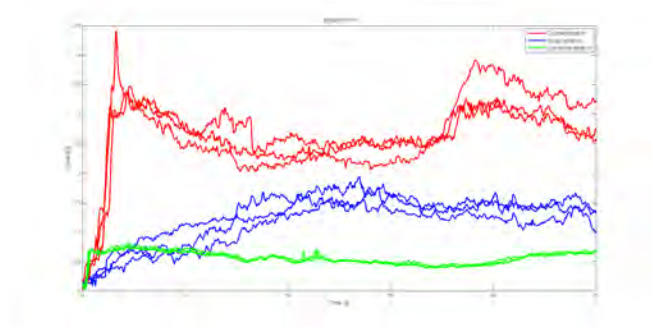

Figure 39: Operation force distribution of 9 runs. The average operation force for the counter rotating knifes is 3.75 N (3.37-4.41 N). For the combination of the Single rotating knife and the fixed knife an average value of 1.76 N (1.56-1.95 N) was found. When only one knife was inserted in the instrument the average operation force was 0.80 N (0.78-0.83 N). The values are indicated as Mean (Min value - Max value).

Figure 40: Failure to cut the gelatin when the Beveled knifes are used.

The remainder of this section entails the results found during the comparison of the knife designs, for both the counter rotating and single rotating knife configuration, where after the results varying the velocity will be analysed. The results are summarized in Table 3

6.2.1 Exclusion of the Beveled knifes

The counter rotating Beveled knife was unable to cut the entire gelatin, as is shown in Figure 40. The shortcoming to debulk along the entire cut out length was caused by the force exerted outwards, pushing the gelatin away from the instruments tip, seen in Figure 45. The left side of the figure shows the initial position of the gelatin, the image on the right shows the position after conducting the debulking process. The results shown in these figures combined with the findings of the video feed gives enough sufficient information to conclude that the Beveled design exerts a force pushing the gelatin away from the tip, thereby reducing the ability to cut along the entire length of the knife.

When the single rotating knife configuration of the Beveled knifes was used the results were even worse, lacking the ability to perform even the smallest cut. The single rotating knifes created an upwards push causing the gelatin to be moved upwards, without debulking the tissue (Fig.43).

Concluding the Beveled knife design showed inadequate results in both the counter rotating and the single rotating configuration therefore this knife design is excluded

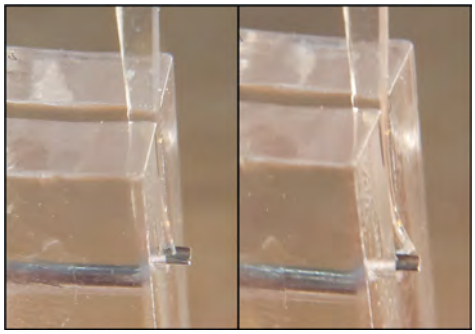

Figure 45: Left: Gelatin position before cut. Right: Gelatin is pushed away during the debulking process.

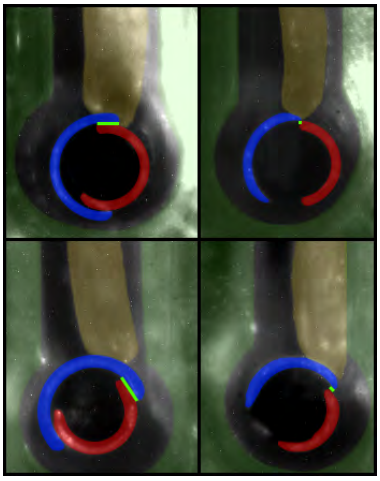

Figure 46: Examples of the knife displacement of both the inner- and outer knife. Up-Left: Counter rotating Reversed beveled knife (0.31 ± 0.01 mm). Up-Right: Counter rotating Straight knife (0.04 ± 0.01 mm). Down-Left: Single rotating Reversed beveled knife (0.35 ± 0.01 mm). Down-Right: Single rotating Straight knife (0.11 ± 0.01 mm).

in the remainder of this study. The comparison between the Straight knifes and the Reverse beveled knifes will be performed by analysing the differences in the displacement of the gelatin along the contour of the knife design, as well as a comparison between gelatin cut angles.

6.2.2 Resection time

The resection times for the Reverse beveled counter rotating knife and single rotating knife are 6.52 s (5.79-7.34 s) and 11.93 s (11.50-12.42 s) respectively. The Straight counter rotating knifes finished the debulking process in 4.29 s (3.88-4.56 s) while the single rotating Straight knifes completed the debulking process in 8.98 s (8.36-9.51 s).

6.2.3 Displacement

The knife displacement of the counter rotating Reverse beveled knifes was 0.31 mm (0.29-0.33 mm), shown in Figure 46. The counter rotating straight knifes gave a displacement of 0.04 mm (0.03-0.05 mm) in the analysed tests. When the Single rotating knifes are considered the Reserved beveled knife and the Straight knife give a displacement of 0.37 mm (0.35-0.39 mm) and 0.13 mm (0.11-0.15 mm) respectively.

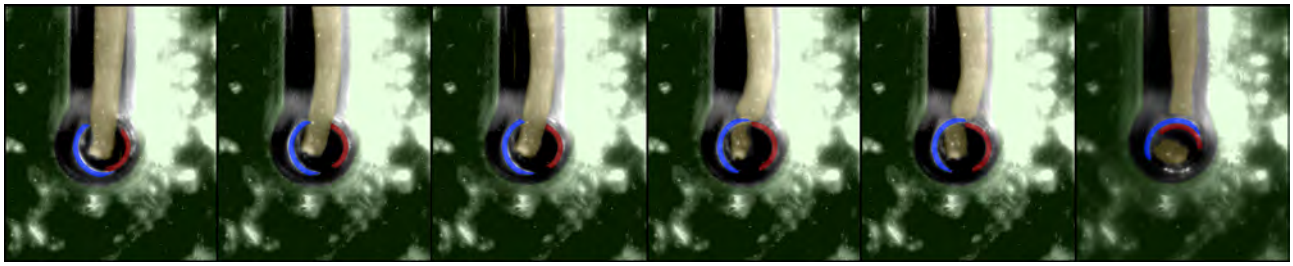

Figure 41: Example of a Straight knife video in snapshots. 1: Moment before impact (0.00 ± 0.01 *s*). 2: Moment before penetration (2.02 ± 0.01 *s*). 3: Moment of Penetration (2.14 ± 0.01 *s*). 4: Moment before debulking (4.44 ± 0.01 *s*). 5: Moment of debulking (4.56 ± 0.01 *s*) 6: Moment after the debulking process (9.22 ± 0.01 *s*).

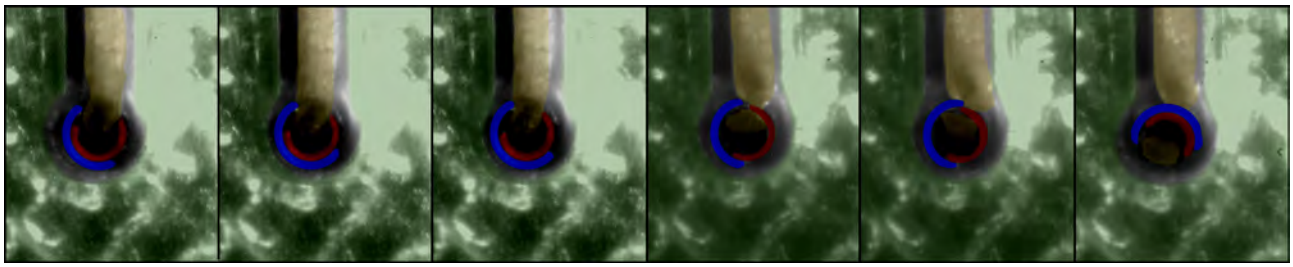

Figure 42: Example of an Reverse beveled knife video in snapshots. 1: Moment before impact (0.00 ± 0.01 *s*). 2: Moment before penetration (1.22 ± 0.01 *s*). 3: Moment of Penetration (1.38 ± 0.01 *s*). 4: Moment before debulking (7.20 ± 0.01 *s*). 5: Moment of debulking (7.34 ± 0.01 *s*) 6: Moment after the debulking process (15.78 ± 0.01 *s*).

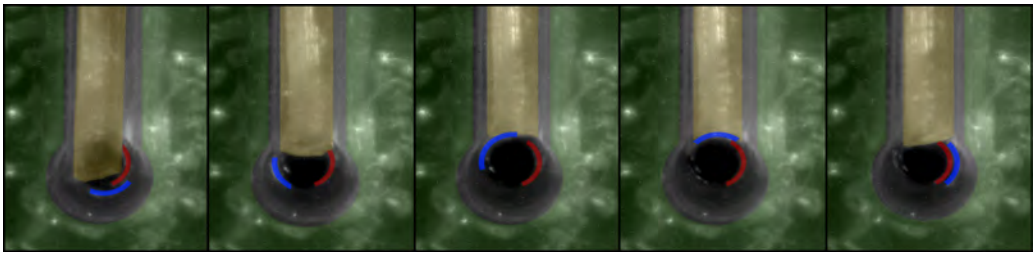

Figure 43: Example of a video snapshots of a Single rotating Beveled knife, pushing the gelatin upwards without making a cut. 1: Starting point (0.00 ± 0.01 *s*). 2: Pushing the gelatin upwards (10.00 ± 0.01 *s*). 3: Highest point for the gelatin (16.00 ± 0.01 *s*). 4: Rotating knife in horizontal position (18.00 ± 0.01 *s*). 5: Gelatin is moved down pushing against the fixated knife (33.00 ± 0.01 *s*).

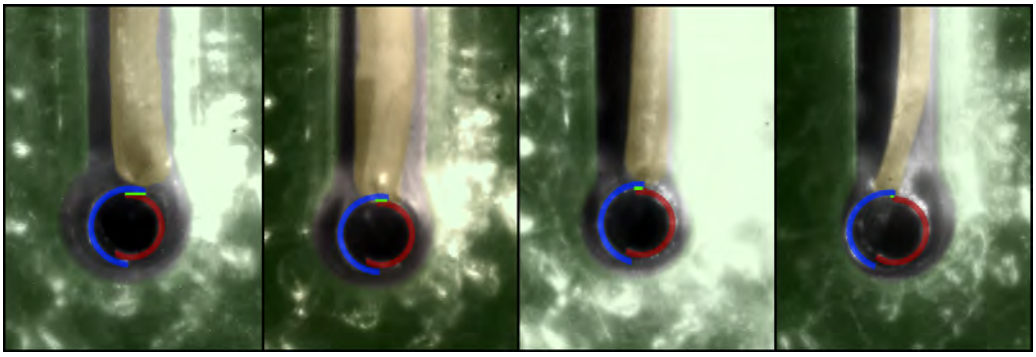

Figure 44: Examples of the displacement of the inner- and outer knife. 1. With a knife velocity of 15.76 ± 0.01 *RPM* a displacement is fount of 0.31 ± 0.01 *mm*. 2. A knife velocity of 31.51 ± 0.01 *RPM* gives a 0.19 ± 0.01 *mm* displacement. 3. A knife velocity of 55.15 ± 0.01 *RPM* results in a displacement of 0.12 ± 0.01 *mm*. 4. A rotational velocity of 94.54 ± 0.01 *RPM* gives a displacement of 0.05 ± 0.01 *mm*.

Table 3: Results of the knife design and rotational configuration comparison. The values are indicated as Mean (Min value - Max value). Not Applicable (NA).

		Resection time [s]	Displacement [mm]	Cut angle [°]
Counter rotating knife	Beveled	NA	NA	NA
	Reversed beveled	6.52 (5.79 - 7.34)	0.31 (0.29 - 0.33)	6.67 (6 - 8)
	Straight	4.29 (3.88 - 4.56)	0.04 (0.03 - 0.05)	18.33 (16 - 21)
Single rotating knife	Beveled	NA	NA	NA
	Reversed beveled	11.93 (11.50 - 12.42)	0.37 (0.35 - 0.39)	40 (38 - 41)
	Straight	8.98 (8.36 - 9.51)	0.13 (0.11 - 0.15)	36.67 (35 - 39)

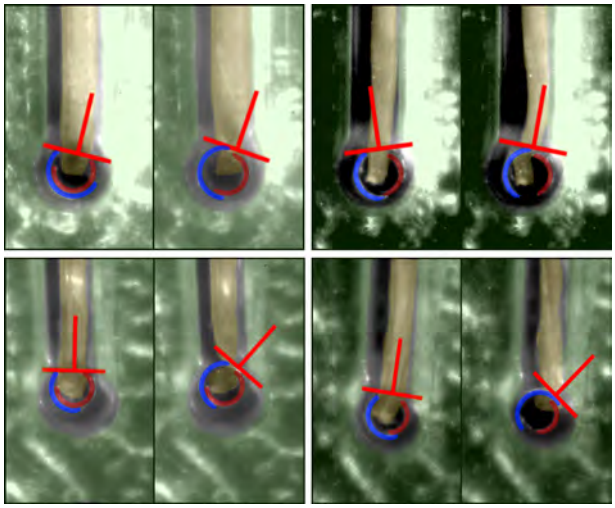

Figure 47: Examples of the tissue cut angles. 1: Counter rotating Reverse beveled knife at moment of impact (0.00 ± 0.01 s) and moment of debulking (7.34 ± 0.01 s), the difference is $6 \pm 0.5°$. 2: Counter rotating straight knife at moment of impact (0.00 ± 0.01 s) and moment of debulking (4.56 ± 0.01 s), the difference is $18 \pm 0.5°$.3: Single rotating Reverse beveled knife at moment of impact (0.00 ± 0.01 s) and moment of debulking (11.50 ± 0.01 s), the difference is $41 \pm 0.5°$. 4: Single rotating straight knife at moment of impact (0.00 ± 0.01 s) and moment of debulking (8.36 ± 0.01 s), the difference is $36 \pm 0.5°$.

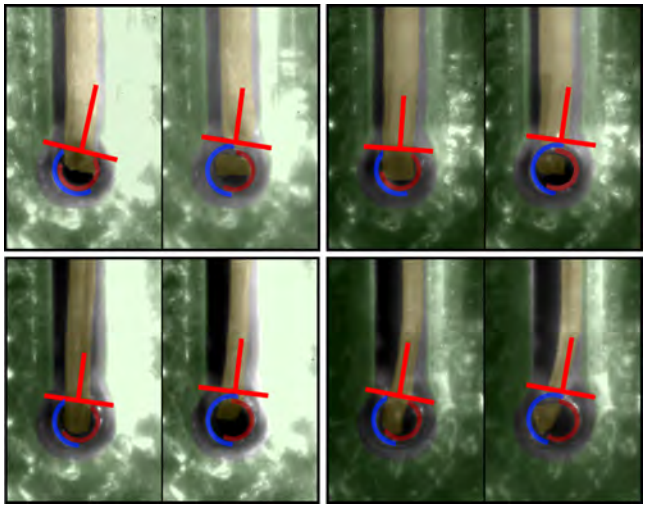

Figure 48: Examples of tissue cut angles for the different velocities, using the counter rotating Reversed beveled knife. 1: 15.56 ± 0.01 RPM at moment of impact (0.00 ± 0.01 s) and moment of debulking (7.34 ± 0.01 s), the difference is $6 \pm 0.5°$. 2: 31.51 ± 0.01 RPM at moment of impact (0.00 ± 0.01 s) and moment of debulking (2.520 ± 0.01 s), the difference is $4 \pm 0.5°$. 3: 55.15 ± 0.01 RPM at moment of impact (0.00 ± 0.01 s) and moment of debulking (1.000 ± 0.01 s), the difference is $2°$. 4: 94.54 ± 0.01 RPM at moment of impact (0.00 ± 0.01 s) and moment of debulking (0.488 ± 0.01 s), the difference is $1 \pm 0.5°$.

6.2.4 Tissue cut angle

The tissue cut angle differences between both moments in time are 6.67° (6-8°) for the counter rotating Reverse beveled knife, 40° (38-41°) for the single rotating Reverse beveled knife, 18.33° (16-21°) for the counter rotating Straight knife and 36.67° (35-39°) for the single rotating Straight knife. As can be seen in Figure 47 the difference between the single rotating and counter rotating method is clearly visible.

6.3 Velocity comparison

The influence of the debulking velocity is tested using the counter rotating Reverse beveled knifes. This knife design was chosen over the Straight knife, due to its better tissue cutting angle, and its larger resection time, creating a larger effect when increasing the blade velocity.

The results shown in Figure 44 show the knife displacements found during the knife velocity comparison. The highest velocity; 94.54 RPM (94.54-94.54 RPM), has the lowest resection time; 0.48 s (0.40-0.56 s), displacement; 0.05 mm (0.04-0.06 mm) and tissue cut angle; 1° (0-2°). The highest values are found for the lowest velocity of 15.76 RPM (15.75-15.76 RPM), with a resection time of 6.52 s (5.79-7.34 s), a displacement of 0.31 mm (0.29-0.33 mm), and a tissue cutting angle of 6.67° (6-8°). The tissue cut angles are illustrated in Figure 48. Table 4 shows the resection time, displacement figures and the tissue cut angles according to the used velocities.

Table 4: Results of the velocity comparison. The values are indicated as Mean (Min value - Max value).

Velocity $[RPM]$	Resection time $[s]$	Displacement $[mm]$	Cut angle $[^\circ]$
15.76 (15.75 - 15.76)	6.52 (5.79 - 7.34)	0.31 (0.29 - 0.33)	6.67 (6 - 8)
31.51 (31.51 - 31.51)	2.59 (2.18 - 3.07)	0.20 (0.19 - 0.22)	4.33 (3 - 6)
55.15 (55.14 - 51.15)	1.05 (0.78 - 1.36)	0.12 (0.11 - 0.14)	1.67 (1 - 2)
94.54 (94.54 - 94.54)	0.48 (0.40 - 0.56)	0.05 (0.04 - 0.06)	1.00 (0 - 2)

Figure 49: Tissue sample caught in the Straight knifes after debulking. This example shows the ability to perform a cut.

6.4 Sample volume

An example of a tissue sample is shown in Figure 49. The taken tissue samples have a cylindrical form, $V = \pi \cdot (d/2)^2 \cdot h$, the minimally obtained size is $h = 2.0\ mm$ by $d = \varnothing 0.8\ mm$ resulting in a volume of $1.0\ mm^3$.

7 Discussion

7.1 Introduction

Throughout this study the potential of the described biopsy instrument is explored. Providing evidence, the novel biopsy instrument is a viable solution to increase the survival rate of breast cancer, was the main tasks.

This chapter will discuss, the potential of the biopsy instrument containing the biopsy tip and actuation mechanism. In the design phase the novel biopsy instrument has shown its ability to achieve all the requirements, and set criteria.

The actuation mechanism has been proven to execute the counter rotational movement, while being robust, with already more than 500 successfully movements, without showing any signs of fatigue. It was observed that the ability of the instrument to debulk the lesion depended on the knife design, as well as the ability to counter rotate both knifes or only a single knife. The highest potential was created by combining the counter rotating movement with either the Straight knife design or the Reverse Beveled knife design, this chapter will discuss the potential of both these knifes and will recommend design improvements.

7.2 Summary of main findings

7.2.1 Operating force

The force exerted on the helix tube, shown in Figure 39, also called operation force, is determined using the said configurations. When the counter rotating knifes are compared to one rotating knife the average operating force used to operate the instrument is a factor of 4.69 higher, in the case of the counter rotating knifes. When the counter rotating knifes are compared to the single rotating knife a factor of 2.20 is found. The reason for this large difference in operation force lays most probably in the friction effects caused by the manufacturing tolerances.

Friction effect

Friction is found in every moving mechanism and although the design of the instrument tried to reduce the friction, it is impossible to reduce this value to zero. The friction effects in the handle were reduced by applying the smallest possible moment arms and choosing the right materials.

The friction effects caused by the rotation of the inner and outer cutting tube were underestimated. Due to the exact fit of the inner and outer diameter, the tubes needed to be round and straight over the entire length to create as little friction as possible. The oxide layer found on the tubes was also an unpredictable factor creating different friction effects after every test.

However, these effects were vastly increased due to the limitations in exact centering of both the cutting tubes, inside the helix tube and outer shell, using the two planar bearings. The manufacturing tolerances of the bearings, helix tube and outer shell, created an inability to precisely center both cutting tubes. Creating an exact $\varnothing 6.0\ mm$ round hole over a length of $93.2\ mm$, in the helix tube, proofed to be the biggest problem. Causing both planer bearings to rotate under a slight angle, while being able to wiggle inside the helix tube. This created an increased friction over the entire length of the cutting tubes.

This effect is clearly illustrated when only one of the cutting tubes is inserted. Without the second cutting tube the average operating force was reduced to a value of $0.56\ N$ (0.55-$0.58\ N$). When both cutting tubes were inserted and one tube was rotated the average operation force increased to $1.21\ N$ (1.06-$1.29\ N$), this can be explained by the alignment of both tubes, created by the tolerances, which apparently were too large.

Using lubrication to minimize friction resulted in a reduced friction between the helix tube and both bearings, but increased the friction between the inner and outer cutting tube, thereby increasing the overall friction. Therefore, it was decided to use no lubrication during the experiment, however the instruments design could be adapted to protect the cutting tubes from the oil.

7.2.2 Resection time

Comparing the resection time between the counter rotating Reversed- and Straight knife gives a better understanding on the exerted debulking forces. Although the Reversed beveled knife has a larger displacement, partly created by the knifes shape, the resection time should not be effected by this phenomenon, due to the exact same position of the end of the knife.

Given the constant rotating velocity of 15.76 ± 0.01 *RPM* (0.825 ± 0.001 mm/s), used in all tests, the resection time of the counter rotating Reversed beveled knife took $6.47 - 4.29 = 2.18$ s longer compared to the Straight knife. Because the only distinguishing factor between the two is the knife design, the higher resection time should be caused by the design difference. Examining the cutting surface, indicated in Blue in Figure 51, gives an indication of the involved forces, were the Straight knife uses the entire cut out length to penetrate the lesion the Reversed beveled knife uses an infinitely small surface area, caused by the angle of the knife. This small area creates a high local pressure resulting in a smooth penetration, however when the Straight knife is used the large cutting surface needs to exert a high force over the entire cut out length before the tissue is abruptly penetrated, where after the entire lesion is debulked very quickly. The sudden penetration is most probably the reason for the faster resection time.

7.2.3 Displacement

The displacement of both knifes suggests a reduced capability of the Reversed beveled knife due to the larger displacement of the gelatin before it was completely debulked. In theory the Reversed beveled knife has an displacement of 0.22 *mm*, caused by the 5° knife angle. However, in reality a displacement of 0.31 *mm* (0.29-0.33 *mm*) was found, thereby indicating a gelatin displacement of 0.09 *mm*. In the case of the Straight knife the theoretical value should be 0.00 *mm*, what turned out to be a displacement of 0.04 *mm* (0.03-0.05 *mm*). Comparing both values indicates that the displacement needed to debulk the tissue is 0.05 *mm* larger in the case of the Reversed beveled knife. This number can be explained by several reasons, the most likely is the differences in knife sharpness, because the knifes where sharpened by hand, without determining the exact difference between the two.

When the single rotating knife configurations are examined the higher displacement is striking, although the displacement will most probably be influenced by the larger increase of tissue cutting angle using the single rotating knife.

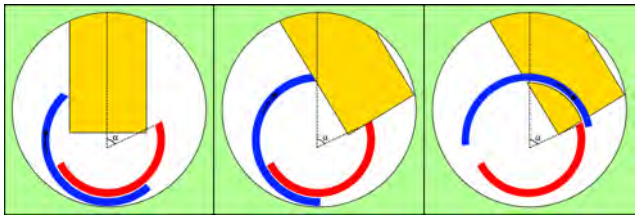

Figure 50: Schematic drawing of what happens if the angle between the lesion and the fixed knife (α) is to large. Left: Initial position of the lesion. Middle: Lesion is pushed against the ductal wall by the single rotating knife. Right: The small part that is debulked. Blue: the outer knife, Red: The inner knife, Yellow: The lesion and Green: The milk duct.

7.2.4 Rotation configurations

During the experiment not only the knife designs were compared, the rotation of a single knife was also compared to the counter rotating knife configuration.

However, when the knife is positioned correctly there still is a downside to the single rotating configuration, caused by the angle, over which the knifes cut, compared to the initial position of the gelatin. When the counter rotating knifes are used the gelatin will in theory stay exactly in the center caused by the perfect counter rotation of both knifes, despite the shape of the lesion. When a single rotating knife is used the penetration will be performed under an angle, despite a perfect positioning against the lesion, creating a larger gelatin cutting angle.

The magnitude of this angle influences the ability to cut along the circumference of the ductal wall. When the angle is large the lesion will be pushed against the ductal wall reducing the volume of the biopsy. The effect of the increased angle is shown in the schematic drawings illustrated in Figure 50. The obtained results found using the experimental images is less dramatic, however the effect is still visible (Fig.47). Using a single rotating knife multiplies the gelatin cut angle by little less than a factor of six, in the case of the Reverse beveled knife and a factor two when using a Straight knife. When the cut angle is increased, and the width of the tissue is constant, the length of the cut will increase, potentially causing a longer recovery for the patient.

7.2.5 Theoretical selection

After performing the experiment combining both the Reversed beveled knife and the Straight knife none of the two tip designs outperforms the other on all points. The debulking surface, force direction, structures integrity and manufacturability were addressed as criteria to determine possible tip designs in section 2.4.2. In this section these criteria are used to determine the theoretical differences.

When the debulking surface of the Straight knife design is examined the theoretical surface area is: The cut out length times the width of the knife, in this case $3 * 0.1 = 0.3$ mm^2.

Examining the surface area of the Reversed beveled knife results in an infinitely small surface area due to the angled shape of the knife. This infinitely smaller surface

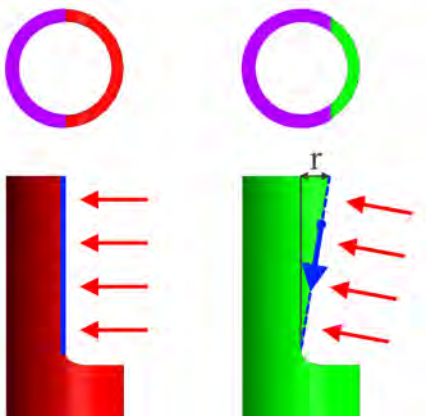

Figure 51: Theoretical selection. Blue: The cutting surface, in the case of the Straight knife the entire cut out length, when using the reversed beveled knife it consists of a point moving along the dotted line. Red: The debulking direction. Purple: The frontal surface area. Grey: The moment arm r.

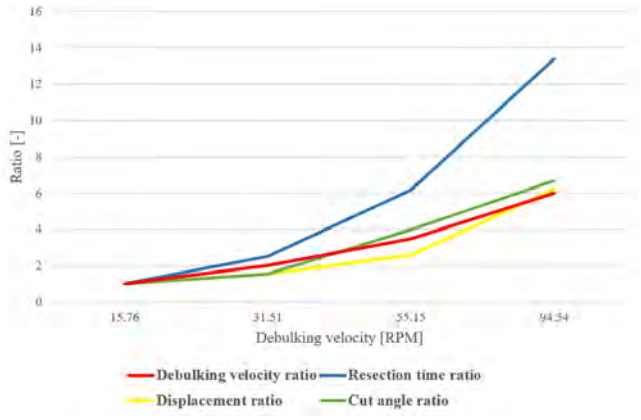

Figure 52: The influence of the increase in debulking velocity (Red) on the dependent variables: the resection time (Blue), displacement (Yellow) and cut angle (Green). A ratio is taken of all values to create a better comparison.

area leads to an infinitely smaller force needed to create the same pressure as is the case using a straight knife. Combining the smaller debulking surface with the force direction pointed inwards, as is shown in Figure 51, creates an advantage for the Reversed beveled knife.

However, the frontal surface area is in favour of the Straight knife. The frontal surface area can be of great importance when a clinical situation is found were the entire duct is filled, as was described in section 2.4.2, when this is the case the knifes need to be pushed into the lesion where after the knifes can be rotated. In this case the Straight knifes frontal surface area is smaller, resulting in a smaller force. When the Reversed beveled knife is used in such a situation the structures integrity can be endangered due to the created moment arm, see Figure 51.

7.2.6 Velocity effects

Using the Reverse beveled knife to determine the influence of the velocity on the biopsy process, showed a decrease in the resection time, displacement and the cut angle.

When the increase of the velocity is compared to the decrease of the dependent variables, as is illustrated in Figure 52, the displacement and cut angle decrease a similar degree as the increase of the velocity. However when the resection time is examined something else happens.

In Figure 52 the resection time is inverted to show the large difference between the debulking velocity ratio and the resection time ratio. If the velocity had no effect on the debulking process the ratios of these two lines should be equal. However, as can be seen from Figure 52 the increase in velocity effects the resection time exponentially. This increase can point out the larger forces involved, caused by the shorter debulking time. The shorter the time from initial contact to penetration the higher the forces, as was shown in section 7.2.2.

The decrease in the tissue cut angle can be explained by the increase of impulse caused by the higher knife velocity. Due to the increase of impulse the gelatin is less effected by the angle under which the knife will come in contact with

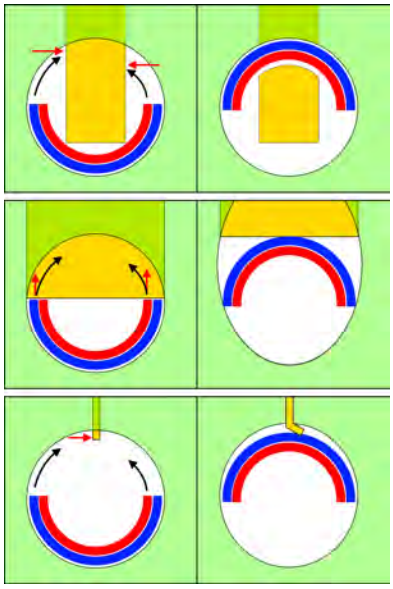

Figure 53: Schematic drawings of some clinical situations: 1. Tested situation, both action forces (Red) are pointed towards the center. 2. Situation filling the duct until the center line. The action forces are pointed upwards resulting in an upwards motion of the lesion, high velocity is needed. 3. Situation describing a small lesion, the outer cutting tube exerts the only action force, pushing the lesion against the ductal wall.

the gelatin, because the gelatin will be cut almost immediately. The tissue cut angle is also influenced by the more rapid change of the force direction, creating a better ability to push the tissue to the center.

However, the higher velocity can also cause dynamic effects, which are much harder to predict. Therefore the operation velocity should only be raised in some cases. Situations, such as extremely tiny lesions or lesions filling the duct until the center-line (see Fig 53), can only be debulked when the debulking velocity is increased. In these cases the reaction force is not exerted by the instrument, therefore a higher velocity is needed, resulting in a reaction force exerted by the lesion itself, instead of the environment when using a slow velocity. Because the instrument does not ex-

ert the reaction force the increased velocity, decreases the possibility of the lesion to move away from the knife, due to the small force loop.

7.2.7 Sample volume

The main objective of the experiment was to proof that the novel biopsy needle instrument was able to debulk a tissue sample usable in pathological examination. To accomplish this goal the sample taken should be large enough. An example of how the tissue is debulked is shown in Figure 49.

The found cancer cells have a diameter of 12-25 μm, as is the commonly quoted range for Circulating tumor cells (CTCs) [44]. Resulting in a volume of $V = 4/3 \cdot \pi \cdot (d/2)^3 = 8.2 \cdot 10^{-6}$ mm^3 per cancer cell. When it is assumed that the tissue sample (1.0 mm^3) of the lesion is homogeneous, thereby containing only cancer cells, the sample contains roughly $1.0/8.2 \cdot 10^{-6} = 1.2 \cdot 10^5$ cancer cells

7.3 Study limitations

7.3.1 Force analyses

Limitations of the study are the inability to determine the debulking forces, the lack of evidence in combining the biopsy instrument with the ductoscope and the reduced validity of the presented results. This section will elaborate on how to improve these limitations.

The problems to determine the tangential forces are addressed in section A.5.3. The lack of the force distribution created a more difficult analyses of the debulking process, the video images created the possibility to proof the working principle of the instrument. Proving that the counter rotating knifes debulked the tissue in a more controlled manner, validated by the better tissue cut angle, resection time and displacement.

However, when the tangential force is measurable more significant differences could be found, which might result in the selection of an ideal knife design and debulking velocity.

7.3.2 Combination with a ductoscope

Although the instrument is designed to be used during ductoscopy, no evidence is provided if the instrument is capable of combining the biopsy needle with a ductoscope. The main reason is the limited length of the current ductoscope, used in the UMCU, with a fiber length of ± 100 mm. The exact same length as described in the requirements, needed for the surgeon to be able to penetrate into the ductal tract. Therefore the potential of using the fiber optical ductoscope in combination with the biopsy needle was not possible in this study, however increasing the fiber length is possible.

Hence, the length of the inner cutting tube (228.2 mm) is to long to fit the fiber. Although techniques might exist to increase the fiber length, this falls out of the scope of this study. Therefore, solutions reducing the inner cutting tube are explored.

The easiest option to reduce the inner cutting tube length is found in decreasing all the margins used to protect the helix tube, and to provide enough strength to the helix tube, a potential reduction of 30.0 mm is possible without changing any other dimensions.

A more rigorous improvement is found in reducing all sizes of the helix tube to a minimum, with a potential inner diameter of 0.1 mm larger than the cutting tubes outer diameter. Although the 45 degree slot angle needs to be taken in consideration providing that the instrument needs to be capable of being used in both directions. When manufacturability isn't taken into account, the 1.3 mm outer diameter results in the reduction of the inner cutting tubes length by a factor $10/1.4 = \pm 7$ providing a minimal length of ± 120 mm, including the 100 mm insertion tube. Although the possibility of reducing the size by this factor is almost impossible given the manufacturability and the strength. A more realistic number will be a factor two or three.

A final approach reduces the angle of rotation. In the current instrument the knifes can rotate over 360° when this is reduced to a little over 90°. Provided that the displacement of the knife design is taken into consideration. The inner cutting tubes length could be decreased with a little less than a factor four.

7.3.3 Experimental validity

The reduced validity of the presented experimental results is another limitation of this study, provided by the minimal amount of repetitions performed and using only one tissue mimicking phantom. Although a proof of principle is provided, more extensive experimentation is needed to transform these findings into significant results and definite answers.

The exploration of the instruments possibilities, was performed to provide proof of the capabilities of the design. Investigating if the biopsy tip could cut a lesion found in the ductal tract, and whether the design showed the potential of being developed into a completely functioning device, was the main target. Although the study has limitation in its in-depth evaluation of the found results, it provides insights in the newly explored matter.

7.4 Design recommendations

7.4.1 Tip design

Cut out length

The biopsy tip provides limitations in debulking tissue larger than 3 mm, when a lesion is found larger than the cut out length the knife would not completely cut the lesion of the duct. However, when a larger lesion is found the surgeon could choose to use the instrument multiple times. In the case of such a large lesion the ability to trigger the instrument once, where after the biopsy tip is pushed further into the duct followed by a second rotation of the knifes, provides the ability to repeat the rotational motion, creating an opportunity to debulk much larger lesions. However, no tests were performed to see if this capability could actually be used.

Multiple rotations are not the only possibility to debulk lesions larger than 3 mm. Due to the overall strength of the knifes the cut out length could also be increased, provided

that the strength of the biopsy tip will remain strong enough to debulk the tissue. After elaborating with Dr.Witkamp the maximal size of the lesions found would not be larger than 10 *mm* in 95% of the time. To determine if the 10 *mm* cut out length is indeed able to debulk the tissue, a similar calculation will be performed as was explained in 4.1.1. Only now the cut out length is increased, therefore the frontal surface area (A) is changed but the moment of inertia (I) stays the same.

$$\begin{aligned} F_{penetration} &= E \cdot A \\ &= (150 \cdot 10^3) \cdot (10 \cdot 10^{-3} \cdot 1 \cdot 10^{-4}) \\ &= 15 \cdot 10^{-2}\ [N] \end{aligned}$$

$$\begin{aligned} \sigma_{max} &= M \cdot y / I \\ &= 2.40 \cdot 10^7\ [Pa] \end{aligned}$$

With this newly obtained stress level $\sigma_{max} = 24.08\ MPa$, it is still safe to say that cut outs are strong enough, compared to the 205 *MPa* needed to permanently deform the stainless steel tube. Therefore it is recommended to increase the span of the cut out to a length capable of debulking the lesions this size.

Cutting tube diameter

The cutting tubes diameter should be reduced providing that the sleeve diameter of 1.4 *mm* is larger than the current ductoscope containing a sleeve of ∅1.2 *mm*. The cutting tubes thickness could be reduced from 0.1 *mm* to 0.05 *mm* with existing tubes. The current tubes with a cut out length of 3 *mm* are strong enough to cut Low-density polyethylene (LDPE) with a Young's modulus of 0.3 *GPa* [45]. These results indicate that the strength of the cut outs is indeed over dimensioned and could be increased to the needed 10 *mm*.

However, to explore the lobules of the ductal epithelial tract the outer diameter has to be reduced to be submillimeter. Because these parts of the ductal epithelium are smaller, therefore harder to enlarge using the fluid, the outer diameter of the instrument needs to be reduced.

To estimate if it is possible to reduce the sleeve to a 1.0*x*0.05 *mm* tube, to explore the lobules, the cutting tubes dimensions need to be adjusted. The outer- and inner-cut out tube are made of a 0.9*x*0.05 *mm* and a 0.8*x*0.05 *mm* tube, with a cut out length of 10 *mm*. To estimate if both tubes are still strong enough the higher stress level on the outer cutting tube is calculated using the following equations:

$$\begin{aligned} F_{penetration} &= E \cdot A \\ &= 7.5 \cdot 10^{-2}\ [N] \end{aligned}$$

$$\begin{aligned} \mathrm{I} &= (D^4 - d^4)/145.7 - D^2 \cdot d^2 (D-d)/(56.5(D+d)) \\ &= 4.47 \cdot 10^{-15}\ [m^4] \end{aligned}$$

$$\begin{aligned} \sigma_{max} &= M \cdot y / \mathrm{I} \\ &= 3.77 \cdot 10^7\ [Pa] \end{aligned}$$

Figure 54: Ideal knife design estimation.

The obtained Stress level of $\sigma_{max} = 37.74\ MPa$ is still under the level of the Young's modulus of the tube (250 *mm*), therefore in theory the outer tubes diameter and cut out length can be reduced to explore the lobules. However the instrument will be more vulnerable and there is 0.1 *mm* less space to fit the ductoscope and the enlargement fluids.

Improved knife design

In section 2.4.2 three knife design categories are suggested, however another category is possible, which combines the advantages of the Straight knife and the Reversed beveled knife into an improved knife design.

Although the comparison of the biopsy tips provided some inside in the knife design, the desire to provide this improved knife design is limited by the obtained results. The found displacement caused by the overlapping of the knifes is slightly better for the Straight knifes, however this can be caused by several factors, most probably by the sharpness of the knife. A larger difference is found for the resection time and the tissue cut angle. When the resection time is looked upon, the Straight knife showed a shorter time of 4.29 *s* (3.88-4.56 *s*) although accompanied by the sorter time comes a larger force needed to debulk the tissue. However, no number can be given to this force increase.

The tissue cut angle is 6.67° (6-8°) for the counter rotating Reversed beveled knifes and 18.33° (16-21°) for the counter rotating Straight knifes, resulting in an advantage for the Reversed beveled knife design. Hence, it can be concluded that both knifes have some advantages over the other and a combination of both designs could be ideal. Based on the limited available information a design as is illustrated in Figure 54, could combine the benefits of both knife designs. The reversed beveled end creates an improved gelatin cut angle while the straight part near the tube reduces the resection time. By combining the two the forces involved would also be lower due to the smaller contact area of the straight edge compared to the normal straight edge.

Another approach could be to look at the best suited knife design for the found clinical situation. Some of these cases were already described in Figure 53. When this approach is considered the Straight knife design should be used in the case of a lesion expanding over fifty percent of the circumference or having a length larger than the knife length of 3 *mm*, because then the frontal surface needs to be penetrated into the tissue. Due to the smaller frontal area and more ridged design the Straight knife design would be picked. Where in other situations the Reversed beveled

knife could be ideal. However, to determine the best suited design for these situations more experiments need to be conducted.

A different possibility to test the ability of the Reversed beveled knife is to enlarge the cutting angle from five degrees to a higher number, thereby exaggerating the effects of the beveled angle. This could lead to a better understanding of the differences in both knifes.

Sharpness of the biopsy tip

Another point of improvement is designing a way to create sharp edges on the biopsy tip, during fabrication. Due to the small size and fragility of the knifes, sharpening the knifes has been done by hand using a delicate file. However, no comparison in sharpness was made therefore the results could be skewed to one of the knife designs.

Tissue entrapment

When the novel biopsy instrument is used the debulked tissue will remain near the tip of the instrument, as is seen in Figure 49. However, when the instrument is withdrawn no certainty is provided that the tissue will remain positioned inside the cutting tubes. This effect creates another downside in the design of the biopsy tip, the inability to provide a method to entrap the debulked tissue using some form of cannula occlusion or some sort of irrigation system. These possibilities should be explored in the future. Methods providing options to be explored can be found in Appendix B.

Due to the exceptionally small sizes of the biopsy needle manufacturing, an enclosing method is more difficult compared to an irrigation system, capable to entrap the tissue sample. The design of the irrigation should consider the fluids used to enlarge the ductal tract and the forces the tissue cells can withstand, to allow for a pathological exam. The allowable forces acting on the tissue cells fell out of the scope of this study, but should be considered when designing an irrigation system

7.4.2 Handle design

In some clinical situations a slow movement of the knifes is essential in taking a biopsy. Therefore a method could be created providing more guidance in performing a slow cut. One could think of a lever which increases the distance the surgeons fingers need to travel to rotate the knifes. Other possibilities could be an automated actuator, capable of moving slowly, although this would increase the complexity of the instrument.

However, in other clinical situations the desire exist for a fast moving knife, therefore a spring driven system could be the solution, due to the simple incorporation of such a spring into the current handle design.

Handle ergonomics

An ergonomic study of the actuation mechanism should be performed to improve the ability to use the instrument. Determining how the instrument is best operated using one hand, allowing the surgeon to use the other hand to maneuver the ductoscope, could be an option. Another possibility is creating a device, which incorporates the use of the ductoscope and the biopsy needle into one ergonomic handle.

7.5 Experimental recommendations

7.5.1 Mimicking the ductal tract

Clinical situations

During the entire experiment the 0.5 ± 0.1 *mm* thick gelatin sheets were used to determine whether the instrument was able to perform a biopsy. However, only one specific clinical situation was tested, created by adding a movable gelatin layer to a perspex block, simulating the ductal tract. Future work could focus on different clinical situations, to determine if the instrument is working in all circumstances. There might be a possibility that testing other clinical situations gives more inside in the differences between the knife designs. Clinical situations, which could be tested on, are a fully filled duct, testing the ability to perform a cut with the frontal surface of the cutting tube and the structures integrity. Another situation describing a duct filled until the center of the duct, tests whether the knifes can perform a cut when the action force directions are pointed upwards instead of towards the center, as is shown in Figure 53.

Tissue density

Another improvement in mimicking the clinical situations could be made by changing the tissue density, in this study it was assumed that when the biopsy tip was able to debulk high stiffness tissues it could also debulk tissues with a lower stiffness, although this is most probably true given the initial tests performed during the pilot phase, see Appendix A.5, there is no certainty it will.

The experimental tests performed, all used the same gelatin stiffness, therefore the provided evidence is only capable of predicting the behavior of this specific stiffness. However, it was planned to perform tests on different gelatin stiffnesses the thin gelatin sheets caused the water to evaporate and thereby increasing the stiffness of the gelatin, therefore only the 150 *kPa* gelatin was tested. For a proof of principle, showing the capability of cutting the strongest breast cancer type will provide sufficient information at this moment. However, a wider variety of breast mimicking substances should be tested, including real breast tissue.

7.5.2 In-vivo study

Although gelatin can mimic the abilities of breast cancer tissue, tests need to be performed using real tissue followed by in-vivo studies, to determine the real potential of the novel biopsy instrument.

7.5.3 Limitations of the video images

The provided video images formed a drawback since the enlargement factor was limited to a factor $11/5$, limiting the capabilities to zoom in to determine the exact moment when the tissue was penetrated. However, sufficient evidence was delivered to indicate the biopsy phases. In the future a camera able to visualise the penetration moment could be included into the study, to examine if there are noticeable differences between the knife designs.

7.5.4 Fixed knife positioning

Creating a possibility to rotate the entire instrument during the experiment, could result in a more controlled single rotating debulking process, due to the lack of this ability the operator needed to guess the position of the fixated knife in comparison to the gelatin. When the user is able to rotate the entire instrument the best suited position could be determined using the camera images. Creating a better ability to compare the counter rotating knifes with the single rotating knifes. Although the difference in gelatin cut angle could be reduced using this method, the advantage of the counter rotating knifes to cut the lesion at its center line remains.

7.6 Future recommendations

7.6.1 Force determination

Exploring methods to determine the involved forces in millimeter biopsy needles could improve the cut out design, and could create the ability to determine if the biopsy phases are comparable with needle-tissue insertion. However, when a method is found the difference between both knife designs could still be small, therefore it might be better to use the video analyses in combination with different tissue densities and clinical situations, to determine if the tip design is suited to combine the ductoscope with a biopsy instrument.

7.6.2 Sterilization

When the novel biopsy instrument is further developed the sterilization process needs to be considered when choosing the handle materials. The tip would be disposable therefore sterilization is of no concern. In this study the main objective was to provide evidence of the capabilities of the instrument, therefore the chosen materials were solely chosen for this purpose. In a future study considering if the instrument, or what parts, need to be reusable can push the material selection in a new direction.

8 Conclusion

In this study an innovative biopsy needle was developed, consisting of two counter rotating blades able to cut tissue along the ductal wall. The biopsy prototype has an innovative tip design, of $\varnothing 1.2$ *mm*, adequate to enter the ductal tract. Thereby, allowing enough space to fit the $\varnothing 0.55$ *mm* ductoscope. The novel handle design actuates the tip by applying a counter rotating motion using two helix paths. Both the tip and the handle design are currently not seen in any other clinical biopsy instrument. The experiments showed the possibility to take a biopsy using the prototype, illustrating the feasibility of combining the novel biopsy instrument with the ductoscope, to screen for and diagnose breast diseases. Continued development of this instrument may, in time, improve the lives of millions of women by increasing the possibility to detect breast cancer, years before the current state of the art.

9 Acknowledgements

First of all, I would like to thank Paul Breedveld, for the guidance throughout this exploratory design study. Secondly, I would like to thank my daily supervisor Aimée Sakes, for the great effort in supporting and guiding me throughout this thesis. Furthermore, I would like to thank Menno Lageweg and Remi van Starkenburg for contributing to the development and manufacturing of the prototype. Special thanks to Wim Velt for educating me how to fabricate, and the mental support during the endless hours of turning and milling. Thanks to Jos van Driel for contributing to the experimental setup. Finally, I would like to thank the Arjen Witkamp, Paul van Diest and Tjeerd de Boorder from the medical center in Utrecht to give me the opportunity to hold a questionnaire.

10 References

[1] W. Al Sarakbi, M. Salhab, and K. Mokbel. “Does mammary ductoscopy have a role in clinical practice”. In: *International Seminars in Surgical Oncology* 16.3 (2006), pp. 1–7.

[2] K. Kaur and E.D. Schraga. *Ductoscopy*. 2015. URL: `http://emedicine.medscape.com/article/1894873-overview` (visited on 06/13/2016).

[3] V. Deshmane. “Intraductal Approach to Breast Cancer: The Role of Mammary Ductoscopy”. In: *Indian J Surg Oncol* 3.1 (2010), pp. 228–231.

[4] S.S.K. Tang et al. “Mammary ductoscopy in the current management of breast disease”. In: *Surg Endosc* 25 (2011), pp. 1712–1722.

[5] C.A. Sparks. “Using ductoscopy to detect breast mass at an early stage”. In: *Aorn J* 76 (2002), pp. 851–4.

[6] E. Kapenhas-Valdes, S.M. Feldman, and S.K. Boolbol. “The Role of Mammary Ductoscopy in Breast Cancer: a Review of the Literature”. In: *Annals of Surgical Oncology* 12.15 (2008), pp. 3350–3360.

[7] E. Yin-Kwee. “Breast imaging A survey”. In: *World J Clin Oncol* 4.2 (2011), pp. 171–178.

[8] E. Kapenhas-Valdes et al. “Mammary ductoscopy for evaluation of nipple discharge.” In: *Annals of surgical oncology* 10.15 (2008), pp. 2720–7.

[9] W.C. Dooley, B.M. Ljung, and U. Veronesi. “Ductal lavage for detection of cellular atypia in women at high risk for breast cancer”. In: *J Natl Cancer Inst* 93 (2001), pp. 1624–32.

[10] J.R. Dietz et al. “Directed duct excision by using mammary ductoscopy in patients with pathologic nipple discharge.” In: *Surgery* 132 (2002), pp. 582–7.

[11] A.B. Hollingsworth, S.E. Singletary, and M. Morrow. “Current comprehensive assessment and management of women at increased risk for breast cancer”. In: *Am J Surg* 187 (2004), pp. 349–62.

[12] F.L. Balci and S.M. Feldman. “Exploring breast with therapeutic ductoscopy”. In: *Gland Surgery* 2.3 (2014), pp. 136–141.

[13] F.M. Iordache, S. Saftoiu, and A. Ciurea. “Autofluorescence imaging and magnification endoscopy.” In: *World Journal of Gastroenterology* 17 (2011), pp. 9–14.

[14] N. Uedo et al. “A novel videoendoscopy system by using autofluorescence and reflectance imaging for diagnosis of esophagogastric cancers”. In: *Gastrointestinal Endoscopy* 62 (2005), pp. 521–528.

[15] J. Haringsma et al. “Autofluorescence endoscopy: Feasibility of detection of {GI} neoplasms unapparent to white light endoscopy with an evolving technology”. In: *Gastrointestinal Endoscopy* 53 (2001), pp. 642–650.

[16] Jhmicall. *Primary Sclerosing Cholangitis:Diagnosis*. 2017. URL: https://www.jhmicall.org/GDL_Disease.aspx?CurrentUDV=31&GDL_Cat_ID=551CDCA7-A3C1-49E5-B6A0-C19DE1F94871&GDL_Disease_ID=80BA0B13-D845-444B-8E1F-A96804DBADA0 (visited on 03/09/2017).

[17] JAMES J. SCIUBBA. “Improving detection of precancerous and cancerous oral lesions”. In: *The Journal of the American Dental Association* 130 (1999), pp. 1445–1457.

[18] US endoscope. *Micro forceps*. 2017. URL: http://www.usendoscopy.com/Products/Moray-micro-forceps.aspx (visited on 03/09/2017).

[19] Olympus. *Stone retrieval baskets*. 2017. URL: http://medical.olympusamerica.com/products/stone-retrieval-baskets (visited on 03/09/2017).

[20] K.D. Hopper et al. “Blinded comparison of biopsy needles and automated devices in vitro 1 Biopsy of diffuse hepatic disease”. In: *Am J Roentgenol* 161 (1993), pp. 1293–7.

[21] D. G. Bostwick. “Evaluating prostate needle biopsy: Therapeutic and prognostic importance”. In: *CA: A Cancer Journal for Clinicians* 47 (1997), pp. 297–319.

[22] Angiotech. *BioPince; Full-Core Biopsy Instruments*. 2016. URL: http://www.mana-tech.com/factsheets/Biopince.pdf (visited on 06/20/2016).

[23] R.B. Kass, D.S.Lind, and W.W. Souba. “Breast procedures”. In: *WebMD* (2007), pp. 1–18.

[24] K.D. Hopper et al. “Percutaneous biopsy of the liver and kidney by using coaxial technique adequacy of the specimen obtained with three different needles in vitro”. In: *Am J Roentgenol* 164 (1995), pp. 221–4.

[25] K. Dowlatshahi et al. “Image-guided surgery of small breast cancers”. In: *The American Journal of Surgery* 182 (2001), pp. 419–425.

[26] S. Diederich et al. “Application of a single needle type for all image-guided biopsies results of 100 consecutive core biopsies in various organs using a novel tri-axial, end-cut needle”. In: *Cancer Imaging* 6 (2006), pp. 43–50.

[27] A.Y. Park et al. “Lesion stiffness measured by shear-wave elastography Preoperativepredictor of the histologic underestimation of US-guided core needle-breast biopsy”. In: *European Journal of Radiology* 8 (2015), pp. 2509–2514.

[28] E.J. Lee et al. “Diagnostic performances of shear wave elastography: which parameter to use in differential diagnosis of solid breast masses”. In: *European Radiology* 23 (2013), pp. 1803–1811.

[29] J.H. Yoona et al. “Qualitative pattern classification of shear wave elastography for breast masses: How it correlates to quantitative measurements”. In: *European Journal of Radiology* 82 (2013), pp. 2199–2204.

[30] S.H. Lee et al. “Differentiation of benign from malignant solid breast masses: comparison of two-dimensional and three-dimensional shear-wave elastography”. In: *European Radiology* 23 (2013), pp. 1015–1026.

[31] O. Orringer and J. Morris. “Applied research on rail fatigue and fracture in the United States”. In: *Theoretical and Applied Fracture Mechanics* 1 (1984), pp. 23–49.

[32] AvE. *Actuator animation*. 2017. URL: https://www.youtube.com/watch?v=fdY5gVvozEo&t=14s (visited on 01/14/2017).

[33] Kanpro. *Section Properties*. 2005. URL: http://www.geocities.jp/iamvocu/Technology/kousiki/kousikidanmen11Eng.htm (visited on 01/04/2017).

[34] AZoM. *Stainless Steel - Grade 304*. 2001. URL: http://www.azom.com/article.aspx?ArticleID=965 (visited on 01/09/2017).

[35] M.F. Ashby, H. Shercliff, and D. Cebon. *Materials; Engineering, Science, Processing and Design*. Elsevier Science & Amp; Technology, 2009. ISBN: 9781856178952.

[36] N. Abolhassani, R. Patel, and M. Moallem. “Needle insertion into soft tissue: A survey”. In: *Med. Eng. Phys.* 29 (2007), pp. 413–431.

[37] N.J. Cowan et al. “Robotic needle steering: Design, modeling, planning, and image guidance.” In: *Surgical Robotics: Systems Applications and Visions* 3 (2011), pp. 557–582.

[38] S. Misra, K.T. Ramesh, and A.M. Okamura. “Modeling of tool tissue interactions for computer-based surgical simulation - a literature review”. In: *Teleoperators and Virtual Environments* 17 (2008), pp. 463–491.

[39] D.J. Van Gerwen. “Needle-Tissue Interaction”. In: (2013).

[40] H. Kataoka et al. “Measurement of the tip and friction force acting on a needle during penetration”. In: *Springer Berlin* 2488 (2002), pp. 216–223.

[41] T.F. Juliano et al. “Multiscale Mechanical Characterization of Biomimetic Physically Associating Gels”. In: *Journal of Materials Research* 8 (2006), pp. 2084–2082.

[42] J.J. Amato et al. “Vascular injuries: An experimental study of high and low velocity missile wounds”. In: *Arch. Surg.* 101 (1970), p. 167.

[43] M.L. Fackler. “Wound ballistics: A target for error”. In: *Int. Def. Rev.* 8 (1988), p. 895.

[44] Zheng et al. “Membrane microfilter device for selective capture, electrolysis and genomic analysis of human circulating tumor cells”. In: *Journal of Chromatography* 1162 (2007), pp. 154–161.

[45] Zhengzhou Orient Power Co. *Properties Compare for LDPE and HDPE*. 2017. URL: http://www.polymer-insulators.com/list1.asp?id=309 (visited on 02/28/2017).

[46] L. Waaijer et al. “Interventional ductoscopy in patients with pathological nipple discharge”. In: *BJS Society Ltd* 102 (2015), pp. 1639–1648.

[47] N. Cabioglu et al. “Surgical decision making and factors determining a diagnosis of breast carcinoma in women presenting with nipple discharge”. In: *J Am Coll Surg.* 196 (2003), pp. 354–364.

[48] T.A. King et al. “A simple approach to nipple discharge”. In: *Am Surg.* 66 (2000), pp. 960–965.

[49] R. M. Moncrief et al. “A Comparison of Ductoscopy-Guided and Conventional Surgical Excision in Women With Spontaneous Nipple Discharge”. In: *Annals of Surgery* 241 (2015), pp. 575–581.

[50] A. Okazaki et al. “Fiberoptic ductoscopy of the breast: a new diagnostic procedure for nipple discharge.” In: *Japanese journal of clinical oncology* 3.21 (1991), pp. 188–93.

[51] H.I. Vargas et al. “Outcomes of clinical and surgical assessment of women with pathological nipple discharge.” In: *The American surgeon* 2.72 (2006), pp. 124–8.

[52] J. Tondre et al. “Technical enhancements to breast ductal lavage”. In: *Annals of surgical oncology* 10.15 (2008), pp. 2734–8.

[53] S. Kamali et al. “Use of ductoscopy as an additional diagnostic method and its applications in nipple discharge”. In: *Minerva chirurgica* 2.69 (2014), pp. 65–73.

[54] S. Kamali et al. “Diagnostic and therapeutic value of ductoscopy in nipple discharge and intraductal proliferations compared with standard methods”. In: *Breast Cancer* 2.21 (2014), pp. 154–61.

[55] S. Kamali et al. “Ductoscopy in the evaluation and management of nipple discharge”. In: *Annals of surgical oncology* 3.17 (2010), pp. 778–83.

[56] E. Kapenhas-Valdes, S.M. Feldmanand J.M. Cohen, and S.K. Boolbol. “Mammary Ductoscopy for Evaluation of Nipple Discharge”. In: *Annals of Surgical Oncology* 10.15 (2008), pp. 2720–2727.

[57] R.M Moncrief et al. “A comparison of ductoscopy-guided and conventional surgical excision in women with spontaneous nipple discharge”. In: *Annals of Surgical Oncology* 241 (2005), pp. 575–581.

[58] J.R. Dietz et al. “Directed duct excision by using mammary ductoscopy in patients with pathologic nipple discharge”. In: *Surgery* 132 (2002), pp. 582–587.

[59] M.F. Dillon et al. “The role of major duct excision and microdochectomy in the detection of breast carcinoma”. In: *BMC Cancer* 6 (2006), p. 164.

[60] Dr. Perry Carter. *Reproductive System*. 2015. URL: http://classes.midlandstech.edu/carterp/Courses/bio211/Chap27/Reproductive_System.html (visited on 05/09/2016).

[61] New Health Guide. *Breast Cancer Pictures*. 2014. URL: http://www.newhealthguide.org/Breast-Cancer-Pictures.html (visited on 06/20/2016).

[62] Breastcancer.org. *Breast cancer types*. 2016. URL: http://www.breastcancer.org/symptoms/types (visited on 06/07/2016).

[63] College of American Pathologists. “Breast Cancer Ductal Carcinoma In Situ”. In: *American Cancer Society* (2006), p. 2.

[64] Mayo Clinic Staff. *Breast cancer types What your type means*. 2015. URL: http://www.mayoclinic.org/diseases-conditions/breast-cancer/in-depth/breast-cancer/art-20045654 (visited on 06/07/2016).

[65] E.V. Newton and J.E. Harris. *Breast Cancer Screening*. 2016. URL: http://emedicine.medscape.com/article/1945498-overview (visited on 06/09/2016).

[66] American Cancer Society. *Experimental breast imaging tests*. 2014. URL: http://www.cancer.org/treatment/understandingyourdiagnosis/examsandtest%20descriptions/mammograms-andotherbreast%20imagingprocedures/mammograms-and-other-breast-imaging-procedures-newer-br-imaging-tests (visited on 06/09/2016).

[67] M. Jochelson. “Advanced Imaging Techniques for the Detection of Breast Cancer”. In: *American Society of Clinical Oncology* (2012), 65*69.

[68] S. Munshie. *Scintimammography - an emerging technique for Breast Imaging*. 2008. URL: https://www.frost.com/sublib/display-market-insight.do?id=137248277 (visited on 06/13/2016).

[69] L. Fass. “Imaging and cancer: A review”. In: *Molecular oncology* 2 (2008), pp. 115–152.

[70] Cancer Quest. *FNA vs CNB*. 2016. URL: http://www.cancerquest.org/fna-vs-core-biopsy.html (visited on 06/15/2016).

[71] Mayo Clinic. *Breast biopsy*. 2013. URL: http://www.mayoclinic.org/tests-procedures/breast-biopsy/basics/what-you-can-expect/prc-20020395 (visited on 06/15/2016).

[72] I. Jatoi, M. Kaufmann, and J.Y. Petit. *Atlas of Breast Surgery*. Springer, 1981. ISBN: 9783540243519.

[73] M.D. Lacambra et al. "Biopsy sampling of breast lesions: comparison of core needle- and vacuum-assisted breast biopsies". In: *Breast Cancer Res Treat* 132 (2012), pp. 917–23.

[74] M. Guenin. *Ultrasound-Guided Breast Biopsy*. 2015. URL: http://www.radiologyinfo.org/en/info.cfm?pg=breastbius (visited on 06/15/2016).

[75] G. Carbognin et al. "MR-guided vacuum-assisted breast biopsy in the management of incidental enhancing lesions detected by breast MR imaging". In: *Breast Radiology /Senologia* 166 (2011), pp. 876–885.

[76] J.T. Hing, A.D. Brooks, and J.P. Desai. "Reality-based needle insertion simulation for haptic feedback in prostate brachytherapy". In: *International Conference on Robotics and Automation* 2006 (2006), pp. 619–624.

[77] J.T. Hing, A.D. Brooks, and J.P. Desai. "A biplanar fluoroscopic approach for the measurement, modeling, and simulation of needle and soft-tissue interaction". In: *Med. Image Anal.* 11 (2007), pp. 62–78.

[78] Tomoe. *Butterfly valve*. 2016. URL: http://patentimages.storage.googleapis.com/EP0018220A1/imgf0002.png (visited on 09/19/2016).

[79] Amazon AWS. *Ball valve*. 2016. URL: http://s3.amazonaws.com/finehomebuilding.s3.tauntoncloud.com/app/uploads/2016/04/09112001/021232038-ball-valves_med.jpg (visited on 09/19/2016).

[80] Wikipedia. *Bimetal*. 2016. URL: https://upload.wikimedia.org/wikipedia/commons/d/d2/Bimetaal.jpg (visited on 10/10/2016).

[81] Wesco. *Kickmaster*. 2016. URL: http://www.culinaris.eu/Shop-by-brand/Wesco/Wesco-Replacement-Parts-Accessories (visited on 09/19/2016).

[82] Wikipedia. *Bicycle valve*. 2016. URL: https://upload.wikimedia.org/wikipedia/commons/thumb/b/bb/Fietsventiel_met_afsluiter.svg/200px-Fietsventiel_met_afsluiter.svg.png (visited on 10/10/2016).

[83] Archtoolbox. *Gate valve*. 2016. URL: https://www.archtoolbox.com/images/materials/plumbing/gateValve.png (visited on 09/19/2016).

[84] Huisentuinmagazine. *S-siphon*. 2016. URL: http://www.huisentuinmagazine.nl/wp-content/uploads/2015/08/soorten-sifon.jpg (visited on 10/10/2016).

[85] Huisentuinmagazine. *Cup-siphon*. 2016. URL: http://www.huisentuinmagazine.nl/wp-content/uploads/2015/08/soorten-sifon.jpg (visited on 10/10/2016).

[86] a2ua. *Gel*. 2016. URL: hhttps://a2ua.com/gel/gel-001.jpg (visited on 10/10/2016).

[87] Isolatie werken afp. *Pur foam*. 2016. URL: http://www.isolatiewerkenafp.be/images/foto.jpg (visited on 10/10/2016).

[88] King national air systems. *Air curtain*. 2016. URL: http://www.kingnationalairsystems.com/s/cc_images/cache_285457504.jpg?t=1351089689 (visited on 10/10/2016).

[89] Ros cardioinvest. *Trikard*. 2016. URL: http://roscardioinvest.ru/eng/image_admin/document/trikard.png (visited on 09/19/2016).

[90] Todays dental cape coral. *UV-light curing adhesive*. 2016. URL: http://www.todaysdentalcapecoral.com/images/uv-light.jpg (visited on 10/10/2016).

[91] Blogspot. *Sphincter*. 2016. URL: http://4.bp.blogspot.com/-nyVeNNF77sQ/VWdR9vziCKI/AAAAAAAAACY/jyRZ7CKxxOA/s1600/Naamloos.jpg (visited on 09/19/2016).

[92] Webmd. *Heart valves*. 2016. URL: http://img.webmd.com/dtmcms/live/webmd/consumer_assets/site_images/media/medical/hw/h9991304_006.jpg (visited on 09/19/2016).

[93] Asha. *Ear drum*. 2016. URL: http://www.asha.org/uploadedImages/inner-ear2.jpg?n=8034 (visited on 10/10/2016).

[94] Izakowski. *Puffin bird beak*. 2016. URL: http://previews.123rf.com/images/izakowski/izakowski1505/izakowski150500152/40547487-Black-and-White-Cartoon-Illustration-of-Atlantic-Puffin-Bird-for-Coloring-Book-Stock-Vector.jpg (visited on 09/19/2016).

[95] Thumb9. *Shark jaw*. 2016. URL: https://thumb9.shutterstock.com/display_pic_with_logo/1768667/304081742/stock-vector-great-white-shark-jaws-304081742.jpg (visited on 09/19/2016).

11 Abbreviations

.

.

ADH Atypical ductal hyperplasia

AF Auto Fluorescence

AFI Auto fluorescence imaging

CNB Core Needle Biopsy

CT Computed Tomography

CTCs Circulating tumor cell

DCIS Ductal Carcinoma In Situ

EIT Electrical Impedance Tomography

FNAB Fine Needle Aspiration Biopsy

IBC Inflammatory Breast Cancer

IDC Invasive Ductal Carcinoma

ILC Invasive Lobular Carcinoma

IP Intraductal Papilloma

LCIS Lobular Carcinoma In Situ

MRI Magnetic Resonance Imaging

MSMAs Magnetic Shape Memory Alloys

NA Not Applicable

NIR Near Infrared

PET Positron Emission Tomography

PND Pathological Nipple Discharge

SMAs Shape Memory Alloys

SMMs Shape Memory Materials

TDLU Terminal Duct-Lobular Unit

UMCU University Medical Centre of Utrecht

VAB Vacuum-Assisted Biopsy

VAD Vacuum-Assisted Device

WLE White light endoscopy

A Appendices

A.1 Breast diseases

Ductoscopy is used in to detect breast diseases at an early stage. This section will elaborate on the different forms of breast cancers that are distinguished.

A.1.1 Pathologic Nipple Discharge (PND)

Pathological nipple discharge (PND) is defined as spontaneous, unilateral hemorrhagic or serous discharge during a non-lactational period [46]. However, not all PND-types are associated with significant pathologic findings, most types correlate with a high likelihood of unilaterality, persistence, emanation from a single duct, and watery-, serous-, or bloody appearance [47, 48]. These forms of discharges are seen as pathologic, and are an indication for surgical excision of the involved duct [49].

PND is the third most common complain among women with breast diseases [50], and causes approximately 3-6% of all women to visit a breast speciality service. Put into figures, this pertains to about 3 500-4 500 new cases a year in the Netherlands and 106 000-137 000 cases in Europe [8, 51–55]

The most common cause of PND is Intraductal Papilloma (IP), found in 36% to 66% of all cases. Followed by ductal carcinoma in situ (DCIS) in 3% to 20% and other benign causes in up to 23% [12]. When PND is caused by an IP, the origin is most often found in the lactiferous sinus or papillomatosis in which the discharge is often spontaneous and extracted from a single duct (Fig. 55) [56]. Although, the underlying cause of PND in the majority of patients is a benign papilloma, many surgeries are performed with a risk of complications and effects on cosmesis, breastfeeding and sensitivity of the nipple [46, 57, 58].

The evaluation of women with PND usually involves mammography and/or ultrasound. The lesions are frequently fount at some distance from the nipple office, resulting in the fact that blind surgical excision is used, which may lead to unsuccessful removal of peripheral lesions [57, 59]. This type of blind surgical procedures can be eliminated using ductoscopy.

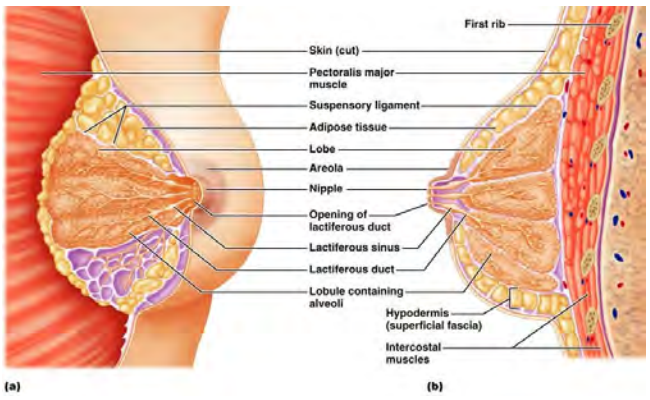

Figure 55: Breast anatomy [60].

A.1.2 Breast cancer

Breast cancer starts in the breast cells of both women and men, most often in the ductal epithelium. Worldwide, breast cancer is the second most common type of cancer after lung cancer. It accounts for 10.9% of all cancer diagnosis in both men and women and is the second leading cause of death in women. The National Breast Cancer Foundation has estimated around 200 000 new breast cancer cases and 40 000 deaths in women every year. The National Cancer Institute, estimates 207 090 new cases and 39 840 deaths due to breast cancer cases in women each year in the United States, despite recent advances in treatment [7].

The most common types of breast cancer are, (Fig. 56): Ductal carcinoma in situ (DCIS); Lobular carcinoma in situ (LCIS); Invasive (or infiltrating) ductal carcinoma (IDC) and Invasive lobular carcinoma (ILC)

Less common types of breast cancer are: Inflammatory breast cancer (IBC) and Paget disease of the nipple, illustrated on the left side of Figure 56.

Ductal Carcinoma In Situ (DCIS)

DCIS is a non-invasive or pre-invasive breast cancer, caused by the absence of spreading beyond the milk duct into any normal surrounding breast tissue. It is the earliest possible, most common and best treatable diagnosis of breast cancer. According to the American Cancer Society, about 60,000 cases of DCIS are diagnosed in the United States each year, about 25% of all breast cancers cases [62, 63].

Lobular carcinoma in situ (LCIS)

This non-invasive form of cancer is found in the lobules, the milk-producing glands at the end of the breast ducts and is less common then DCIS. LCIS will not always become ILC. However it increases the risk for invasive breast cancer, therefore close follow-up is very important.

Invasive (or infiltrating) Ductal Carcinoma (IDC)

This is the most common type of invasive breast cancer. IDC starts in the milk ducts of the breast, where after it spreads through the fatty tissue of the breast. Followed by the possibility of metastasizes to other parts of the body via the lymphatic system and bloodstream. IDC accounts for 80% of all invasive breast cancers [62].

Invasive (or infiltrating) Lobular Carcinoma (ILC)

ILC starts in the milk-producing glands (lobules) and is able to metastasize. More than 180 000 women are diagnosed with ILC each year, about 10% of all invasive breast cancers [62].

Inflammatory breast cancer (IBC)

This uncommon and aggressive type of invasive breast cancer accounts for about 1% to 3% of all breast cancers [64]. Due to the lack of a single lump or tumor this form of cancer is hard to diagnose. IBC makes the skin on the breast look red and feel warm, or it gives the breast skin a thick, pitted appearance.

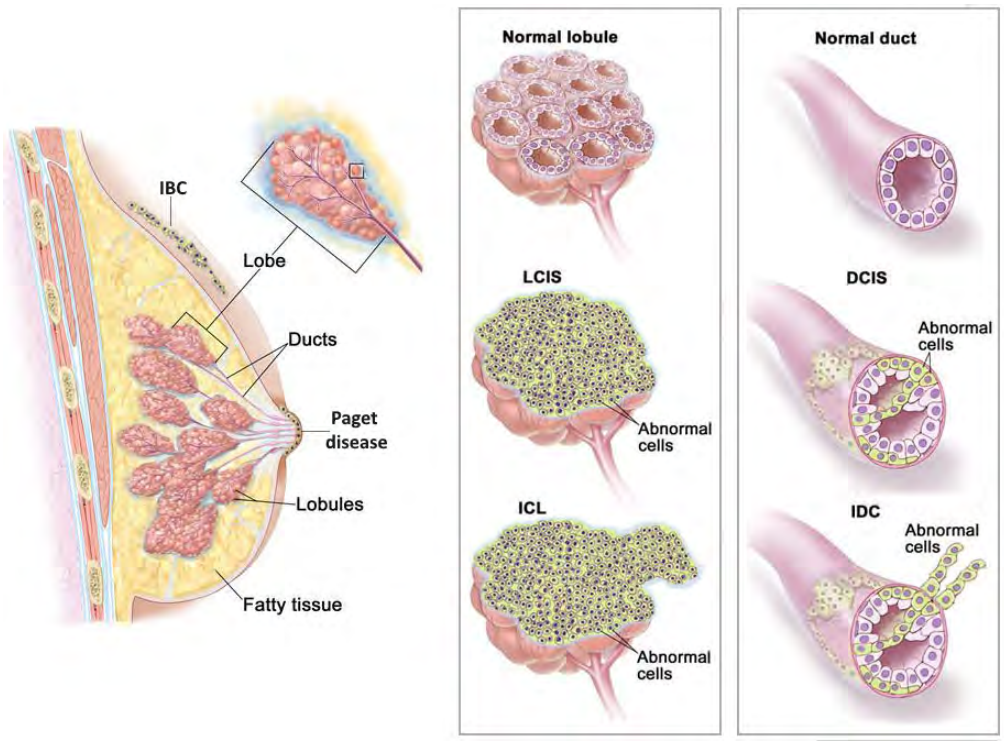

Figure 56: Breast cancer types: Ductal carcinoma in situ (DCIS), Lobular carcinoma in situ (LCIS), Invasive ductal carcinoma (IDC), Invasive lobular carcinoma (ILC), Inflammatory breast cancer (IBC) and Paget disease of the nipple, adapted from [61].

Paget disease of the nipple

This type of breast cancer starts in the breast ducts, spreading to the areola via the skin of the nipple. Most often it is associated with either DCIS or IDC. Treatment often requires mastectomy. Paget disiease accounts for only about 1% of all breast cancer cases [62].

A.2 Cancer diagnosis

Early diagnosis of breast cancer is considered vital, because statistics have shown a five-year survival rate of 96% for women whose cancer was detected in the early stages [7]. Although, ductoscopy seems to have an advantage over the other diagnosing methods. This section will elaborate on the performance of commonly used diagnosing methods such as cancer imaging techniques and biopsy methods.

A.2.1 Cancer imaging techniques

The currently used cancer imaging modalities include [7, 65–67]:

- Mammography
- Ultrasonography
- Magnetic Resonance Imaging (MRI)
- Optical Imaging
- Tomography
- Thermography
- Scintimammography

Mammography

Mammography applies low-dose x-ray imaging to create detailed images of the breast. Currently it is the only breast imaging examination method, which is proven to reduce breast cancer mortality. Hence, it is the preferred population-based method to detect early stage breast cancer before the lesions become clinically palpable. There are 2 types of mammography examination:

- Screening mammography: Performed in asymptomatic women; most often women in the risk-groups
- Diagnostic mammography: Performed in symptomatic women; when self-examination or mammographic screening shows an abnormality

Although mammography remains the most cost-effective approach for breast cancer screening, the sensitivity (67.8%) and specificity (75%) are not as high as other methods. However the sensitivity of mammography in high-risk women with dense breasts is even worse with a number in the range of 50% [65].

Another form of mammography is called Scintimammography, this technique use radioisotopes to visualize lesions of the breast. This method is capable to detect breast cancer in dense tissue, reducing the difficulties found in mammography. Scintimammography is able to image breasts with implants, large and palpable abnormalities, and it can be used when multiple tumors are suspected [68].

Ultrasonography

The ultrasound transducer directs high-frequency sound waves into the breast tissues and detects the reflected sound waves. Doing so the ultrasound image can detect breast lesions and is used as an adjunct tool for detecting the location of the suspicious lesion, after mammography or physical examination. Ultrasound is inexpensive, utilizes no radiation, and is widely available. However as a screening method, ultrasonography is limited by a number of factors, it is unable to detect microcalcifications and has a poor specificity (34%) [65].

Therefor, ultrasonographic screening is only recommended for for special situations, such as highly anxious patients who request it or for women who have a history of mammographically occult carcinoma.

Magnetic Resonance Imaging (MRI)

MRI has been explored as a modality for detecting breast cancer in high risk women and in younger women, due to the absence of radiation. MRI has proven to be exquisitely sensitive for the detection of breast cancer, with a sensitivity range from 79% to 98% to malignant changes in the breast [67]. However, MRI has limited use as a general screening tool, with a 10-fold higher cost than mammography and poor specificity (26%), resulting in an increase of false-positive reads that generate significant additional diagnostic costs and procedures [65]. However MRI remains the most sensitive examination for the detection of early-stage breast cancer in a high-risk screening population [67].

Optical Imaging

Optical imaging uses near infrared (NIR) wavelength light to detect lesions inside the breast [7]. An advantage of this method is the absence of radiation and breast compression. Due to the fact that Optical imaging is a recently discovered method, more research needs to be conducted before it can be used in clinics [66].

Tomography

Tomographic breast imaging techniques include: Positron Emission Tomography (PET), Electrical Impedance Tomography (EIT) and Computed Tomography (CT).

PET includes a nuclear medicine, which exist of a radionuclide that emits γ-rays. These rays are then detected by the imaging techniques producing three dimensional images. The contrast on PET images between normal and cancerous cells is caused by the increased glucose metabolism in malignant tumors compared with normal cells. The downside of using this method is the high cost and the poor resolution images. Furthermore, when PET is used the patient will be subjected to radiation exposure [69].

During EIT the lower impedance levels of the cancerous breast tissues, compared to normal tissues, create the possibility to image the potential lesions. In EIT, 2D or 3D images are reconstructed from a large number of impedance values, which are captured by placing electrodes around the breast surface in a circular fashion. When EIT is used there is no need to compress the breast and an absence of radiation. It is approved by the Food and Drug Administration (FDA) to help classify tumors found on mammograms. But more clinical testing should be done before it is used in breast cancer screening [7, 66].

CT scans generate 2D images by applying X-rays on the body parts that need to be examined. Where after algorithms are used to generate a corresponding 3D images, which provide more anatomical information such as the location of the malignant tumors. One of the downsides of CT is the low contrast [7].

Thermography

In Thermography the higher metabolic rate and the corresponding higher temperature emitted by the cancerous and pre-cancerous tissues, create the possibility to image the lesions. These effects are caused by the higher metabolic rate, which increases the growth of new blood vessels, delivering nutrients to the fast growing cancer cells. Resulting, in an increased temperature of the area surrounding the pre-cancerous and cancerous breast tissue, compared to normal breast tissue temperatures [7].

A.3 Biopsy methods

When a suspected lesion is found the next step is to perform a biopsy. The definition of a biopsy is: a sample of tissue removed from a living body in order to examine it for the presence, cause, or extent of a disease.

A breast biopsy is performed to remove cells from a suspicious area in the breast for examination and under a microscope. This can be performed surgically or, more commonly, by a radiologist using a less invasive procedure that involves a hollow needle and image-guidance.

There are 2 types of surgical biopsies:

- Incisional biopsy; removes only a small part of the suspicious lesion, to make a diagnosis. This biopsy type is used during:
  - Fine Needle Aspiration Biopsy (FNAB)
  - Core Needle Biopsy (CNB)
  - Vacuum-Assisted Biopsy (VAB)
- Excisional biopsy; removes the entire tumor or suspicious lesion, with or without trying to remove a small portion of normal breast tissue depending on the reason of the excisional biopsy. It is performed during:
  - Surgical Biopsy

Fine Needle Aspiration Biopsy (FNAB)

The simplest type of breast biopsy and evaluates an abnormal growth that can be felt during a clinical breast exam. It removes only a very small portion of the lesion.

The 22-27 gauge (0.361-0.64mm) needle is attached to a syringe to collect a sample of cells or fluid from the lump, sometimes performed under the guidance of ultrasound [70]. Fine-needle aspiration is a quick way to distinguish between a fluid-filled cyst and a solid mass, and could possibly avoid a more invasive biopsy procedure. If, however, the mass is solid, it will need further evaluation [71].

FNAB has a very low false-positive rate. However, the false-negative rate is much higher [72], due to the small sample area. If no malignant cells are detected using FNAB, many surgeons will proceed with excisional biopsy to definitely exclude the possibility of cancer.

Although, FNAB has a limited ability to specifically diagnose benign lesions and has no ability to differentiate between in situ and invasive breast cancer, it is inexpensive, quick, readily available, and very safe.

Sensitivity: 75.8-98.7% Specificity: 60-100%, Positive Predictive Value: 93.5-100% [70]

Core Needle Biospy (CNB)

Core needle biopsy assesses a lesion visible on a mammogram or ultrasound, or palpable by the doctor during a clinical breast exam. A radiologist or surgeon uses a, 11-20 gauge (0.81-2.31mm), hollow needle to remove tissue samples from the breast mass, most often with ultrasound-guided core needle biopsy [71].

Several samples, each about the size of a grain of rice, are collected and analyzed to identify features indicating the presence of diseases [71]. Depending on the lesions location different methods are performed such as stereotactic-guided core-needle biopsy, a method which uses mammography or MRI, to guide the core needle to the right position.

The advantage over FNAB is the ability to perform additional studies on the biopsy and the more specific diagnostic abilities. However, CNB is more expensive and time consuming than FNA [70].

Sensitivity: 91-99.6%, Specificity: 98-100%, Positive Predictive Value: 98-100% [70, 73]

Vacuum Assisted Biopsy (VAB)

VAB also known as Vacuum Assisted Device biopsy (VAD), a needle, 11-14 gauge (1.63-2.31mm), is inserted through the skin to the site of the abnormality, where vacuum pressure enables the surgeon to collect and remove a sample for analysis. VAB is able to retreat several samples without withdrawing and reinserting the needle by rotating the instrument. Typically, eight to 10 samples of tissue are collected from around the lesion [74].

Sensitivity: 92-100%, Specificity: 100%, Positive Predictive Value: 100% [73, 75]

Surgical Biopsy

During surgical biopsy, the surgeon removes all (excisional biopsy) or part (incisional biopsy) of the abnormal lesion. Often a small amount of normal-looking tissue, known as the "margin" is contained as well. If the lump cannot be easily felt, the surgeon can use a mammogram or ultrasound, or mark the location of the suspicious lesion using wire localization [74]. During wire localization a needle is inserted containing a small wire. The tip of the needle is placed near the abnormal tissue under mammographic guidance, where after the wire is secured.

A.4 Questionnaire

On the 4th of July a questionnaire was held at the Medical center in Utrecht (UMCU). Attending this meeting from Utrecht; surgeon A.J. Witkamp, pathologist P. van Diest clinical physicist T. de Boorder, from the Tu Delft; P. Breedveld and A. Sakes. In advance a questionnaire was sent to all attendees and the questions where answered during a one hour meeting.

1 Q) What is the advantage of using a ductoscope over stereotactic-guided biopsy (MRI or Mammography).

1 A) With ductoscopy lesions can be visualised that are impossible to see on any other method.

2 Q) Is the instrument used during both pathological nipple discharge (PND) and breast cancer diagnosis.

2 A) Yes

3 Q) What are the concerns using the current biopsy devices; size, shape, usability etc.

3 A) Can't be used during ductoscopy, and are not able to visualise the lesion during the biopsy procedure, therefore the current devices are more harm full.

4 Q) What needle diameter and length are needed.

4 A) Comparable to the current ductoscopic instrument, ±1mm in diameter and ±100mm in length.

5 Q) Is it needed to reach the Terminal ductlobular unit (TDLU) and is it possible to give an indication of the diameter of both the Milk ducts and the TDLU.

5 A) The ductoscope should reach as far as possible into the ductal system however it isn't needed to go into the TDLU, certainly not for the first prototypes which should prove the working principle.

6 Q) Does a fluid exists which enlarges the duct diameter, if this is the case is an irrigation channel needed.

6 A) Yes, there is a fluid which enlarges the milk ducts, which is used during all procedures. The fluid is proceeded to the tip of the instrument via the cannula, however no real channel is needed to irrigate the fluid.

7 Q) Is it possible to give an indication of the tissue stiffness of breast tissue, Papilloma, Ductal carcinoma in situ (DCIS), Invasive ductal carcinoma (IDC) and Invasive lobular carcinoma (ILC).

7 A) Papilloma is mushy, where as the different cancer types are comparable to an Adipose tissue.

8 Q) Do you wish to take several samples without leaving the malign side, such as happens during VAB, or is one sample enough due to the small lesion.

8 A) It will suffice to take one sample, because the lesion is clearly visible.

9 Q) Is there a minimal volume needed to analyze the sample (sample size), the current smallest size is 20 gauge by 1cm, resulting in a maximal volume of 254.5 mm^3.

9 A) The minimal volume is 10 cells which all have to be in perfect condition therefore it is preferred to use a blade cut the lesion from the side instead of using suction.

10 Q) Is it needed to see the malign tissue while taking the sample.

10 A) It is not necessarily to see the malign tissue during the cut, however the surgeon should be certain that the instrument engulfs the malign lesion when taking the tissue sample.

11 Q) What cutting method is preferred an end cut or a side cut.

11 A) A front cut is preferred due to the better visibility, however an end cut can be used as well when the surgeon is able to see the lesion during the procedure.

12 Q) Are the requirements for the visualization system known and what are the dimensions.

12 A) Yes, an auto fluorescence endoscopic imaging system (OncoLIFE, Xillix Technologies Corporation, British Columbia, Canada, now Pinpoint, NOvadaq Technologies Corporation, Ontario Canada).

13 Q) What steps are taken during the procedure.

13 A) At first the nipple is anaesthetised, where after a trocar is placed to enlarge the nipple orifice, than the canula containing the ductoscope is inserted through the trocar and a fluid is inserted to enlarge the ducts, where after the surgeon can visualize the ductal system.

14 Q) Is there a possibility to preform some tests on human breast tissue.

14 A) Yes, this is possible in Utrecht.

Side note

To ensure the best quality samples it is desirable to use a fixation fluid (Formaline) as quickly as possible.

A.5 Pilot experiment

A.5.1 Purpose

This section will discuss the results of the pilot tests, conducted to determine if all the variables could be measured and analysed, given the found sensor data and video feed. The pilot test also examines the ideal velocity to compare the knife designs and the knife rotation configurations. Besides checking the measurement protocol the pilot test will also determine which knife is used during the velocity tests.

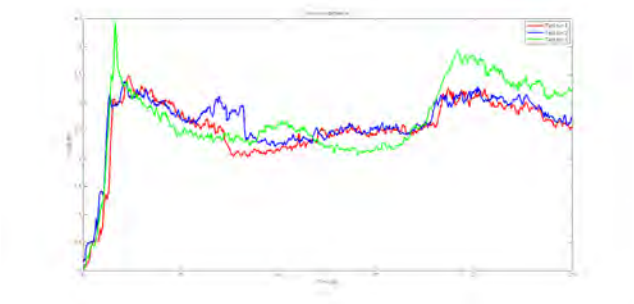

Figure 57: Differences in Force distributions.

A.5.2 Force measurement

Tangential force Characteristics

The biopsy instrument consists of a slender stainless steel tube or "cannula" containing two cutting tubes. The cutting tubes have a sharp tip at the end of the slender shaft. The hollow space inside the inner cutting tube is called the lumen, inside the lumen the ductoscope is placed to examine the milk duct. The tip of the cutting tubes consists of a cut out as was explained before, in all but the straight cut out the cutting surface exists of a point which moves along the cut out length whereas the Straight knifes cutting surface has a constant surface area. The tangential force is defined here as the force acting on the biopsy instruments knife hub in the direction of insertion. The tangential force consists of a puncture force, debulking force and a friction force created during the gelatin puncture process.

Friction forces

When needle insertion theory is interpreted the axial load distribution was found to be largely uniform, when the needle is inserted into homogeneous isotropic artificial materials. The question now is whether this is also true when a tangential motion is used to insert/cut the material. If the load distribution turns out to be uniform, it results in a linear rise of the friction force with the insertion distance. When the normal force exerted by the linear stage is contact and the coefficient of friction is the same during the entire knife movement. To determine if the theory will hold, the friction force needs to be measured.

In needle-tissue interaction literature several different approaches can be adopted to measure the friction forces acting on the needle or in this case the knife. One method is to assume that the forces acting on the needle during withdraw are solely caused by the friction, which allows for a direct friction force measurement [76, 77].

A second method suggest to exclude the needle tip, done by pushing the needle tip through the tissue phantom, resulting in a friction force exerted by the instrument and the tissue cannula.

Another approach is to measure the force acting on the tip as well as the total force [40]. In Addition, friction force can also be determined using an in explicit method, which uses a force-position diagram.

This study will measure the friction force by determining the forces exerted on the helix tube, otherwise explained as the operation force. Due to the constant rotation velocity the forces can be related to time.

A.5.3 Exclusion Tangential forces

In advance of the pilot test it was thought the friction forces inside the instrument might give a constant value for constant velocities. When this is the case the axial operation forces, minus the constant friction force, results in the tangential force caused by the tissue resisting the deformation. Resulting in the ability to determine the tangential force, which can be derived to the phantom penetration function.

However, initial testing resulted in the elimination of the load cell data, due to large disturbances in the measurements. Figure 57 contains the force disturbances of three consecutive runs, measured under the same conditions. As can be seen there is a wide range in the force disturbance, with a maximum difference of 1.61 N. Due to the large differences between runs the exerted gelatin penetration force is unnoticeable in the data.

The gelatin penetration force is estimated using the given gelatin Young's modules, namely 150 kPa and the knife surface accounting for a maximal area of $3 \cdot 0.1 = 0.3\ mm^2$. This force is an estimation, which doesn't include the nonlinear effects of gelatin, the sharpened edges and the different cut out designs. However, the force will not be higher when these characteristics are accounted for. The following formula calculates a rough estimate of the involved forces:

$$F = E \cdot A = (150 \cdot 10^3) \cdot (3 \cdot 10^{-3} \cdot 1 \cdot 10^{-4}) = 4.5\dot{1}0^{-2}\ [N]$$

When the calculated penetration force is compared to the maximal difference between runs, shown in Figure 57, it can be concluded that the found force distribution is useless in estimating the tangential forces, resulting in the gelatin penetration forces.

Concluding, although the force measurements had the needed accuracy to determine the gelatin debulking forces, $\pm 0.5\dot{1}0^{-2}$ with a possibility to use a more accurate sensor, it was unable to provide usable data, about the tangential forces. Therefore the tangential force measurements will be excluded from further results.

A.5.4 Adaptation of experiment

The pilot experiment also determined, if the set parameters needed to be adapted before the actual experiment started. During these initial tests the tissue mimicking phantom and the biopsy phases were adapted to improve the experiment.

Tissue stiffness

The influence of the tissue stiffness is tested on artificial tissue in the form of gelatin, the stiffness and non-linear effects will not be the same as in real life operations. Therefore it is important to determine if the same results hold for other tissue stiffnesses as well.

Using the 0.5 ± 0.1 mm thick gelatin sheets with stiffnesses ranging from normal breast tissue (30 kPa) to IDC (150 kPa), created by changing the weight percentage of the 250 bloom type A gelatin, from 5 $wt\%$ to 20 $wt\%$, caused a problem. Because the sheets were very thin, the water inside the lower stiffness gelatin sheets evaporated quickly creating an uncontrollable tissue stiffness. During tests with 10 $wt\%$ the gelatin sheets became solid within an hour, preforming tests with the 20 $wt\%$ gelatin increased this time to six hours. Due to the longer solidification time it was assumed that when the 20 $wt\%$ gelatin was used within two hours from taking it out of the refrigerator the results would be good to compare.

As this study holds a proof of principle for the novel biopsy instrument, a constant tissue stiffness comparable with the stiffest tissue found during ductoscopy is used, namely 150 kPa, equal to the stiffness of IDC. Using this constant stiffness tissue phantom will generate first insights in the ability of the biopsy tip.

When the knifes are able to cut the high stiffness gelatin, it is assumed that the knifes will be able to debulk lower stiffness tissue as well.

Knife positioning

Initial testing of the knife rotation configurations, preformed in the pilot tests, shows the importance of knife placement during this procedure. When the fixated knife is positioned directly under the gelatin, as is shown in Figure 58:left, the rotating knife acts as a single-sided knife, only exerting an action force, caused by the inability of the fixated knife to exert the reaction force, resulting in an upward motion of the gelatin, and the inability to cut the tissue. When the fixated knife was positioned against the gelatin, shown in Figure 58:right, the tissue is debulked. This difference is caused by the reaction force delivered by the fixated knife.

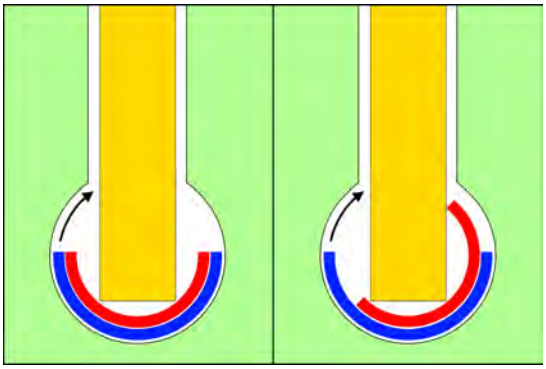

Figure 58: Schematic drawing of knife positioning. Left: The fixated knife (Red) is positioned directly beneath the gelatin creating a single sided cut. Right: The fixated knife (Red) is positioned against the gelatin creating the ideal position to debulk the tissue. Blue: the outer knife, Red: The inner knife, Yellow: The gelatin and Green: The perspex duct.

A.5.5 Determination of constants

Ideal knife operation velocity

Conducting the experiment in a repeatable manner is of great importance, due to the small amount of repetitions made during the actual experiment, increasing the chance of finding comparable results, was the main reason to conduct the pilot tests. Determining the ideal operation velocity as well as the best suited knife design used during the velocity comparisons increased the ability to compare the results.

The ideal knife operation velocity is found by varying the linear stage velocities. Because the used linear stage couldn't be programmed very precisely the lowest possible stage velocity was 0.413 mm/s, or in rounds per minute 7.88 *RPM*, where after the velocity could be increased with steps equal to this velocity. The four chosen velocities are 15.76 *RPM*, 31.51 *RPM*, 55.15 *RPM* and 94.54 *RPM*. These velocities gave the full range of moving the knifes very slowly to a rapid movement of the knifes.

Determining the ideal velocity to compare the different knife designs was done by performing several test for all the different velocities. When these tests were examined they showed a preference to a slower movement of the knifes. Because the prototype wasn't proven to work over and over again, the slowest speed was chosen to prevent the possibility of damaging the instrument.

Another factor contributing to this choice was the ability to debulk the gelatin when it was positioned near the edges of the knife, when a higher velocity was used in some of the tests the gelatin was pushed up, by the rotational movement, because the gelatin wasn't fixated in the perspex duct. Although the slower moving knifes where not affected by the position of the gelatin, in these cases the gelatin was moved towards the center of the duct the ideal place for the debulking process. Due to the better ability to debulk the tissue with knifes rotating with slower velocities together with a reduced possibility for dynamic effect in the debulking process. The slowest knife operation velocity of 15.76 *RPM* was chosen as the ideal velocity for comparing the biopsy tips.

B Tissue entrapment methods

Table 5: An overview of the different possibilities to entrap the debulked tissue.

	Working principle	Industry	Medical	Biology
Gas	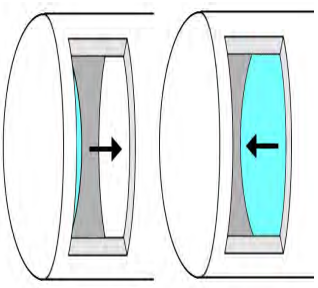	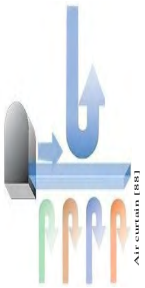 Air curtain [88]		
Liquid	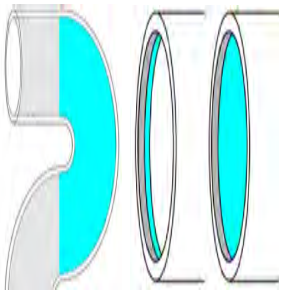	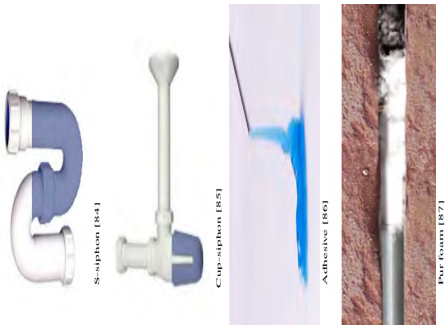 S-siphon [84] Cup-siphon [85] Adhesive [86] Pur foam [87]	 Ur-light earring [90]	 Ear wax [93]
Solid	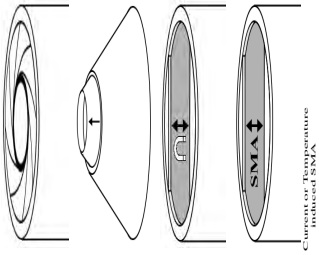 Current or Temperature induced SMA	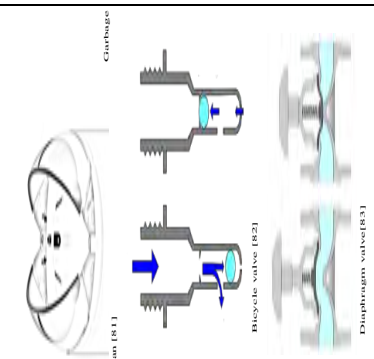 Garbage can [81] Bicycle valve [82] Diaphragm valve[83]	 Blood pressure monitor [89]	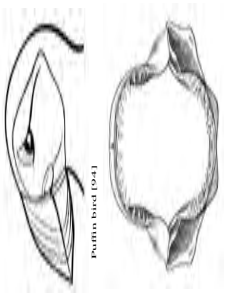 Puffin bird [94] Shark jaw [95]
	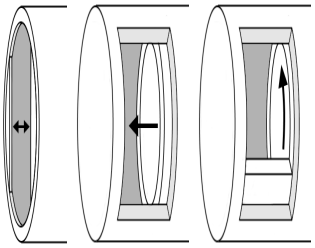	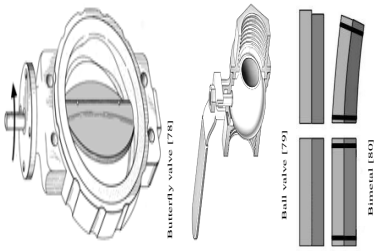 Butterfly valve [78] Ball valve [79] Bimetal [80]	 Tribard [89]	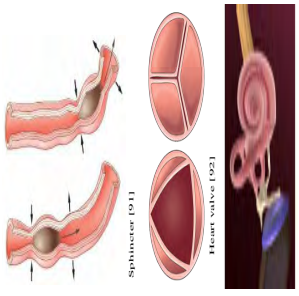 Sphincter [91] Heart valve [92] Ear drum [93]

C Drawings

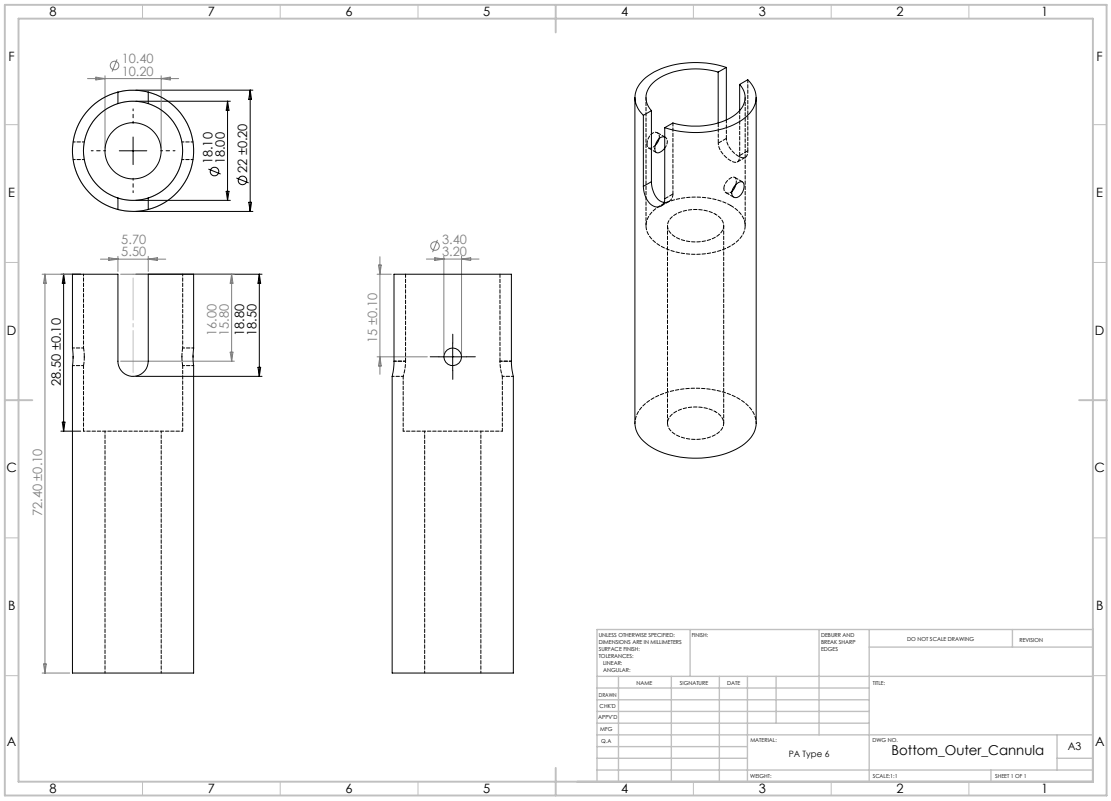

Figure 59: Outer shell bottom.

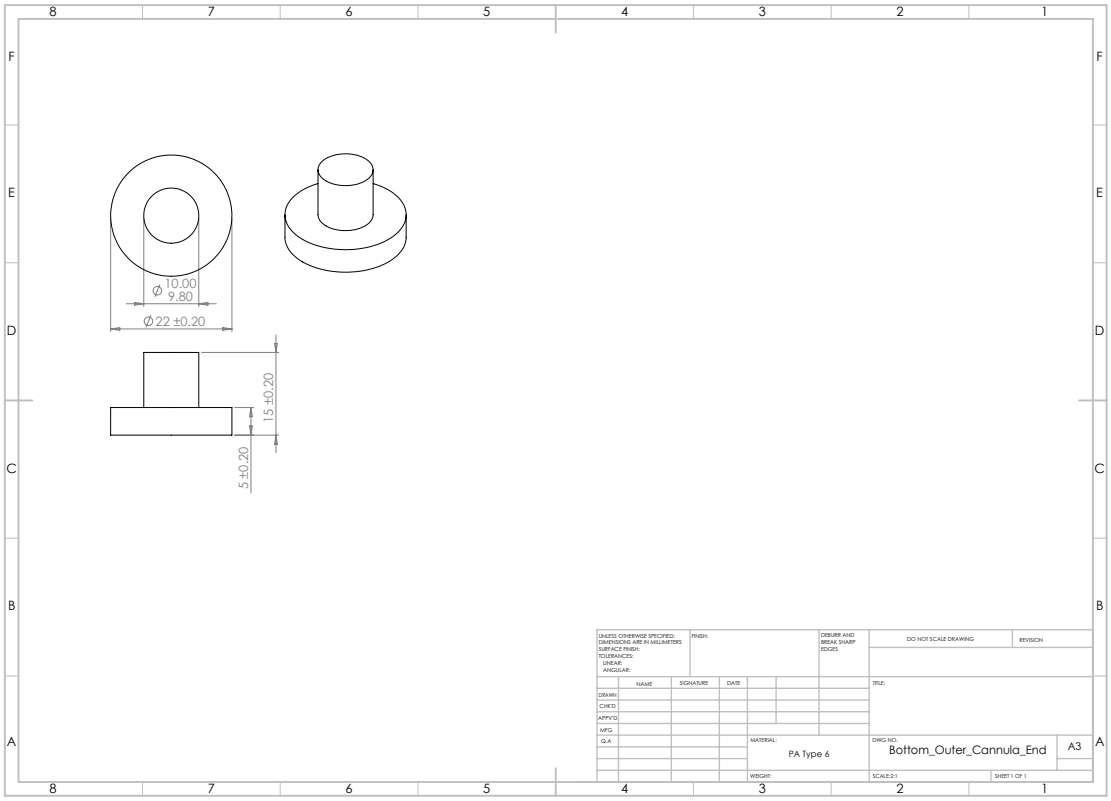

Figure 60: Outer shell bottom end.

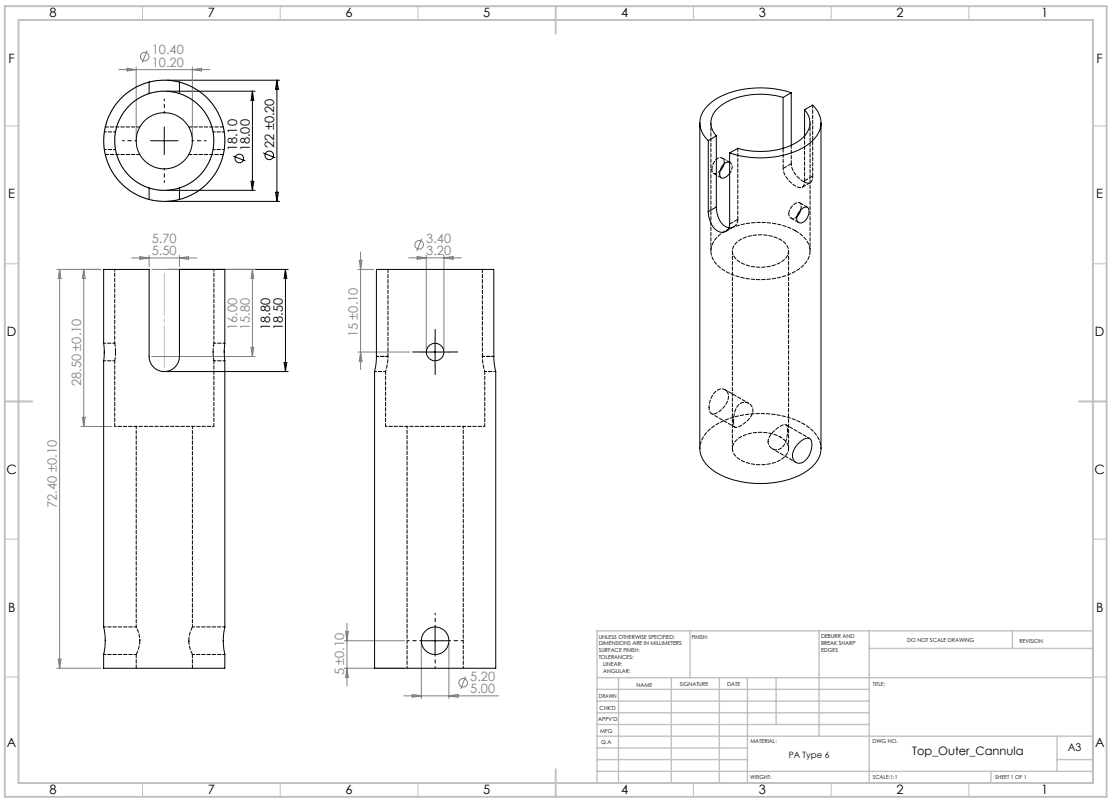

Figure 61: Outer shell top.

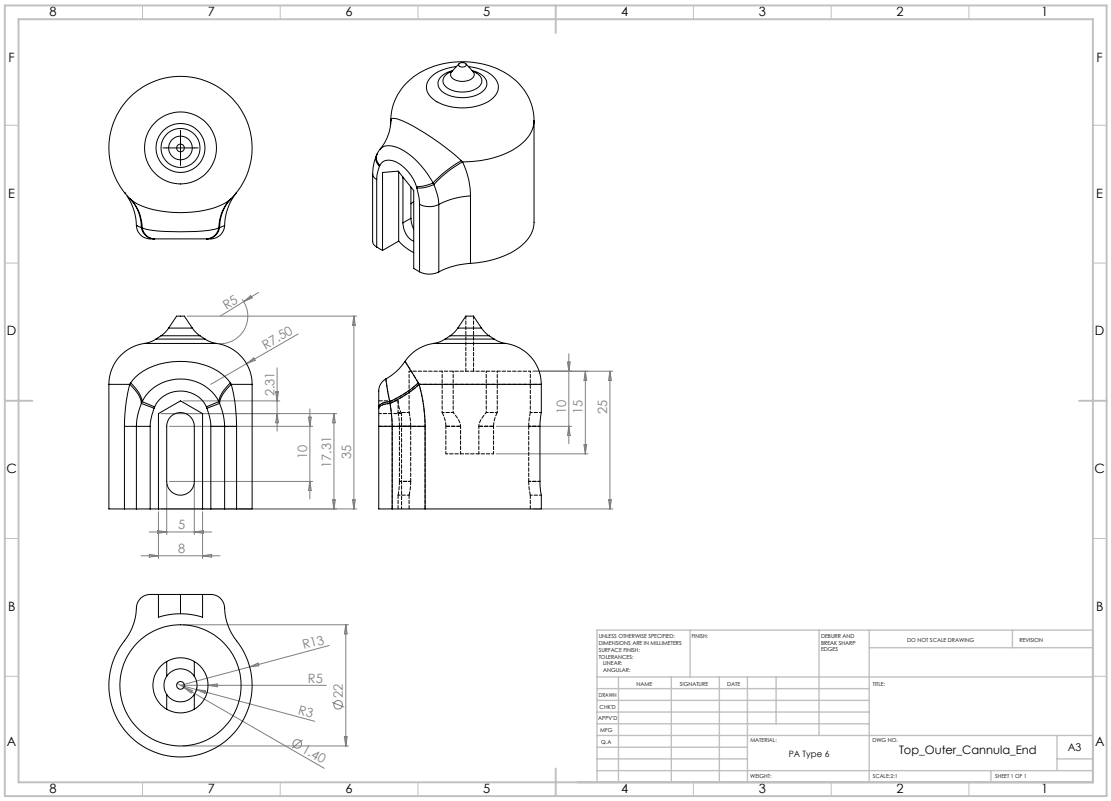

Figure 62: Outer sleeve.

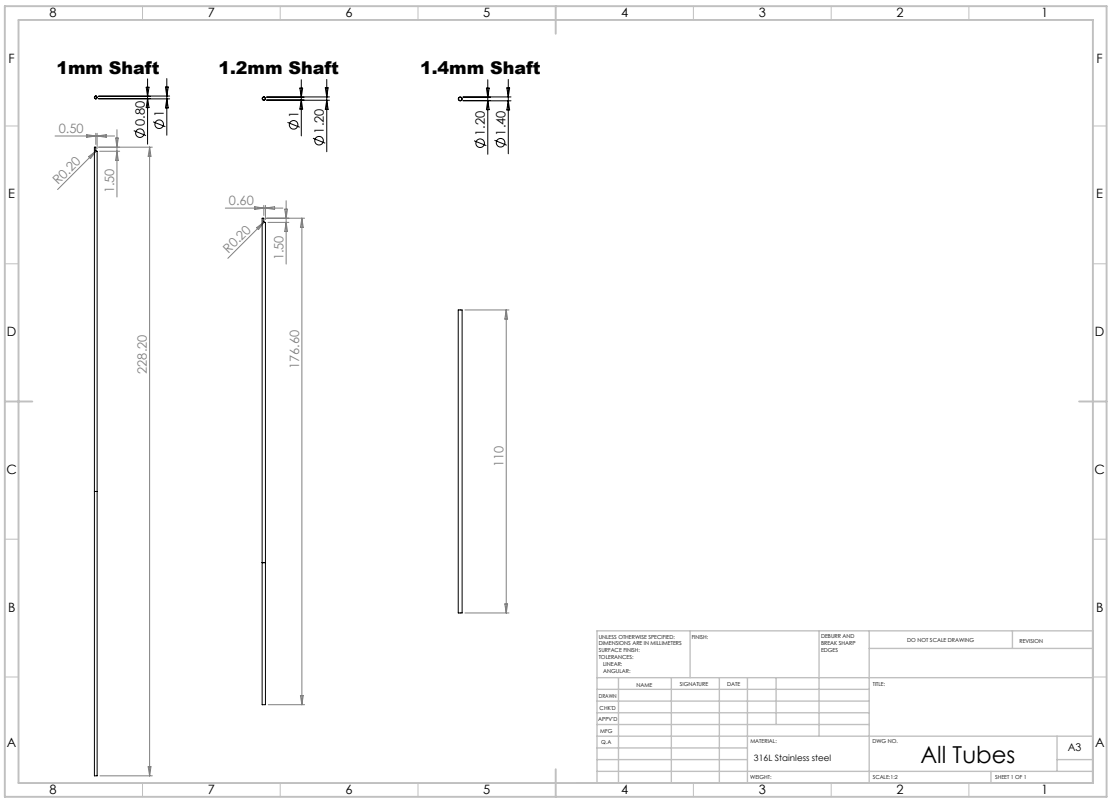

Figure 63: Straight cutting tube

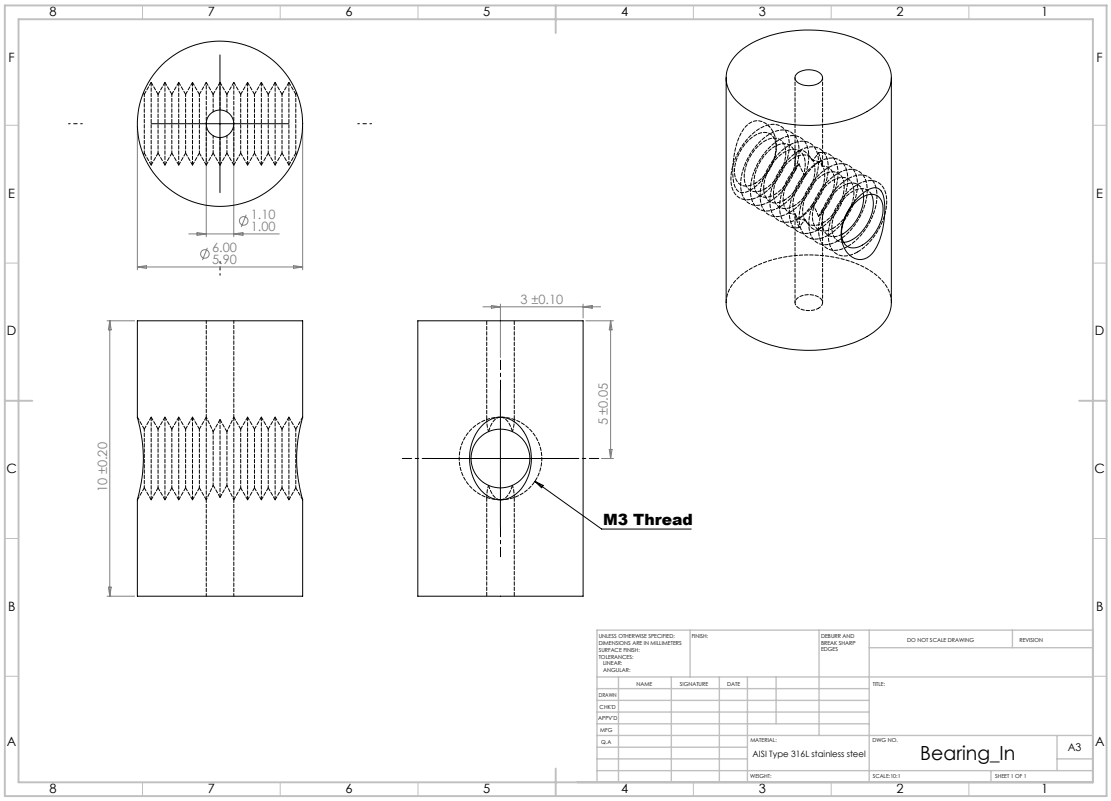

Figure 64: Inner bearing.

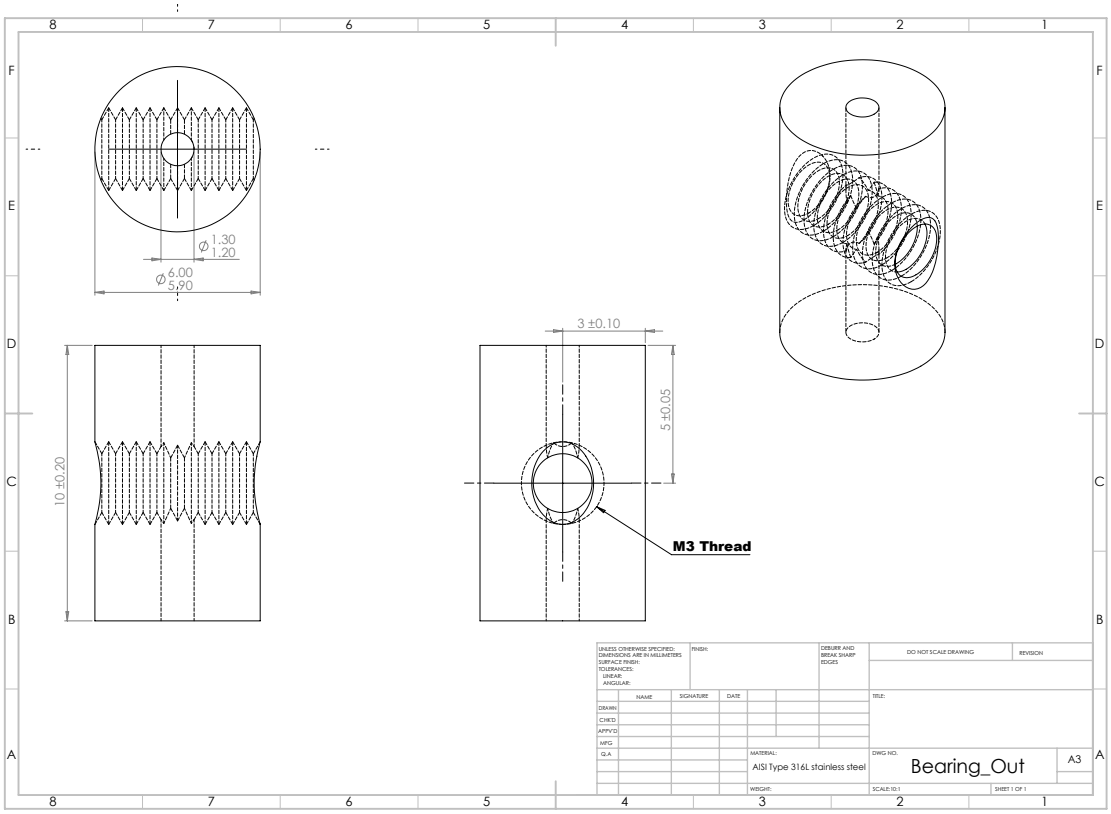

Figure 65: Outer bearing.

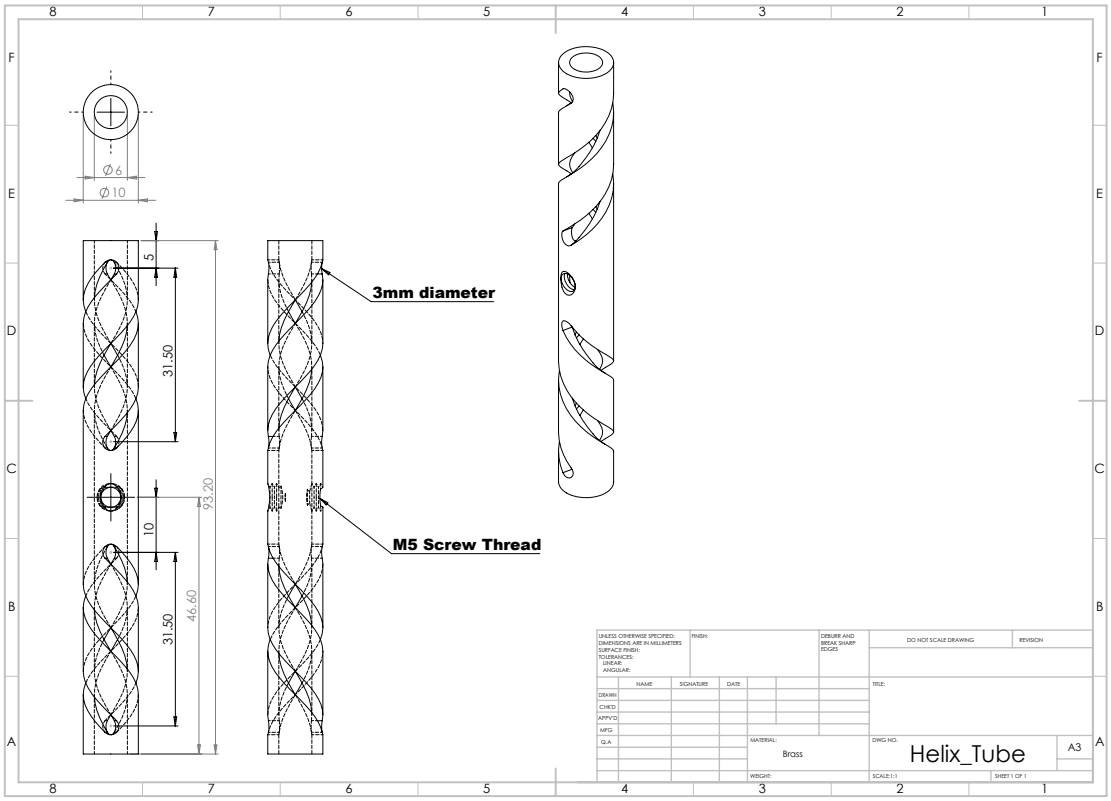

Figure 66: Helix tube.

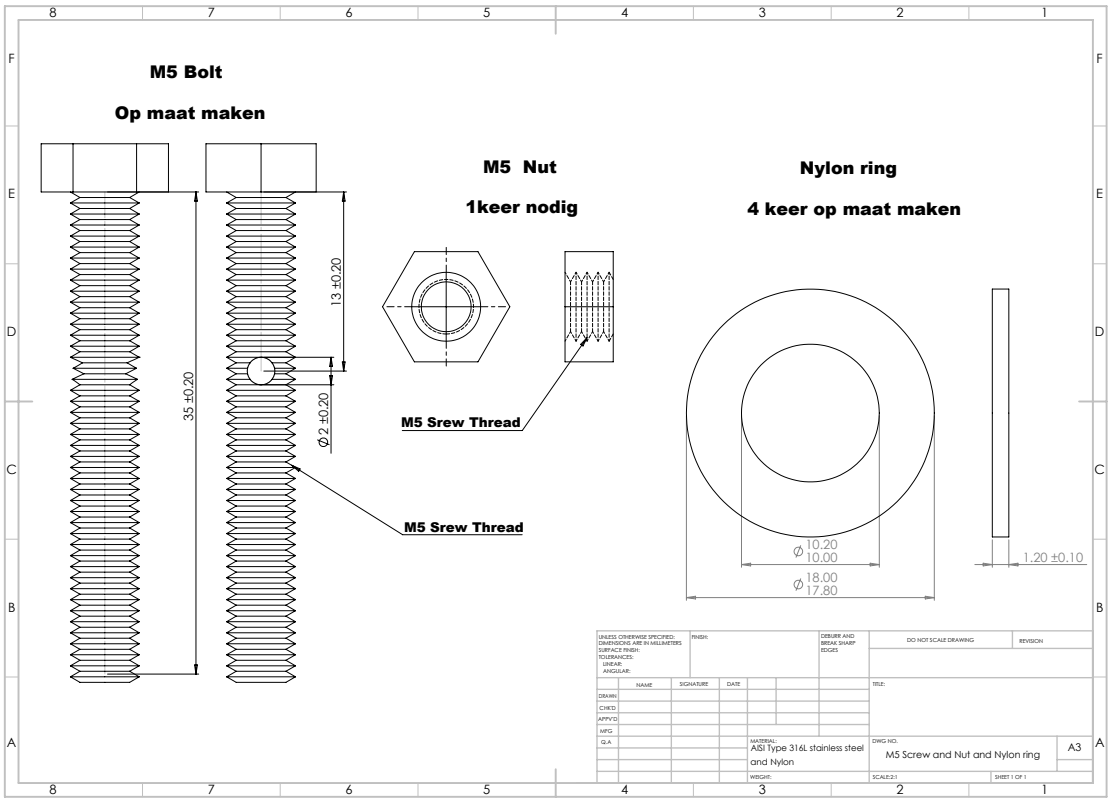

Figure 67: Nylon rings.

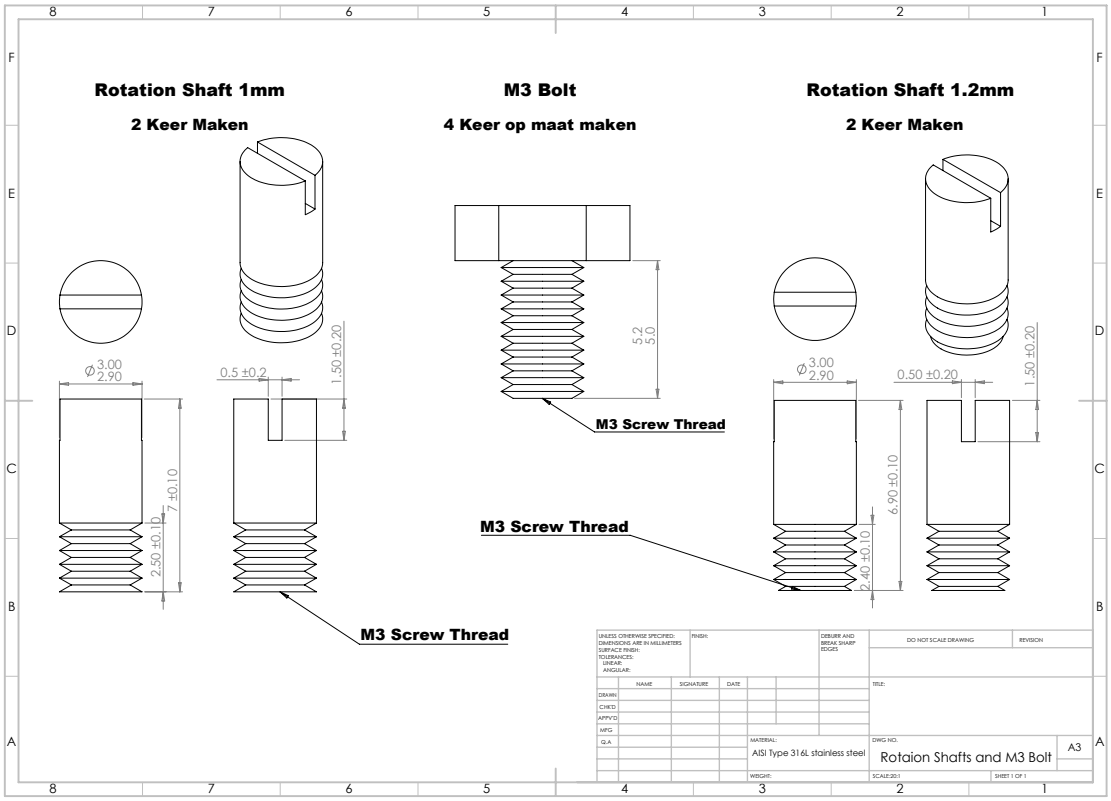

Figure 68: Bearing rotating pins.

D Data analysing

D.1 Q-programmer

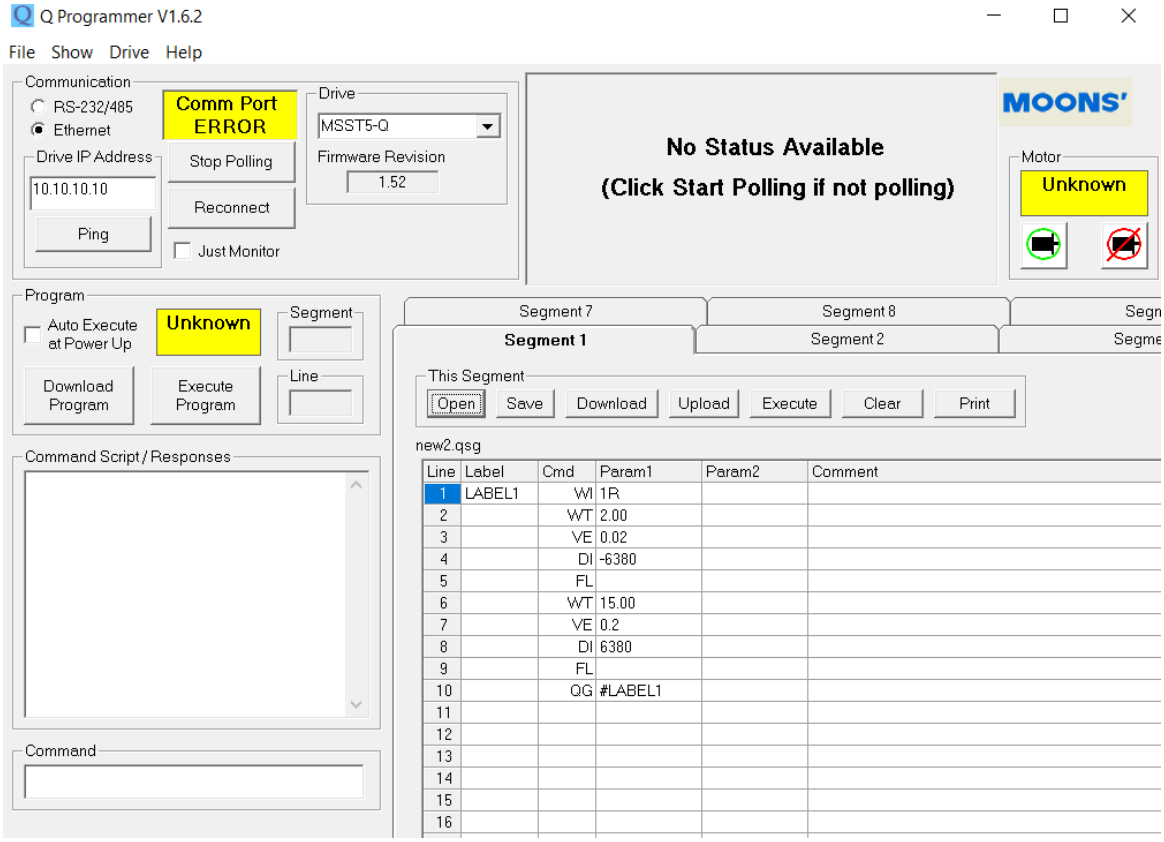

Figure 69: Q-programmer input.

D.2 Labview

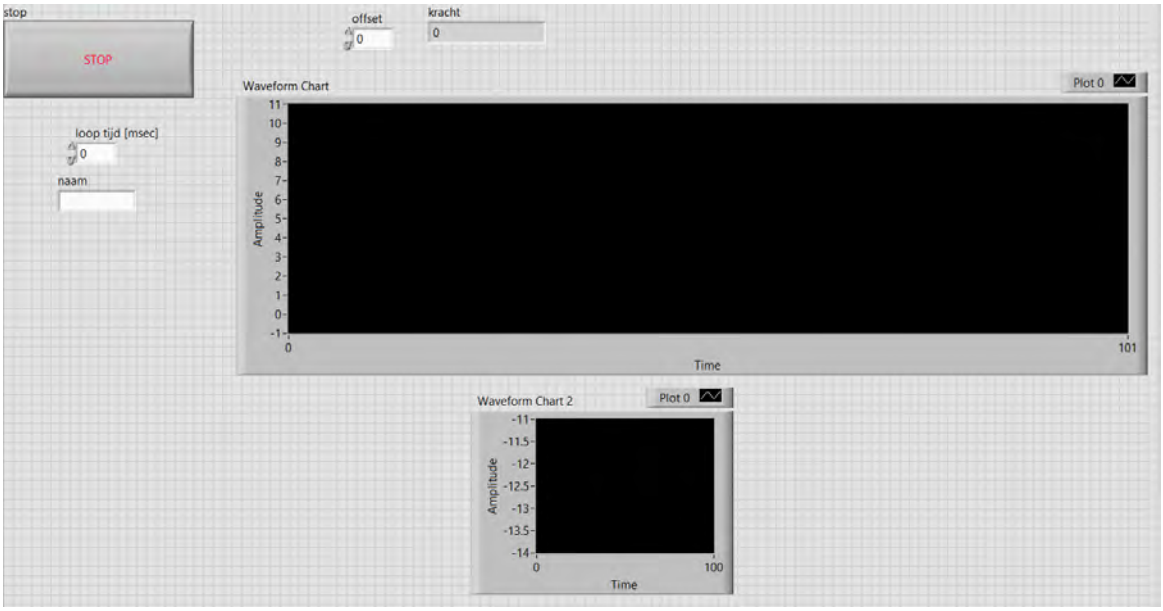

Figure 70: Labview initial GUI.

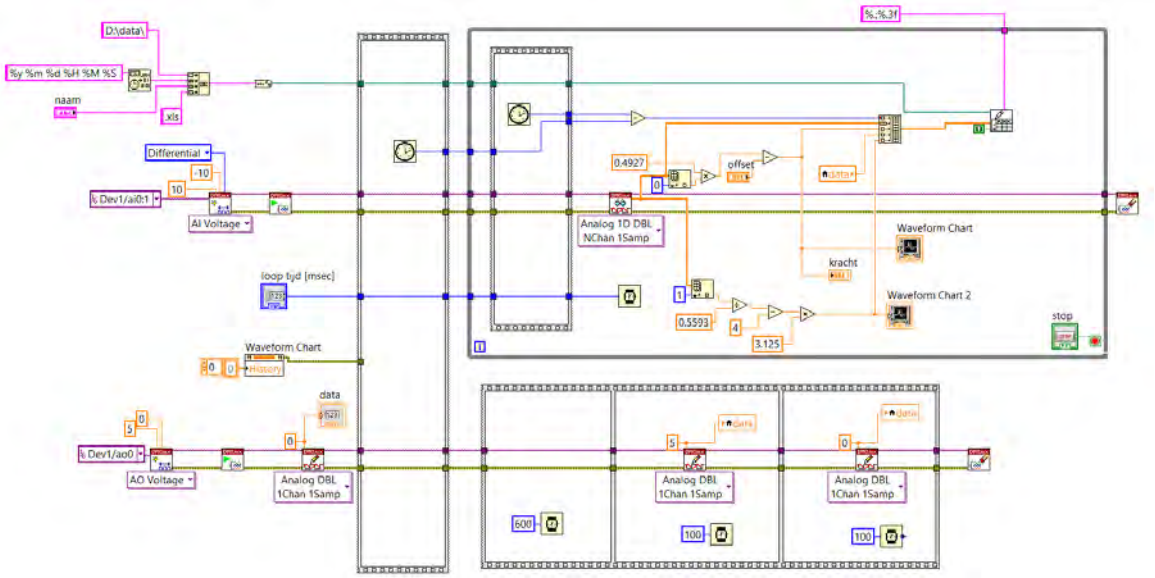

Figure 71: Labview block-diagram

.

D.3 Matlab Code

```
E = 150*10^3;   % Young's modulus Gelatin

D_o = 1.2*10^-3;    % Outer tube diameter 1.2 mm
D_i = 0.9*10^-3;    % Inner tube diameter 0.9 mm

d_1  = 0.1*10^-3;   % Tube Thickness 0.1 mm
d_05 = 0.05*10^-3;  % Tube Thickness 0.05 mm

y_o = D_o/2;        % Half outer tube diameter 0.6 mm
y_i = D_i/2;        % Half inner tube diameter 0.45 mm

L_3  = 3*10^-3;     % Cut out length 3mm
L_10 = 10*10^-3;    % Cut out length 10 mm


A_3_1   = L_3*d_1;      % Frontal area cut out 3mm x 0.1mm
A_3_05  = L_3*d_05;     % Frontal area cut out 3mm x 0.05mm
A_10_1  = L_10*d_1;     % Frontal area cut out 10mm x 0.1mm
A_10_05 = L_10*d_05;    % Frontal area cut out 10mm x 0.05mm

F_3_1   = E*A_3_1;      % Force needed to cut the tissue 3mm x 0.1mm
F_3_05  = E*A_3_05;     % Force needed to cut the tissue 3mm x 0.05mm
F_10_1  = E*A_10_1;     % Force needed to cut the tissue 10mm x 0.1mm
F_10_05 = E*A_10_05;    % Force needed to cut the tissue 10mm x 0.05mm

r_3  = L_3/2;        % Moment arm 3mm
r_10 = L_10/2;       % Moment arm 10mm

M_3_1  = F_3_1*r_3;         % Moment on the tube 3mm x 0.1mm
M_3_05  = F_3_05*r_3;       % Moment on the tube 3mm x 0.05mm
M_10_1 = F_10_1*r_10;       % Moment on the tube 10mm x 0.1mm
M_10_05 = F_10_05*r_10;     % Moment on the tube 10mm x 0.05mm

I_o_1 = (D_o^4-d_1^4)/145.7-D_o^2*d_1^2*(D_o-d_1)/(56.5*(D_o+d_1));
                % Secondairy moment of inertia half a tube 1.2mm x 0.1
I_i_1 = (D_i^4-d_1^4)/145.7-D_i^2*d_1^2*(D_i-d_1)/(56.5*(D_i+d_1));
                % Secondairy moment of inertia half a tube 0.9mm x 0.1
I_o_05 = (D_o^4-d_05^4)/145.7-D_o^2*d_05^2*(D_o-d_05)/(56.5*(D_o+d_05));
                % Secondairy moment of inertia half a tube 1.2mm x 0.05
I_i_05 = (D_i^4-d_05^4)/145.7-D_i^2*d_05^2*(D_i-d_05)/(56.5*(D_i+d_05));
                % Secondairy moment of inertia half a tube 0.9mm x 0.05

sigma_3_o_1  = (M_3_1*y_o)/I_o_1 % Stress 1.2mm x 0.1mm x 3mm
sigma_3_i_1  = (M_3_05*y_i)/I_i_1 % Stress 1.0mm x 0.1mm x 3mm
sigma_10_o_1 = (M_10_1*y_i)/I_o_1 % Stress 1.2mm x 0.1mm x 10mm
sigma_10_i_1 = (M_10_05*y_i)/I_i_1 % Stress 1.0mm x 0.1mm x 10mm

sigma_3_o_05  = (M_3_1*y_o)/I_o_05 % Stress 1.2mm x 0.05mm x 3mm
sigma_3_i_05  = (M_3_05*y_i)/I_i_05 % Stress 1.0mm x 0.05mm x 3mm
sigma_10_o_05 = (M_10_1*y_i)/I_o_05 % Stress 1.2mm x 0.05mm x 10mm
sigma_10_i_05 = (M_10_05*y_i)/I_i_05 % Stress 1.0mm x 0.05mm x 10mm
```

```
Operation  = xlsread('Operation2.xlsx');

Operation  = Operation(291:2790,:);

Counter    = Operation(:,1:3);
Single     = Operation(:,4:6);
One_blade  = Operation(:,7:9);

Mean_Counter   = mean(mean(Counter))
Mean_Single    = mean(mean(Single))
Mean_One_blade = mean(mean(One_blade))

Ratio_Operating_Force_C_O = Mean_Counter/Mean_One_blade
Ratio_Operating_Force_C_S = Mean_Counter/Mean_Single
Ratio_Operating_Force_S_O = Mean_Single/Mean_One_blade

Max_Counter_1 = max(Counter(:,1))
Max_Counter_2 = max(Counter(:,2))
Max_Counter_3 = max(Counter(:,3))

Max_Counter_1_2 = max(Counter(:,1)-Counter(:,2));
Min_Counter_1_2 = min(Counter(:,1)-Counter(:,2));

Max_Counter_2_3 = max(Counter(:,2)-Counter(:,3));
Min_Counter_2_3 = min(Counter(:,2)-Counter(:,3));

Max_Counter_1_3 = max(Counter(:,1)-Counter(:,3));
Min_Counter_1_3 = min(Counter(:,1)-Counter(:,3));


max_Counter   = max(Counter);
max_Single    = max(Single);
max_One_blade = max(One_blade);

std_Counter   = std(max_Counter)
std_Single    = std(max_Single)
std_One_blade = std(max_One_blade)



AvgMax_Counter   = mean(max_Counter)
AvgMax_Single    = mean(max_Single)
AvgMax_One_blade = mean(max_One_blade)

max_all =[max_Counter max_Single max_One_blade];

Max = max(max_all)



t2 = [1:1:2500]/100;

figure
plot(t2,Counter(:,1),'r','LineWidth',2);
hold on
plot(t2,Counter(:,2),'b','LineWidth',2);
plot(t2,Counter(:,3),'g','LineWidth',2);
title('Force disturbance')
xlabel('Time [s]')
ylabel('Force [N]')
legend('Test run 1','Test run 2','Test run 3')



figure
p1 = plot(t2,Counter(:,1),'r','LineWidth',2);
hold on
plot(t2,Counter(:,2),'r','LineWidth',2);
plot(t2,Counter(:,3),'r','LineWidth',2);

p3 = plot(t2,Single(:,1),'b','LineWidth',2);
plot(t2,Single(:,2),'b','LineWidth',2);
plot(t2,Single(:,3),'b','LineWidth',2);

```

```
p4 = plot(t2, One_blade(:,1),'g','LineWidth',2);
plot(t2, One_blade(:,2),'g','LineWidth',2);
plot(t2, One_blade(:,3),'g','LineWidth',2);

title('Operation force')
xlabel('Time [s]')
ylabel('Force [N]')

legend([p1 p3 p4],{'Counter rotation','Single rotation', 'One blade rotation'} )
```

```
close all
clear all
clc



%% Data Analyse (Run Once)
%D  = xlsread('A.xlsx');
%D1 = xlsread('A1.xlsx');
D_0_005  = xlsread('0.005.xlsx');
D_0_006  = xlsread('0.006.xlsx');
D_0_007  = xlsread('0.007.xlsx');
D_0_008  = xlsread('0.008.xlsx');
D_0_009  = xlsread('0.009.xlsx');
D_0_010  = xlsread('0.010.xlsx');
D_0_011  = xlsread('0.011.xlsx');
D_0_012  = xlsread('0.012.xlsx');
D_0_013  = xlsread('0.013.xlsx');
D_0_014  = xlsread('0.014.xlsx');
D_0_015  = xlsread('0.015.xlsx');
D_0_020  = xlsread('0.020.xlsx');
D_0_025  = xlsread('0.025.xlsx');
D_0_030  = xlsread('0.030.xlsx');
D_0_035  = xlsread('0.035.xlsx');
D_0_040  = xlsread('0.040.xlsx');
D_0_045  = xlsread('0.045.xlsx');
D_0_050  = xlsread('0.050.xlsx');


Time_start = 600;                                                   % [ms]
Dist_Push = 31.6;                                                   %
Dist_knife = pi*1;


Velocity_Q_programmer_0_005 = 0.005;                                 %[-]
Velocity_Q_programmer_0_006 = 0.006;                                 %[-]
Velocity_Q_programmer_0_007 = 0.007;                                 %[-]
Velocity_Q_programmer_0_008 = 0.008;                                 %[-]
Velocity_Q_programmer_0_009 = 0.009;                                 %[-]
Velocity_Q_programmer_0_010 = 0.010;                                 %[-]
Velocity_Q_programmer_0_011 = 0.011;                                 %[-]
Velocity_Q_programmer_0_012 = 0.012;                                 %[-]
Velocity_Q_programmer_0_013 = 0.013;                                 %[-]
Velocity_Q_programmer_0_014 = 0.014;                                 %[-]
Velocity_Q_programmer_0_015 = 0.015;                                 %[-]
Velocity_Q_programmer_0_020 = 0.020;                                 %[-]
Velocity_Q_programmer_0_025 = 0.025;                                 %[-]
Velocity_Q_programmer_0_030 = 0.030;                                 %[-]
Velocity_Q_programmer_0_035 = 0.035;                                 %[-]
Velocity_Q_programmer_0_040 = 0.040;                                 %[-]
Velocity_Q_programmer_0_045 = 0.045;                                 %[-]
Velocity_Q_programmer_0_050 = 0.050;                                 %[-]
Velocity_Q_programmer = 0.05;
%%

% M  = VectorLength(D,Time_start);
% M1 = VectorLength(D1,Time_start);

[Max_Dist_0_005, M_0_005] = VectorLength(D_0_005,Time_start);
[Max_Dist_0_006, M_0_006] = VectorLength(D_0_006,Time_start);
[Max_Dist_0_007, M_0_007] = VectorLength(D_0_007,Time_start);
[Max_Dist_0_008, M_0_008] = VectorLength(D_0_008,Time_start);
[Max_Dist_0_009, M_0_009] = VectorLength(D_0_009,Time_start);
```

```
[Max_Dist_0_010, M_0_010] = VectorLength(D_0_010,Time_start);
[Max_Dist_0_011, M_0_011] = VectorLength(D_0_011,Time_start);
[Max_Dist_0_012, M_0_012] = VectorLength(D_0_012,Time_start);
[Max_Dist_0_013, M_0_013] = VectorLength(D_0_013,Time_start);
[Max_Dist_0_014, M_0_014] = VectorLength(D_0_014,Time_start);
[Max_Dist_0_015, M_0_015] = VectorLength(D_0_015,Time_start);
[Max_Dist_0_020, M_0_020] = VectorLength(D_0_020,Time_start);
[Max_Dist_0_025, M_0_025] = VectorLength(D_0_025,Time_start);
[Max_Dist_0_030, M_0_030] = VectorLength(D_0_030,Time_start);
[Max_Dist_0_035, M_0_035] = VectorLength(D_0_035,Time_start);
[Max_Dist_0_040, M_0_040] = VectorLength(D_0_040,Time_start);
[Max_Dist_0_045, M_0_045] = VectorLength(D_0_045,Time_start);
[Max_Dist_0_050, M_0_050] = VectorLength(D_0_050,Time_start);



% X       = Speed_Calc( D,Time_start,Velocity_Q_programmer,Dist_Push,Dist_knife);
% X1      = Speed_Calc( D1,Time_start,Velocity_Q_programmer,Dist_Push,Dist_knife);
X_0_005 = Speed_Calc2( M_0_005,Velocity_Q_programmer_0_005,Dist_Push,Dist_knife,Max_Dist_0_005)
X_0_006 = Speed_Calc2( M_0_006,Velocity_Q_programmer_0_006,Dist_Push,Dist_knife,Max_Dist_0_006)
X_0_007 = Speed_Calc2( M_0_007,Velocity_Q_programmer_0_007,Dist_Push,Dist_knife,Max_Dist_0_007)
X_0_008 = Speed_Calc2( M_0_008,Velocity_Q_programmer_0_008,Dist_Push,Dist_knife,Max_Dist_0_008)
X_0_009 = Speed_Calc2( M_0_009,Velocity_Q_programmer_0_009,Dist_Push,Dist_knife,Max_Dist_0_009)
X_0_010 = Speed_Calc2( M_0_010,Velocity_Q_programmer_0_010,Dist_Push,Dist_knife,Max_Dist_0_010)
X_0_011 = Speed_Calc2( M_0_011,Velocity_Q_programmer_0_011,Dist_Push,Dist_knife,Max_Dist_0_011)
X_0_012 = Speed_Calc2( M_0_012,Velocity_Q_programmer_0_012,Dist_Push,Dist_knife,Max_Dist_0_012)
X_0_013 = Speed_Calc2( M_0_013,Velocity_Q_programmer_0_013,Dist_Push,Dist_knife,Max_Dist_0_013)
X_0_014 = Speed_Calc2( M_0_014,Velocity_Q_programmer_0_014,Dist_Push,Dist_knife,Max_Dist_0_014)
X_0_015 = Speed_Calc2( M_0_015,Velocity_Q_programmer_0_015,Dist_Push,Dist_knife,Max_Dist_0_015)
X_0_020 = Speed_Calc2( M_0_020,Velocity_Q_programmer_0_020,Dist_Push,Dist_knife,Max_Dist_0_020)
X_0_025 = Speed_Calc2( M_0_025,Velocity_Q_programmer_0_025,Dist_Push,Dist_knife,Max_Dist_0_025)
X_0_030 = Speed_Calc2( M_0_030,Velocity_Q_programmer_0_030,Dist_Push,Dist_knife,Max_Dist_0_030)
X_0_035 = Speed_Calc2( M_0_035,Velocity_Q_programmer_0_035,Dist_Push,Dist_knife,Max_Dist_0_035)
X_0_040 = Speed_Calc2( M_0_040,Velocity_Q_programmer_0_040,Dist_Push,Dist_knife,Max_Dist_0_040)
X_0_045 = Speed_Calc2( M_0_045,Velocity_Q_programmer_0_045,Dist_Push,Dist_knife,Max_Dist_0_045)
X_0_050 = Speed_Calc2( M_0_050,Velocity_Q_programmer_0_050,Dist_Push,Dist_knife,Max_Dist_0_050)


% figure
% plot(M(:,1),M(:,2),M1(:,1),M1(:,2))
% xlabel('Time [s]')
% ylabel('Force [N]')
%
%
% figure
% plot(M(:,3),M(:,2),M1(:,3),M1(:,2))
% xlabel('Distance [mm]')
% ylabel('Force [N]')
```

```
function [X] = Speed_Calc2( D,Velocity_Q_programmer,Dist_Push,Dist_knife,Max_Dist)

Time  = D(:,1);                                    % [ms] Time array
Dist  = D(:,3);                                    % [mm] Distance array

Value_Max_Dist_min = find(Dist<Max_Dist-0.2,1);    % [-]  Position of the value where this is
    through
Max_Dist_min = Dist(Value_Max_Dist_min);           % [mm] Distance belongin to the value
Time_Max_Dist_min = Time(Value_Max_Dist_min);      % [ms] Time belonging to the value

[Min_Dist,Position_Min_Dist]= min(Dist);           % [mm] Min Distance value and Positions in Array
     of the Min Distance
Length_Dist_Total = Max_Dist - Min_Dist;           % [mm] Total Distance traveled
Length_Dist_Velocity = Max_Dist_min - Min_Dist;    % [mm] Distance traveled when moving
Time_Min_Dist = ((Time(Position_Min_Dist))-Time_Max_Dist_min)/1000;        % [s] Time to reach
    minimal distance

Velocity_Platform = Length_Dist_Velocity/Time_Min_Dist;      % [mm/s] Velocity of the platform
Ratio_velocity_platform_Q = Velocity_Platform/Velocity_Q_programmer;

Ratio_Push_Knife = (Length_Dist_Total/Dist_Push)*(Dist_Push/Dist_knife);

Velocity_Knife = Ratio_Push_Knife*Velocity_Platform;


X = [ Length_Dist_Total,Length_Dist_Velocity, Time_Min_Dist, Velocity_Platform,
    Ratio_velocity_platform_Q,Velocity_Knife ];

end
```

```
function [Max_Dist, M ] = VectorLength(D,Time_start)

Time  = D(:,1);                                    % [ms] Time array
Dist  = D(:,6);                                    % [mm] Distance array
Forces = D(:,4);                                   % [N]  Force array



Position_Time_start = find(Time>Time_start,1);     % [-]  Position where 600ms is reached
[~,Position_Max_Dist]= max(Dist);                  % [mm] Min Distance value and Positions in Array
     of the Min Distance

Max_Dist = max(Dist(1:Position_Time_start));       % [mm] Max Distance value before starting

Time_Vector  = (Time(Position_Time_start:Position_Max_Dist)-600);          % [ms]  Start untill end
    movement
Force_Vector = Forces(Position_Time_start:Position_Max_Dist);              % [N]  Start untill end
    movement
Dist_Vector  = Dist(Position_Time_start:Position_Max_Dist);                % [mm] Start untill end
    movement

M=[Time_Vector,Force_Vector,Dist_Vector];

end
```